Supplemental Materials

Molecular Biology of the Cell

Bennett et al.

Supplemental Table S1. List of cloning and expression vectors used in this study.

Name	Source	Application/Features
pDONR221	Invitrogen	Donor vector for gateway cloning.
pWPXLd/LAP-N/blast/DEST	Jackson Lab Kanie et al. (2018) *Dev. Cell*	Lentiviral destination vector for cloning stable expression vectors for N-terminally tagged GFP fusion proteins. Other features: EF1alpha promoter, blasticidin resistance.
pMCB306	Bassik Lab (Stanford)	sgRNA expression vector for generating KO cell lines. Lentiviral vectors containing sgRNAs were generated by ligating oligonucleotides encoding sgRNAs into the pMCB306 vector digested with BstXI and BlpI restriction enzymes.
pCMV-VSV-G	Weinberg	Envelope plasmid
pCMV-dR8.2 dvpr	Weinberg	Lentiviral packaging vector
cDNA vectors		
pCMV6-mNEK8	Origene MC203539, Procured by Cimprich Lab	mNEK8 cDNA
pCMV-mANKS6-Myc-DDK	Origene MR224239	mANKS6 cDNA
Entry Vectors		
pENTR221-mNEK8	This study	
pENTR221-mNEK8-K33M	This study	Generated by quick change of pENTR221-mNEK8
pENTR221-mNEK8-G448V	This study	Generated by quick change of pENTR221-mNEK8
pENTR221-mANKS6	This study	
pENTR221-mANKS6-(n.s.)	This study	No stop codon, for C-terminal tagging
pENTR221-hNPHP2	Genecopoeia GC-H1881	
pENTR221-hNPHP3-(n.s.)	Genecopoeia GC-H2370-CF	No stop codon, for C-terminal tagging
Expression vectors, *generated by LR cloning reaction using entry vectors (listed above) and destination vectors.*		
pWPXLd/LAP-N-mNEK8/blast	This study	
pWPXLd/LAP-N-mNEK8-K33M/blast	This study	
pWPXLd/LAP-N-mNEK8-G448V/blast	This study	
pWPXLd/LAP-N-mANKS6/blast	This study	
pWPXLd/LAP-N-hNPHP2/blast	This study	
pWPXLd/hNPHP3-LAPC/blast	This study	

Supplemental Table S2. List of primer and guide RNA sequences used in this study.

	Name	**Sequence (5'—3')**
Primers for Gateway cloning of mANKS6 for N-term tagging:		
	HWB.P069F	GGGACAACGTTTGTACAAAAAAGCAGGCTTCATGG GCGAGGGCGCGCTGGCC
	HWB.P069R	GGGGACCACTTTGTACAAGAAAGCTGGGTCCTACC TCCTGCTAGACACGGTTTC
Primers for Gateway cloning of mNEK8 for N-term tagging:		
	HWB.P056F	GGGGACAAGTTTGTACAAAAAAGCAGGCTTCATGG AGAAGTACGAGCGG
	HWB.P056R	GGGACCACTTTGTACAAGAAAGCTGGGTCTCAGG GGGGAACTGGTTCATC
Quickchange primers for G448V mutation:		
	HWB.QC03.F	CCACCATTGTAGAAGCCTTGCTTGTCTATGAGATG GTGCAGGTGGCCTGTGG
	HWB.QC03.RC	CCACAGGCCACCTGCACCATCTCATAGACAAGCAA GGCTTCTACAATGGTGG
Quickchange primers for K33M mutation:		
	HWB.QC04.F	GGCCGACCAGAAGCTGGTGATCCTCATGCAGATC CCAGTGGAACAGATGACC
	HWB.QC04.RC	GGTCATCTGTTCCACTGGGATCTGCATGAGGATCA CCAGCTTCTGGTCGGCC
TIDE primers for NEK8-KO genotyping:		
	HWB.P090F	GAGGCCCATTTCATTTTCCAGAC
	HWB.P098R	GCCAACAACCCCTCTCCTTT
TIDE primers for INVS-KO genotyping:		
	HWB.P091F	GTCACCTAATTTGCCACCTAATGC
	HWB.P076R	TCCACTGTTTCATTCGAGATCTGT
Guide RNA sequences		
Target Gene and Guide number	**Targeted Exon**	**Sequence (5' – 3')**
ANKS6 Guide #1	Exon 4	TTGGATGCTAGCAGCTGTTACGTTTAAGAGC
ANKS6 Guide #4	Exon 5	TTGGCAGCATCACCAGGTCAAGTTTAAGAGC
INVS Guide #1	Exon 1	TTGGATGAACCAGCAAACAGCGTTTAAGAGC
NEK8 Guide #1	Exon 2	TTGGTAGTACTCAATGACATTGTTTAAGAGC
NEK8 Guide #2	Exon 2	TTGGGCTGCCTGCCGCTCTTCCTGTTTAAGAGC
NPHP3 Guide #1	Exon 1	TTGGTCGCTCGTGAGCCCCGCGTTTAAGAGC
NPHP3 Guide #2	Exon 1	TTGGTGATCGAGGACACGTACGTTTAAGAGC
NPHP3 Guide #3	Exon 1	TTGGCGCAACTCGTTCCGCCGGTTTAAGAGC

Supplemental Table S3. List of primary antibodies and concentrations or dilutions used to prepare samples for each microscopy technique used in this study, or western blot (WB).

Primary Antibody (Host, clonality)	Manufacturer (Cat. Number)	Lot number	Dilution or working concentration
Anti-INVS (Rabbit, polyclonal)	Proteintech Group (10585-1-AP)	NA	2 µg/mL (3D SM SR) 1 µg/mL (DLM and SIM)
Anti-NPHP3 (Rabbit, polyclonal)	Proteintech Group (22026-1-AP)	NA	2 µg/mL (3D SM SR) 1 µg/mL (SIM) 0.5 µg/mL (DLM) 1 µg/mL (WB)
Anti-ANKS6 (Rabbit, polyclonal)	Sigma (HPA008355)	A82684	2 µg/mL (3D SM SR*) 0.2 µg/mL (3D SM SR, SIM, DLM) 1 µg/mL (WB)
Anti-GFP (Chicken, IgY)	Invitrogen (A10262)		1:1000 (SIM)
Anti-GFP (Rabbit, polyclonal)	Invitrogen (A11122)		2 µg/mL (SIM) 1 µg/mL (WB)
Anti-GFP 3E6 (Mouse, monoclonal IgG2a)	Invitrogen (A11120)	1563696	2 µg/mL (3D SM SR)
Anti-Acetylated Tubulin Clone 6-11B-1 (Mouse, monoclonal IgG2b)	Sigma (T7451)	018M4873	2 µg/mL (3D SM SR) 0.25 µg/mL (DLM and SIM)
Anti-Alpha Tubulin DM1A (Mouse, monoclonal)	Sigma (T6199)	116M4802V	0.2 µg/mL (WB)
Anti-ARL13B (Rabbit, polyclonal)	Proteintech Group (17711-1-AP)	NA	2 µg/mL (3D SM SR) 0.54 µg/mL (SIM) 0.27 µg/mL (DLM)
Anti-ARL13B Clone N295B/66 (Mouse, monoclonal IgG2a)	Neuromab, Davis (75-287)		1 µg/mL (SIM) 0.5 µg/mL (DLM)
Anti-CEP164 (Rabbit, polyclonal)	Sigma (HPA0373606)		1:1000 (SIM) 1:2000 (DLM)
Anti-CEP170 Clone 72-413-1 (Mouse, monoclonal IgG1)	ThermoFisher Scientific (41-3200)		0.25 µg/mL (DLM)
Anti-Polyglutamylated Tubulin GT335 (Mouse, monoclonal IgG1)	Adipogen (AG-20B-0020-C050)		1 µg/mL (SIM)
Anti-Polyglutamate IN105 (Rabbit, polyclonal)	Adipogen (AG-25B-0030-C050)	A26381411	1.4 µg/mL (3D SM SR) 0.5 µg/mL (SIM)
Anti-EHD1 (Rabbit, polyclonal)	Novus Biologicals (NBP2-56412)		1:100
Anti-PACSIN2 (Rabbit, polyclonal)	Abcam (ab37615)		1:100
Anti-RPGRIP1L (Rabbit, polyclonal)	Proteintech Group (55160-1-AP)	NA	0.19 µg/mL (SIM)
Anti-IFT88 (Rabbit, polyclonal)	Proteintech Group (13967-1-AP)	NA	0.5 µg/mL (SIM)
Anti-GPR161 (Rabbit, polyclonal)	Dr. Saikat Mukopadhyay (Mukhopadhyay et al., 2013, Cell)	YZ2308AP	1:250 (SIM)

Supplemental Table S4. List of fluorescent antibodies and concentrations or dilutions used to prepare samples for each microscopy technique used in this study, or western blot (WB).

Fluorescent Secondary Antibody	Manufacturer (Cat. Number)	Lot number	Dilution or working concentration
Donkey anti-Rabbit AF647	Abcam (ab150067)	GR217553-2	2 µg/mL (3D SR SM)
Goat anti-Mouse AF647	Abcam (ab150119)	GR3192716-2	2 µg/mL (3D SR SM)
Donkey anti-Rabbit CF568	Biotium (20087-1)	17C0207	2 µg/mL (3D SR SM)
Goat anti-Mouse CF568	Biotium (20105)		2 µg/mL (3D SR SM)
Donkey anti-Chicken AF488	Jackson ImmunoResearch (703-545-155)		2 µg/mL (SIM) 1 µg/mL (DLM)
Donkey anti-Rabbit AF488	Jackson ImmunoResearch (711-545-152)		2 µg/mL (SIM) 1 µg/mL (DLM)
Donkey anti-Rabbit AF568	ThermoFisher Scientific (A10042)		2 µg/mL (SIM) 1 µg/mL (DLM)
Donkey anti-Rabbit AF647	ThermoFisher Scientific (A-31573)		2 µg/mL (SIM) 1 µg/mL (DLM)
Goat anti-Mouse IgG1 AF568	ThermoFisher Scientific (A-21124)		2 µg/mL (SIM) 1 µg/mL (DLM)
Goat anti-Mouse IgG2a AF568	ThermoFisher Scientific (A-21134)		2 µg/mL (SIM) 1 µg/mL (DLM)
Goat anti-Mouse IgG2a AF647	ThermoFisher Scientific (A-21241)		2 µg/mL (SIM) 1 µg/mL (DLM)
Goat anti-Mouse IgG2b AF647	ThermoFisher Scientific (A-21242)		2 µg/mL (SIM) 1 µg/mL (DLM)
Donkey anti-Mouse AF647	Jackson ImmunoResearch (715-605-151)		2 µg/mL (SIM) 1 µg/mL (DLM)
Donkey anti-Rabbit IRDye 800	Li-Cor Biosciences (962-32213)		0.1 µg/mL (WB)
Donkey anti-Mouse IRDye 680	Li-Cor Biosciences (962-68072)		0.1 µg/mL (WB)

Supplemental Movies:

All supplemental movies correspond to cilia marked with asterisks in Figure 2.

Supplemental Movie 1
Two-color 3D SM SR reconstruction of a cilium where NPHP3 (green) and AcTub (magenta) are labeled.

Supplemental Movie 2
3D SM SR reconstruction of a cilium where ARL13B is labeled. Color corresponds to Z position in the sample.

Supplemental Movie 3
3D SM SR reconstruction of a cilium where INVS is labeled. Color corresponds to Z position in the sample.

Supplemental Movie 4
3D SM SR reconstruction of a cilium where ANKS6 is labeled. Color corresponds to Z position in the sample.

Supplemental Movie 5
3D SM SR reconstruction of a cilium where NPHP3 is labeled. Color corresponds to Z position in the sample.

Supplemental Figure Legends:

Supplemental Figure S1. Workflow for quantitative analysis of cilia and INVcs in RPE1 cells measured by DLM.
Schematic of DLM sample preparation (A) and image acquisition (B) in this study. See Materials and Methods section for detailed descriptions of cell culture, IF, and imaging conditions. (C) Tif images were imported into MATLAB and plotted as figures to determine ideal contrast settings for the ciliary marker. Cilia positions were then annotated for each image in FIJI. The coordinates for these annotations were exported as csv files. (D) The cilia coordinates for each image were used to save mosaic files containing multi-channel images of individual cilia in a given sample. Cilia masks were made by thresholding the contrast-adjusted ciliary marker channel, usually ARL13B or acetylated tubulin (AcTub). Masks could also be generated using the sum of two ciliary markers (ARL13B + AcTub). These masks were used to measure cilia length and the densities of each marker within the masked region. (E) A function was written that prompt user-defined masking of the INVc in a chosen sample by using the curser to draw around the region marked by the protein of interest. These user-defined masks were then used to measure INVc length and protein density within the INVc. Pixel intensity-based measurements in D and E were always performed on the raw images (no contrast adjustment). (F) The results of these analyses were reported using two different graphical representations: either images (cilia plots), or combination box and bar plots. Cilia plots take advantage of the cilium masking step to reformat each cilium mosaic so that it is oriented vertically based on a mask orientation measurement, and also cropped tightly to allow for efficient side-by-side comparisons of many cilia, as well as counting the number of INVc-positive cilia. Cilia which were also stained with a basal body marker were automatically oriented tip up. For the main figures in this paper we have corrected the ciliary orientation to always point tip up. Cilia can be ordered by any parameter measured, for example longest to shortest, or brightest to dimmest as in F. Cilia within the same plot were shown with the same contrast settings, as were cilia plots of the same marker compared side by side (compare NPHP3 staining in WT and INVS-KO cells in Figure 3B as an example). Contrast settings were chosen to best represent the features of particular interest for the specified experiment. Only samples prepared at the same time, and subsequently imaged with the same conditions were considered comparable. Samples were always prepared in technical replicates to identify potential staining errors.

Supplemental Figure S2. Definition of morphological features and measurements of the INVc. (A) Diagram of a cilium illustrating some of the mapping the structural features cilia and the INVc used for analyses in this structure. Definitions of the parameters measured for cilia and the INVc in this study are listed below. (B) Diagram of three cilia of fixed length (gray) with INVcs (green) of varying lengths demonstrating the relationship between absolute compartment length and relative compartment length. (C) Diagram of how local background corrections are applied to pixel intensity based measurements of DLM images for both the cilium (magenta) and INVc (green). Ring masks used to measure background dilated 300 nm from the ciliary mask and were 300 nm wide. (D) Definition of compartment height: the distance between the basal body or start of the AcTub-positive axoneme and the proximal compartment boundary (PCB). (E) Diagrams of cilia illustrating range of variation in compartment density for an INVc protein (green). Relative values of the expected ciliary density and compartment densities are shown below to demonstrate the relationship between these two measurements. INVc protein density is expected

to be higher in the INVc than the cilium, unless the INVc extends the full length of the cilium as in the fourth illustration(*).

Supplemental Figure S3. DLM images of 100 cilia stained with anti-INVS representing variation in INVc length and density in RPE1 cells; and cilia and sub-compartment masks. (A) Schematic illustrating the coloring and relative positioning of fluorescent markers in the images in B and C. (B) 100 cilia from WT RPE1 cells stained with anti-INVS (green), anti-ARL13B (red), and anti-AcTub (blue). Cilia which do not contain well-defined inversin compartments are indicated by red triangular markers at their base. Here 86% of cilia contain inversin compartments. The 100 cilia come from seven individual images of the same coverslip, imaged with a 63X objective (DLM). Each field of view: 100x160 µm. (C-E) show the same 100 cilia with: (C) INVS (the green channel) shifted 600 nm to the right as is our convention for DLM images of INVc proteins, (D) the perimeter of the cilia mask in white, and (E) the perimeter of the sub-compartment mask (drawn around the INVS-positive region of the cilium) in white.

Supplemental Figure S4. Localization of GFP-pINVc expressed in RPE1 cells. (A) DLM images of cilia in RPE1 cells stably expressing GFP-ANKS6, ANKS6-GFP, and NPHP3-GFP. Some cilia are faintly positive for these GFP fusion proteins but the low ciliary signal above background relative to cilia stained by antibodies against endogenous ANKS6 and NPHP3 suggests that these GFP proteins are neither robust nor faithful INVc reporters. (B-D) Comparison of GFP-INVS signal to anti-INVS staining in cilia from INVS-KO cells rescued with GFP-INVS. (B) Schematic illustrating the coloring and relative positioning of fluorescent markers in the images in C and D. (C) SIM reconstructions of cilia in which GFP-INVS was detected by native GFP fluorescence (green) or indirect immunolabeling with anti-INVS and and Alexa Fluor AF568-conjugated secondary (red). (D) SIM reconstructions of cilia in which GFP-INVS was detected by indirect immunolabeling of GFP with an Alexa Fluor 488-conjugated secondary (green) and indirect immunolabeling with anti-INVS and an Alexa Fluor 568-conjugated secondary (red). GFP-INVS detected by native GFP fluorescence was also found at the ciliary base (white arrow heads) in most cilia but was not labeled by anti-INVS or anti-GFP (C and D, empty arrow heads). The diameter of this GFP-INVS-positive ciliary base structure, and the gap between it and the start of the acetylated tubulin-positive axoneme, suggests this GFP-INVS-positive structure is below the transition zone in an outer distal appendage-like conformation. This pool of GFP-INVS may not be accessible to antibody labeling due to antigen masking as diagrammed in (E), therefore it may be present but undetectable in WT RPE1 cells. (F) In some cilia GFP-INVS also localized to the ciliary tip. Tip localization of INVS was not observed in WT cells where endogenous INVS was detected by the anti-INVS antibody (Figure 1C top, and S3) thus this was likely an artifact of the GFP allele. Interestingly, ciliary tips positive for GFP-INVS were not co-stained with ANKS6 or NPHP3 (G and H). (G) Schematic (left) illustrating the coloring and relative positioning of fluorescent markers in this panel. DLM images (right) of cilia in WT and INVS-KO cells expressing GFP-INVS (green) in which ANKS6 or NPHP3 (red) were detected by IF. Top row: all cilia in which GFP-INVS was found at the ciliary tip. Bottom row: cilia from the same samples in which GFP-INVS was not found in the ciliary tip. (H) SIM reconstruction of a cilium with GFP-INVS (green) present at the ciliary tip in a WT cell. This sample was stained with anti-NPHP3 (red), though little NPHP3 was present in this INVc, and no NPHP3 was detected at the ciliary tip.

Supplemental Figure S5. INVc length does not correlate with cilium length or ciliary pocket depth.
(A) Scatter plot of cilium length (X-axis) vs. INVc length (Y-axis). Cilium length was measured as half the perimeter of a ciliary mask generated by thresholding AcTub and ARL13B intensities in WT RPE1 cells. Compartment length was measured as half the perimeter of a user-defined sub-compartment mask around the INVS-positive region of the cilium. The modest correlation noted between cilium length and INVc length here is likely driven by the fact that the INVc cannot be longer than the cilium. (B) Pie chart showing the percentage of cilia that were positive for both ciliary pocket markers (EHD1 or PACSIN2) and GFP-NEK8 or GFP-INVS in which 1. the distal compartment boundary (DCB) was equal to the top of the ciliary pocket, 2. the DCB of the INVc was shorter (more proximal) than the top of the ciliary pocket, or 3. the DCB of the INVc extended higher than the top of the ciliary pocket as diagrammed in the top right corner (see Supplemental Figure S2 for INVc morphology definitions). Only 21 cilia were measured as only 15% of cilia were positive for both INVc and ciliary pocket markers in the four samples analyzed, nonetheless, the majority of INVcs extended farther than the ciliary pocket markers suggesting that the length of the INVc is not determined by the ciliary pocket. DLM images of NEK8-KO GFP-NEK8 cells stained with antibodies against EHD1 (C) or PACSIN2 (D). Schematics (right) illustrate the coloring and relative positioning of fluorescent markers in these panels.

Supplemental Figure S6. SIM of the INVc and ciliary pocket markers.
(A) Schematic of the three possible relationships between INVc length and ciliary pocket depth. The relationship concluded for each SIM reconstruction (B-E) is annotated below the merge. (B) SIM of cilia in RPE1 cells expressing GFP-INVS stained with anti-GFP (green), EHD1 (red), and AcTub (blue). (B') Schematic illustrating the coloring and relative positioning of fluorescent markers in B and C. (C) SIM of RPE1 cells expressing GFP-INVS stained with anti-GFP (green), PACSIN2 (red), and AcTub (blue). (D) SIM of RPE1 cells expressing GFP-NEK8 stained with anti-GFP (green), PACSIN2 (red), and AcTub (blue). (D') Schematic illustrating the coloring and relative positioning of fluorescent markers in D and E. (E) SIM of RPE1 cells expressing GFP-NEK8 stained with anti-GFP (green), PACSIN2 (red), and AcTub (blue).

Supplemental Figure S7. The length of the INVc does not correlate with the length of the polyglutamylated region of the axoneme.
(A) Schematic (left) illustrating the coloring and relative positioning of fluorescent markers in the SIM reconstructions (right) in this panel. Co-localization of NPHP3 (green) with polyglutamylated tubulin (GT335, red) measured in cilia of WT RPE1 cells. In the representative examples shown, the INVc (labeled here by NPHP3) can end before or after the end of the polyglutamylated region of the axoneme suggesting that INVc length does not correlate with tubulin glutamylation in RPE1 cells. (B) Illustration of two distinct polyglutamylated regions in the axoneme, detected by two glutamylation-specific antibodies: IN105 (green), which labels at least four consecutive glutamate residues (>4E), and GT335 (red), which labels the branchpoint of the glutamate chain on the C-terminal tail of the tubulin protein. The INVc can overlap with both the IN105 and GT335 staining regions of the axoneme, and does not seem to be particularly bounded by either one. (C) SIM reconstructions of cilia in WT RPE1 cells stained with IN105 (green, AF488 secondary), GT335 (red, AF568 secondary), and anti-acetylated tubulin (AcTub, blue, AF647 secondary antibody) to mark the full length of the axoneme. Three SIM reconstructions are shown, two of which demonstrate that GT335 often stains a longer region of

the axoneme than IN105, which is rather enriched at the ciliary base, suggesting that polyglutamylation of the axoneme is more extensive at the ciliary base. Based on DLM measurements of >100 cilia (not shown) it is estimated that GT335 staining extends beyond the IN105 region in 40% of cilia as summarized in the illustration (right) of the coloring and relative positioning of fluorescent markers in this panel.

Supplemental Figure S8. The INVc does not start directly above the transition zone (TZ). (A-B) Schematics (left) illustrating the coloring and relative positioning of fluorescent markers in the SIM reconstructions (right) that measure co-localization of INVc proteins with the transition zone protein RPGRIP1L (red, AF568 secondary antibody) by SIM. (A) GFP-INVS (green, detected with anti-GFP primary antibody, AF488 secondary) and (B) GFP-NEK8 (green, detected with anti-GFP primary antibody, AF488 secondary). AcTub (blue, AF647 secondary antibody) marks the axoneme. (C) Distribution of INVc to TZ distances measured in GFP-NEK8 cells by SIM, using the start of the AcTub-positive axoneme (blue) to approximate the distal end of the TZ. (D) Table of INVc size statistics measured from 114 images of GFP-NEK8-positive cilia. INVc size parameters are diagrammed in the image (right): (a) INVc length. (b) Cilium length, measured by tracing the path of the AcTub-labeled axoneme from base to tip. (c) INVc height, the distance from the start of the AcTub-labeled axoneme to the PCB (Supplemental Figure S2A and S0D). This is the same parameter plotted in panel C. (d) Distance from the DCB (Supplemental Figure S2A) to the cilium tip. (e) Approximate values of compartment diameter, measured either as the distance between GFP-NEK8 signal peaks on either side of the axoneme in SIM reconstructions, or the most separated fibrilloids at the base of 3D SM SR reconstructions of the INVc.

Supplemental Figure S9. Co-localization of the INVc with IFT.
(A) Schematic (left) illustrating the coloring and relative positioning of fluorescent markers in the SIM reconstructions (right) that measure co-localization of GFP-INVS (green, detected with anti-GFP primary antibody, AF488 secondary) with IFT88 (red, AF568 secondary) in WT cells. (B) Schematic of channels and markers (left) and SIM reconstruction of IFT88 (red, AF568 secondary) in INVS-KO cells (right). No obvious changes in ciliary localization of IFT88 were noted between WT and INVS-KO cells in these experiments. Substantial IFT defects can result in notable decreases in the number of IFT particles observed along the axoneme in SIM reconstructions as described previously (Kanie et al. 2017), however, these were also coupled with defects in ciliation frequency and cilia length which were not observed in INVS-KO cells (Supplemental Figure S27). All samples (A and B) were stained with anti-AcTub (blue, AF647 secondary) to mark the axoneme.

Supplemental Figure S10. Co-localization of the INVc with ciliary membrane proteins.
(A) Schematic detailing the colors and relative positioning of channels and markers as they appear in panels B-D. All samples are stained with anti-AcTub (blue, AF647 secondary antibody) to mark the axoneme. (B) Co-localization of GFP-INVS (green, detected with anti-GFP primary antibody, AF488 secondary) with GPR161 (red, AF568 secondary) by SIM. GPR161 is a transmembrane protein enriched in the ciliary membrane. (C-D) Co-localization of ANKS6 (C, green, AF488 secondary) and NPHP3 (D, green, AF488 secondary) with ARL13B (red, AF568 secondary) by SIM in WT RPE1 cells. ARL13B is a ciliary protein which associates with both the ciliary membrane and the axoneme.

Supplemental Figure S11. INVc length and density in INVcs containing endogenous INVS and GFP-INVS.
(A-B) Scatter plots of INVc length (X-axis) vs. INVc density (Y-axis). INVc length was measured as half the perimeter of a user-defined sub-compartment mask around the INVS-positive region of the cilium labelling either endogenous INVS in both WT cells (A) and INVS-KO GFP-INVS cells (B). (C) Box plot of the distribution of INVS densities in the cilium measured as the mean pixel intensity in arbitrary units (AF568 channel, A.U.). INVS was detected in both WT cells and INVS-KO GFP-INVS cells by indirect immunofluorescence using anti-INVS primary, and AF568-conjugated secondary antibodies. For each cell line, two replicates are shown. The bars behind the box plot represent the percent of cilia in each sample with an INVc. The median density of anti-INVS (AF568) in INVS-KO GFP-INVS compartments is 2.5X greater than in endogenous INVS compartments.

Supplemental Figure S12. Additional SIM reconstructions of GFP-NEK8 and INVS in WT cells.
As in Figure 1D, SIM IF of INVS (red, AF568 secondary antibody) in the INVcs of WT RPE1 cells stably expressing GFP-NEK8 (green, detected with anti-GFP primary antibody, AF488 secondary) and stained with anti-AcTub (blue, AF647 secondary antibody) to mark the axoneme. 20 cilia are shown. Merged images of all three markers are shown in the top row. In the bottom row the channels are shifted relative to the merge to show each channel individually: left to right: AcTub, GFP-NEK8, and INVS. "ID no." is the identification number for an individual cilium in our SIM dataset.

Supplemental Figure S13. Additional SIM reconstructions of GFP-NEK8 and ANKS6 in WT cells.
As in Figure 1D, SIM IF of ANKS6 (red, AF568 secondary antibody) in the INVcs compartments of WT RPE1 cells stably expressing GFP-NEK8 (green, detected with anti-GFP primary antibody, AF488 secondary) and stained with anti-AcTub (blue, AF647 secondary antibody) to mark the axoneme. 20 cilia are shown. Merged images of all three markers are shown in the top row. In the bottom row the channels are shifted relative to the merge to show each channel individually: left to right: AcTub, GFP-NEK8, and ANKS6. "ID no." is the identification number for an individual cilium in our SIM dataset.

Supplemental Figure S14. Additional SIM reconstructions of GFP-NEK8 and NPHP3 in WT cells.
As in Figure 1D, SIM IF of NPHP3 (red, AF568 secondary antibody) in the INVcs of WT RPE1 cells stably expressing GFP-NEK8 (green, detected with anti-GFP primary antibody, AF488 secondary) and stained with anti-AcTub (blue, AF647 secondary antibody) to mark the axoneme. 20 cilia are shown. Merged images of all three markers are shown in the top row. In the bottom row the channels are shifted relative to the merge to show each channel individually: left to right: AcTub, GFP-NEK8, and NPHP3. "ID no." is the identification number for an individual cilium in our SIM dataset.

Supplemental Figure S15. Expected and observed geometries of ciliary proteins measured by SIM.
(A) SIM reconstructions of two different ring structures (IFT88 and CEP164) present at the base of the cilium. Because the face of the ring is oriented perpendicular to the imaging plane in most

cilia in RPE1 cells, these structures appear as two dots in SIM reconstructions. (B) SIM of three different ciliary markers: acetylated tubulin (AcTub) and polyglutamylated tubulin (PgTub) both of which mark the axoneme, and ARL13B, an abundant peri-axonemal protein which can associate with the ciliary membrane. Interpretations of the arrangements of each marker in the cilium are diagrammed above the images. ARL13B detected by AF488 (green, left) and PgTub detected by AF488 (green, right) and AF568 (red) appear as two parallel lines. For the PgTub signal these lines coalesce as polyglutamylation of the axoneme tapers off. AcTub (detected by AF647) appears as a single line. (C) Diagram of a 9+0 axoneme in cross-section, illustrating relative locations of peri-axonemal proteins (green) and modified tubulin epitope surfaces: anti-AcTub (blue) should bind to the microtubule lumens, and anti-PgTub (red) should bind to the microtubule surfaces. (D) Diagram of the expected appearance for a hollow tube in a SIM reconstruction (left) compared with actual measurements (right). Compare these results with (A): cylindrical structures appear as stacks of rings, consistent with the presence of a hollow center. SIM reconstructions of structures labeled with AF647, AF568, or AF488 will have different resolutions. AF647 cannot resolve an AcTub stained cilium as a hollow structure. AF488 can almost resolve the hollow in the proximal half of the axoneme as emphasized in the inset. Note that the tip of this cilium has a hairpin bend that accounts for the double line observed in the AcTub channel at the very tip of the cilium. (E) Illustration of known structural features of the cilium compared to the conformations observed in SIM reconstructions. All SIM reconstructions shown in this study are sum projections of 3D-SIM reconstructions. The axially cut appearance of ring and cylindrical structures is not due to optical sectioning of a portion of the structure, but rather an axial distortion due to the ratio of lateral and axial resolutions (approximately 100 nm to 300 nm (Schermelleh, Heintzmann, and Leonhardt 2010)). The diameters of these structures are approximately equal to the Z-resolution of this SIM imaging system.

Supplemental Figure S16. The INVc is asymmetric in some cilia measured by SIM.
(A) Illustrations and SIM reconstructions of symmetric (top) or asymmetric (bottom) INVcs. SIM reconstructions WT RPE1 cells expressing GFP-NEK8 stained with anti-GFP primary antibody (green, AF488 secondary) and anti-NPHP3 (red, AF568 secondary) and anti-AcTub (blue, AF647 secondary). The schematic containing left and right bars (representing the left and right sides of the axoneme where INVc protein was detected) with green fill is introduced as a method for representing interpretations of compartment symmetry or asymmetry as used in (D) and Supplemental Figure S17B-C. (B) Interpretation of compartment symmetry or asymmetry regarding the structure of the INVc. Symmetric compartments suggest that INVc proteins are evenly distributed about the axoneme. Asymmetric compartments are not compatible with interpretation, with the exception of compartments which tapering at their distal end due to a narrowing of the axoneme. (C) Schematic illustrating the coloring and relative positioning of fluorescent markers in the SIM reconstructions in D. (D) Six SIM reconstructions of cilia in WT cells expressing GFP-NEK8 stained with anti-GFP primary antibody (green, AF488 secondary) and anti-ANKS6 (red, AF568 secondary) and anti-AcTub (blue, AF647 secondary). The observed symmetry or asymmetry of the compartment is diagrammed below each cilium.

Supplemental Figure S17. Asymmetries are more likely to be detected by SIM in low density compartments.
(A) Multi-channel cilia image format guide defining the markers shown (B and C). (B) Three SIM measurements of GFP-NEK8-positive cilia stained with anti-GFP (green, AF488 secondary) and co-stained with ARL13B (red, AF568 secondary) and anti-AcTub (blue, AF647

secondary). (C) Three SIM measurements of GFP-INVS-positive cilia, stained with anti-GFP (green, AF488 secondary) and co-stained with ARL13B (red, AF568 secondary) and anti-AcTub (blue, AF647 secondary). Compartment symmetry or asymmetry is diagrammed below each cilium using the schematic introduced in Supplemental Figure S16A. (D) Quantification of percent of cilia with symmetric distributions for the following ciliary proteins: ARL13B, GFP-NEK8, GFP-INVS, and polyglutamylated tubulin (PgTub). Ciliary proteins were considered asymmetric if >300 nm of signal (or approximately three granules in the reconstruction) was unpaired. The number (n) of SIM reconstructions surveyed is noted at the top of the graph. It should be noted that all of the asymmetric PgTub stained cilia were asymmetric at the tip of the PgTub-positive compartment likely indicating a tapering of the axoneme and also a reduction in local PgTub density. Some of the asymmetries driven by the INVc could also represent axoneme narrowing if the INVc is directly associated with the axoneme. However, many examples of asymmetric INVcs (B and Supplemental Figure S16D) are asymmetric at the proximal end of the compartment as well. Further, in the examples shown in B, GFP-NEK8 is asymmetric where ARL13B is not, demonstrating that the asymmetries observed in these cilia are not driven by general changes in cilium morphology. (E) Box plot representing the distributions of GFP densities in the INVcs containing either GFP-NEK8 or GFP-INVS. The median GFP-INVS density is 6X greater than the median GFP-NEK8 density, supporting the observation that sparse compartments detected by GFP-INVS are less likely to present asymmetric distributions in SIM reconstructions. “GFP” density for GFP-negative INVcs (detected by immunolabeling of endogenous INVc proteins in the red channel, AF568) was measured as a control for background fluorescence in the green channel (GFP).

Supplemental Figure S18. 3D SM SR reconstruction statistics for two-color NPHP3 and AcTub and single-color ARL13B experiments.
Histograms showing the signal photons per localization, background photons per pixel, double-helix PSF lobe distance, and the localization precisions in x, y, and z for the representative cilia shown in Figure 2A and 2B (marked with asterisks) and in Supplemental Movies 1-2. Each data set has been filtered to remove localizations with a lobe distance between 5.8 pixels and 7.2 pixels (when imaging with Alexa Fluor 647 using the 686 nm DH phase mask: (A) NPHP3 and (C) ARL13B) or between 5.3 pixels and 7.5 pixels (when imaging with CF568 using the 615 nm DH phase mask: (B) AcTub), and localizations with a localization precision in x or y larger than 30 nm. The resulting median values are indicated above each histogram.

Supplemental Figure S19. 3D SM SR reconstruction statistics for single-color INVS, ANKS6 and NPHP3 experiments.
Histograms showing the signal photons per localization, background photons per pixel, double-helix PSF lobe distance, and the localization precisions in x, y, and z for the representative cilia shown in Figure 2C, 2E, and 2F (marked with asterisks) and in Supplemental Movies 3-5. Each data set has been filtered to remove localizations with a lobe distance between 5.8 pixels and 7.2 pixels and localizations with a localization precision in x or y larger than 30 nm. The resulting median values are indicated above each histogram.

Supplemental Figure S20. DLM images of 3D SM SR labeling controls.
Diffraction-limited images of samples that were used for 3D SM SR imaging, immunolabeled as indicated. The top row shows the signal in the red channel (Red Ch) when the sample were excited by 647 nm light, and the bottom row shows the signal in the green channel (Green Ch)

when the same samples were excited by 560 nm light. Image intensities are self-normalized to show potential structure also in the dimmer samples. The resulting signal photons are reported on each image: average photons per pixel measured in the six brightest pixels in labeled cilia and in a 50x50 pixel region of interest (ROI) at the highest intensity found in the controls. Five cilia/ROIs were measured for each labeling condition and the values report mean ± standard deviation between the measurements. Species host and specificity of the antibodies have been abbreviated: R (Rabbit), D (Donkey), and M (Mouse).

Supplemental Figure S21. Additional 3D SM SR reconstructions and fibrilloid measurements. (A) 3D SM SR reconstruction of the base of an axoneme labeled with anti-acetylated tubulin (CF568 secondary). As in Figure 2B-F, the color of each localization in the reconstruction maps to its Z-position in the sample, and this view is looking down the axis of the axoneme. The depth range of the color scale is unique to each reconstruction. This cross-section represents the most proximal 200 nm of the cilium where the axoneme is resolved as a hollow structure. (B) Histogram of localization frequency (bin size 20 nm) for a 30 nm wide line-scan in the x-y plane of the axoneme cross-section in panel A. (C) Two-color 3D SM SR reconstruction of a larger field-of-view of the same cilium shown in Figure 2A immunolabeled with anti-NPHP3 to detect the inversin compartment (green, AF647 secondary) and anti-acetylated tubulin to detect the axoneme (magenta, CF568 secondary). (D) Two-color 3D SM SR reconstruction of a cilium immunolabeled with anti-GFP to detect the inversin compartment in cells expressing GFP-INVS (green, AF647 secondary) and anti-polyglutamylated-tubulin (GT335) to detect the axoneme (magenta, CF568 secondary). (E-H) Additional one-color reconstructions of cilia labeled for ARL13B (E), INVS (F), ANKS6 (G), and NPHP3 (H). (I) Total compartment lengths plotted against the number of fibrilloids per cilium demonstrating that INVc length does not appear to be strongly correlated with fibrilloid number. Measurements from 19 cilia are included. (J) Individual fibrilloid lengths plotted against total compartment length. The dotted line indicates where fibrilloid length would be equal to compartment length. Measurements from 19 cilia are included covering all INVc 3D SM SR measurements made (provided here in panels E-H and in Figure 2C-F). Our reconstructions yielded measurements for a total of 58 fibrilloids and one afibrilloid ANKS6 compartment (fibrilloid length = 0). The marker type of each data point in G and H indicates which INVc protein was labeled to generate the reconstruction.

Supplemental Figure S22. Artificially sparse reconstructions of ARL13B.
(A) Complete reconstruction of ARL13B-labeled cilium (the same cilium as shown in Figure 2B) including 54,466 localizations. (B) Four reconstructions of the cilium in A, each using only 8000 localizations. The 8000 localizations used in each reconstruction were randomly sampled from the original 3D SM SR dataset for this cilium.

Supplemental Figure S23. Knockout cell line generation and validation of INVS-KO.
(A) Outline of knockout (KO) cell line generation and validation steps employed in this study. KO validation methods varied by gene of interest depending on which reagents were available. TIDE (C) and IF (G) were used to confirm mutation of the INVS gene and loss of INVS protein from the INVc respectively. Full rescue of INVc assembly by GFP-INVS (Figure 4 and Supplemental Figure S31) further confirmed phenotypic loss of INVS activity in INVS-KO cell line that we generated. We found that the anti-INVS antibody used here for IF could not be reliably used for immunoblot as it did not detect an INVS-specific band. (B) Annotated schematic of the INVS gene (green, NC_000009.12:100091700-100302175). Exons appear in

red. The guide RNA target site, and binding regions for the primers used to amplify this locus for TIDE analysis (HWB.P091.For and HWB.P076.Rev) are noted on the inset for Exon 2. Primer and guide RNA sequences are provided in Supplemental Table S2. The Ankyrin Repeat Domain (ARD) spans Exons 1-12, and the immunogen region for the anti-INVS antibody used in this study spans exons 1-3. INVS gene schematic was generated using Geneious version 10.2 created by Biomatters (available from https://www.geneious.com). (C) TIDE results for INVS-KO single cell clones, which were then mixed to generate the superclonal KO line used in this study. Clones with insertions or deletions predicted to introduce frame shift mutations (sizes not divisible by 3) were chosen. (D) Schematic illustrating the coloring and relative positioning of fluorescent markers in the images in E-G. (E) 50 representative cilia in WT cells stained with anti-INVS (green). (E') INVS (green) channel shown alone with enhanced contrast. (F) 50 representative cilia in WT Cas9-BFP cells stained with anti-INVS (green). (F') INVS (green) channel shown alone with enhanced contrast. (G) 50 representative cilia in INVS-KO Cas9-BFP cells stained with anti-INVS (green). (G') INVS (green) channel shown alone with enhanced contrast to confirm absence of INVS-positive cilia. Non-specific anti-INVS staining of the basal body is noted (black arrowheads).

Supplemental Figure S24: NEK8-KO genotyping by TIDE and validation of ANKS6-KO cell line by IF.
(A) Annotated schematic of the NEK8 gene (green, NC_000017.11:28727700-28743457). Exons appear in gray. The guide RNA target sites (guides #1 and #2), and binding regions for the primers used to amplify this locus for TIDE analysis (HWB.P090.For and HWB.P098.Rev) are noted on the inset for Exon 2. Primer and guide RNA sequences are provided in Supplemental Table S2. The Kinase Domain (KD) spans Exons 1-5, and the RCC1 Repeat Domain (RRD) spans exons 6-9. NEK8 gene schematic was generated using Geneious version 10.2 created by Biomatters (available from https://www.geneious.com). (B) Annotated schematic of the ANKS6 gene (green, NG_042237.1). Exons appear in gray. The guide RNA target sites are noted on the insets for exon 4 (guide #1) and exon 5 (guide #4). Guide RNA sequences are provided in Supplemental Table S2. The Ankyrin Repeat Domain spans Exons 1-6, and the RCC1 Repeat Domain (RRD) spans exons 6-9. The anti-ANKS6 HPA008355 immunogen spans exons 12-15. ANKS6 gene schematic was generated using Geneious version 10.2 created by Biomatters (available from https://www.geneious.com). (C) TIDE results for the seven NEK8-KO single cell clones, which were then mixed to generate the superclonal NEK8-KO line used throughout this study. Clones with insertions or deletions predicted to introduce frame shift mutations (sizes not divisible by 3) were chosen. In addition to TIDE genotyping, each of these clones was phenotyped by loss of loss of ciliary ANKS6 followed by rescue with stable re-expression of GFP-mNEK8 (data not shown). (D) Schematic illustrating the coloring and relative positioning of fluorescent markers in the images E-G. (E) 50 representative cilia in WT cells stained with anti-ANKS6 (green). (E') ANKS6 (green) channel shown alone with enhanced contrast.
(F) 50 representative cilia in WT Cas9-BFP cells stained with anti-ANKS6 (green). (F') ANKS6 (green) channel shown alone with enhanced contrast.
(G) 50 representative cilia in superclonal ANKS6-KO Cas9-BFP cells stained with anti-ANKS6 (green). (G') ANKS6 (green) channel shown alone with enhanced contrast to confirm absence of ANKS6-positive cilia. Some non-specific anti-ANKS6 staining of the basal body is noted (black arrowheads). Due to the availability of the ANKS6 antibody, the specificity of which had been confirmed by siANKS6 (data not shown) single cell clones selected from sgANKS6-targeted Cas9-BFP cells were not genotyped by TIDE but rather phenotyped directly by IF with anti-

ANKS6 to detect loss of the INVc. Loss of ANKS6 protein in this cell line was further confirmed by immunoblot (Supplemental Figure S26A).

Supplemental Figure S25. Validation of NPHP3-KO cell line by IF.
(A) Annotated schematic of the NPHP3 gene (green, NC_000003.12:c132743384-132659683). Exons appear in gray. The guide RNA target sites (guides #1, #2, and #3) are noted on the inset for exon 1. Guide RNA sequences are provided in Supplemental Table S2. The anti-NPHP3 immunogen is encoded by exon 1. NPHP3 gene schematic was generated using Geneious version 10.2 created by Biomatters (available from https://www.geneious.com). (B) Schematic illustrating the coloring and relative positioning of fluorescent markers in the images in C-F. (C) 50 representative cilia in WT cells stained with anti-NPHP3 (green). (C') NPHP3 (green) channel shown alone with enhanced contrast. (D) 50 representative cilia in WT Cas9-BFP cells stained with anti-NPHP3 (green). (D') NPHP3 (green) channel shown alone with enhanced contrast. (E) 50 representative cilia in superclonal NPHP3-KO Cas9-BFP cells stained with anti-NPHP3 (green). (E') NPHP3 (green) channel shown alone with enhanced contrast to confirm absence of NPHP3-positive cilia compared to INVS-KO cells stained with anti-NPHP3 (F and F') where ciliary NPHP3 is reduced, but still notably present in a fraction of cilia. Due to the availability of the NPHP3 antibody, single cell clones selected from sgNPHP3-targeted Cas9-BFP cells were not genotyped by TIDE but rather phenotyped directly by IF with anti-NPHP3 to detect loss of the ciliary NPHP3 signal. Loss of NPHP3 protein in this cell line was further confirmed by immunoblot (Supplemental Figure S26B).

Supplemental Figure S26. Validation of ANKS6-KO and NPHP3-KO cell lines by immunoblot.
Immunoblots of whole cell lysates from WT and gINVc-KO cell lines, blotted for alpha-tubulin as a loading control (red, detected with IRdye680 fluorescent secondary antibodies, bottom panels) and either ANKS6 (A) or NPHP3 (B) (green, detected with IRdye800 fluorescent secondary antibodies, top panels). In both A and B, the subconfluent asynchronous INVS-KO and ANKS6-KO samples are noticeably underloaded. The confluent, serum-starved samples confirm that ANKS6 is still expressed in INVS-KO cells, and is undetectable in the ANKS6-KO cells. Whole cell lysates were prepared from subconfluent asynchronous cells growing in media containing 10% FBS, or confluent cells that had been cultured in serum-free media for 24 h as in our ciliation assay conditions. Lysates were prepared by scraping cells from plate in NP40 lysis buffer (1% NP40, 150 mM NaCL, 50 mM Tris-Cl pH 8.0, supplemented with phosphatase inhibitors and protease inhibitors), incubation on ice for >20 min, and clarification by centrifugation at 15,000 RPM (21,000 g) for 10 min at 4ºC. Protein concentration was estimated by BCA assay (Pierce, ThermoFisher Scientific Cat#23225) according to manufacturer's instructions. Lysates were diluted to the same final concentration with additional NP40 lysis buffer and then boiled at 95ºC for 5 min in 1X LDS (with 2.5% BME) before loading 7.5 µg protein in each lane of a Novex NuPAGE 4-12% Bis-Tris polyacrylamide gradient gel (Invitrogen NP0323BOX). Novex Sharp Pre-stained Protein Standard (ThermoFisher Scientific, LC5800) was run as a molecular weight reference. Gels were run at 200V for 1 h in MOPS buffer (50 mM MOPS, 50 mM Tris Base, 0.1% SDS, 1 mM EDTA, pH 7.7) at room temperature (RT), then transferred to an Immobilon-FL PVDF membrane (pore size 0.45 µm, Millipore IPFL00010) at 50V for 1.5 h at 4ºC in Towbin transfer buffer (25 mM Tris, 192 mM glycine, pH 8.3, 10% MeOH). Membranes were blocked in 3% milk (prepared in 1X TBST), incubated with primary antibodies diluted in blocking solution (See Supplemental Table S3 for concentrations),

for 2 h at RT, washed in TBST, then incubated with fluorescent secondary antibodies diluted in blocking solution supplemented with 0.01% SDS (See Supplemental Table S4 for antibody concentrations) for 1 h at RT. Membranes were scanned on an Odyssey CLx Imaging System (LI-COR).

Supplemental Figure S27. gINVc-KO cell lines do not have ciliation or cilia length defects.
(A) Ciliation frequency measured for WT and gINVc-KO cell lines by comparing the total number of CEP164-positive basal bodies with the number of basal bodies associated with an AcTub- or ARL13B-positive cilium detected by IF. The number of basal bodies (n) measured represents the total number counted for four different coverslips prepared for each cell line in two separate experiments. Error bars represent the standard deviation between the four coverslips. (B) Distributions of cilium length for WT and gINVc-KO cell lines. Mean cilium length, standard deviation, and number of cilia measured for each cell line are listed in the table (right). No substantial difference in cilium length was observed between WT cells and any of the g-INVc-KO cell lines. (C) Distributions of GFP-INVS-positive INVc length in WT and gINVc-KO cell lines stably expressing GFP-INVS. Mean INVc length, standard deviation, and number of cilia measured for each cell line are listed in the table (right). No substantial difference in GFP-INVS-positive INVc length was observed between WT cells and any of the g-INVc-KO cell lines.

Supplemental Figure S28. Summary of T-test results for significant differences in ciliary pINVc density in WT and gINVc-KO cells.
Matrices present the p-values for two-tailed T-tests comparing the ciliary densities for each immunofluorescence sample plotted in the box plots in Figure 3C. Results are shown for densities of: endogenous INVS (A), endogenous ANKS6 (B), endogenous NPHP3 (C), and ciliary GFP for cell lines stably expressing GFP-NEK8 (D), and GFP-INVS (E).

Supplemental Figure S29. Validation of GFP-INVS and GFP-NEK8 expression by immunoblot.
Immunoblots of whole cell lysates from the WT and gINVc-KO cell lines stably expressing GFP-INVS (A) or GFP-NEK8 (B) generated in this study. Samples were blotted for alpha-tubulin as a loading control (red, detected with IRdye680 fluorescent secondary antibodies, bottom panels) and anti-GFP to detect GFP fusion proteins (green, detected with IRdye800 fluorescent secondary antibodies, top panels). See legend for Supplemental Figure S26 for details on whole cell lysate preparation and immunoblotting conditions.

Supplemental Figure S30. Rescue of NEK8-KO cells with GFP-NEK8.
IF of (A) ANKS6 and (B) NPHP3 (red) in WT, NEK8-KO, and NEK8-KO cells rescued with GFP-NEK8 (green, shifted 600 nm to the right). Expression of GFP-NEK8 was confirmed by immunoblot in Supplemental Figure S29. Cilia are arranged in order of ANKS6 or NPHP3 ciliary density. 50 cilia from each sample are shown. ARL13B was included as a ciliary marker (blue, shifted 600 nm to the left). (C-F) Quantification of samples shown in A-B. ANKS6 and NPHP3 densities were measured in arbitrary units (A.U.) in: (C) the ciliary volume which was automatically masked by ARL13B-positive region, and (D) INVc volume masked by a user-defined region. The mean intensity of the peri-ciliary or peri-compartment background has been subtracted from the reported values. (E) Distribution of cilia lengths (measured in μm) in WT (n = 577), NEK8-KO (n = 579), and NEK8-KO cells rescued with GFP-INVS. WT cells expressing

GFP-NEK8 are also included (n = 367). (F) Distribution of INV compartment lengths (measured in µm) from manually drawn masks around GFP and INVS/ANKS6/NPHP3-positive regions in WT cells (n = 452), NEK8-KO cells (n = 23), and NEK8-KO cells rescued with GFP-NEK8 (n = 276). NEK8-KO cells expressing GFP-INVS are also included (n = 178). As in WT and INVS-KO cells (Supplemental Figure S31F), stable expression of GFP-INVS also increased INVc length in NEK8-KO cells.

Supplemental Figure S31. Rescue of INVS-KO cells with GFP-INVS.
IF of (A) ANKS6 and (B) NPHP3 (red) in WT, INVS-KO, and INVS-KO cells rescued with GFP-INVS (green, shifted 600 nm to the right). Cilia are arranged in order of ANKS6 or NPHP3 ciliary density. 50 cilia from each sample are shown. ARL13B was included as a ciliary marker (blue, shifted to 600 nm to the left). (C-F) Quantification of samples shown in A-B. ANKS6 and NPHP3 densities were measured in arbitrary units (A.U.) in: (C) the ciliary volume which was automatically masked by ARL13B-positive region (as demonstrated in Supplemental Figures S1D, S2A, and S3D), and (D) INVc volume masked by a user-defined region (as demonstrated in Supplemental Figures S1E, S2A, and S3E). The mean intensity of the peri-ciliary or peri-compartment background has been subtracted from the reported values. (E) Distribution of cilia lengths (measured in µm) in WT (n = 577), INVS-KO (n = 515), and INVS-KO cells rescued with GFP-INVS (n = 380). WT cells expressing GFP-INVS are also included (n = 317). (F) Distribution of INVc lengths (measured in µm) from manually drawn masks around GFP and INVS/ANKS6/NPHP3-positive regions in WT cells (n = 452) and INVS-KO cells rescued with GFP-INVS (n = 361). WT cells expressing GFP-INVS are also included (n=290). INVS-KO cells do not have INV compartments so no length is reported. INV compartments are longer in the rescued cell line and WT cells expressing GFP-INVS than in WT cells.

Supplemental Figure S32. Additional DLM images of ANKS6 localization and INVc-specific density measurements of ANKS6 and NPHP3 in gINVc-KO cell lines expressing GFP-INVS.
Additional images of the samples presented in Figure 4B. (A) Schematic illustrating the coloring and relative positioning of fluorescent markers in the images in B-E. ANKS6 (red) shown shifted 600 nm to the right of ARL13B (blue, cilia marker). Although the cell lines in C-E were GFP-positive, the GFP channel has been omitted from these images to better display ANKS6 localization. (B) WT cells (not transduced with GFP-protein). (C) INVS-KO cells rescued with GFP-INVS. (D) NEK8-KO cells expressing GFP-INVS. ANKS6 weakly localizes to the INVc. (E) NPHP3-KO cells expressing GFP-INVS, which results in an increase in ANKS6 compartment density. (F) Box and bar plots quantifying INVc compartments in gINVc-KO cell lines and gINVc-KO cell lines stably expressing GFP-INVS where ANKS6 (top) or NPHP3 (bottom) was detected by IF. The percentage of cilia positive for INV compartments detected by the presence of ANKS6, NPHP3, or GFP-INVS is represented as a bar plot (right axis) behind a box plot (left axis) representing the distribution of ANKS6 and NPHP3 densities in the INV compartments of the cell lines measured. Cilia with no INVc are plotted with a density of 0 arbitrary units (A.U.). The number of cilia (n) measured for each sample is noted above each box and bar.

Supplemental Figure S33. Additional DLM images of NPHP3 localization in gINVc-KO cell lines expressing GFP-INVS.
Additional images of the samples presented in Figure 4E. (A) WT cells (not transduced with GFP-protein). (B) INVS-KO cells (not transduced with GFP-protein). (C) INVS-KO cells

rescued with GFP-INVS. (D) ANKS6-KO cells expressing GFP-INVS (GFP-INVS$_{ANKS6\text{-}KO}$). NPHP3 weakly localizes to the INVc, but is not sequestered in the INVc. (E) NEK8-KO cells expressing GFP-INVS (GFP-INVS$_{NEK8\text{-}KO}$). NPHP3 weakly localizes to the INVc, but is not sequestered in the INVc. (F) NPHP3-KO cells expressing GFP-INVS to demonstrate that weak compartment staining in GFP-INVS$_{ANKS6\text{-}KO}$ (D and Figure 4E) and GFP-INVS$_{NEK8\text{-}KO}$ (E and Figure 4E) compartments is not the result of bleedthrough or non-specific staining.

Supplemental Figure S34. Summary of T-test results for significant differences in ciliary ANKS6 and NPHP3 density in cell lines expressing GFP-INVS.
Matrices present the p-values for two-tailed T-tests comparing the ciliary densities for each immunofluorescence sample plotted in the box plots in Figures 4C and 4F. (A) ANKS6 densities (Figure 4C). (B) NPHP3 densities (Figure 4F).

Supplemental Figure S35. Summary of ANKS6 localization in WT, INVS-KO, NEK8-KO, and NPHP3-KO cell lines expressing GFP-INVS.
SIM IF of cilia positive for INVc proteins: ANKS6 (red, AF568 secondary antibody) and GFP-INVS (green, detected with anti-GFP antibody, AF488 secondary antibody). Cilia were stained with anti-AcTub (blue, AF647 secondary antibody) to mark the axoneme. (A) Schematic illustrating the coloring and relative positioning of fluorescent markers in the SIM reconstructions in B-E. Cilia were measured in the following cell lines: (B) WT, (C) INVS-KO, (D) NEK8-KO, and (E) NPHP3-KO cells all stably expressing GFP-INVS. For each cell line, 6 cilia are shown. Merged images of all three markers are shown in the top row. In the bottom row the channels are shifted relative to the merge to show each channel individually, as diagrammed in panel A. (B'-E') Enlarged images of the cilia marked by white arrowheads are shown to the right. The values on the far right represent (% Loc. in INVc) the percentage of GFP-INVS and ANKS6-positive cilia in which ANKS6 co-localized exclusively with GFP-INVS in the INVc (rather than being localized along the axoneme either above or below the INVc like NPHP3 in Figure 5), and the total number of cilia (n) measured from each cell line is noted below. Supplemental figures S45-S49.

Supplemental Figure S36. Correlation of GFP-NEK8 and GFP-INVS with ANKS6 and NPHP3 in NEK8-KO and INVS-KO cell lines rescued with GFP fusion proteins.
(A-D) Scatter plots and pairwise correlations of GFP-NEK8 or GFP-INVS (X-axis) with ANKS6 and NPHP3 (Y-axis) in RPE1 NEK8-KO cells stably expressing GFP-NEK8 or RPE1 INVS-KO cells expressing GFP-INVS. GFP-NEK8 and GFP-INVS were detected directly by native GFP fluorescence. Endogenous ANKS6 and NPHP3 were detected by indirect IF with AF568 secondary. The densities of the GFP-alleles and endogenous proteins within the INVc were measured as the mean pixel intensity in arbitrary units (A.U.) within a user-defined sub-compartment mask drawn around the GFP- or AF568-positive region of each cilium. The Pearson's *r* value, *p* value, and number of compartments (n) measured for each sample are noted on the plot. Correlation between (A) ANKS6 and GFP-NEK8 in NEK8-KO cells, (B) NPHP3 and GFP-NEK8 in NEK8-KO cells, (C) ANKS6 and GFP-INVS in INVS-KO cells, and (D) NPHP3 and GFP-INVS in INVS-KO cells.

Supplemental Figure S37. SIM reconstructions of NPHP3(1-200) in WT cells.
(A) SIM IF of GFP-NPHP3(1-200) (green, detected with anti-GFP primary antibody, AF488 secondary antibody) in the cilia of WT RPE1 cells. Cilia were stained with anti-INVS (red,

AF568 secondary antibody) to mark the INVc, and anti-AcTub (blue, AF647 secondary antibody) to mark the axoneme. Six cilia are shown. Merged images of all three markers are shown in the top row. In the bottom row the channels are shifted relative to the merge to show each channel individually: Left to right: AcTub, NPHP3(1-200), and INVS.

Supplemental Figure S38. Additional SIM reconstructions of NPHP3 in WT cells.
Additional SIM reconstructions of NPHP3 in WT cells, as in Figure 5A. SIM IF of NPHP3 (green, AF488 secondary antibody) in the INVc. Cilia were stained with anti-polyglutamylated tubulin (red, "PgTub-GT335", AF568 secondary antibody) to mark a proximal region of the cilium and anti-AcTub (blue, AF647 secondary antibody) to mark the axoneme. 20 cilia are shown. Merged images of all three markers are shown in the top row. In the bottom row the channels are shifted relative to the merge to show each channel individually: left to right: AcTub, NPHP3, and PgTub. "ID no." is the identification number for an individual cilium in our SIM dataset. Note: In Figure 5A, polyglutamylated tubulin was not shown, and NPHP3 was shown in red rather than green to be consistent with colors chosen for reconstructions of GFP-INVS expressing cells.

Supplemental Figure S39. Additional SIM reconstructions of NPHP3 in INVS-KO cells.
Additional SIM reconstructions of NPHP3 in INVS-KO cells, as in Figure 5A. SIM IF of NPHP3 (green, AF488 secondary antibody). Cilia were stained with anti-polyglutamylated tubulin (red, PgTub-GT335, AF568 secondary antibody) to mark a proximal region of the cilium and anti-AcTub (blue, AF647 secondary antibody) to mark the axoneme. 16 cilia are shown. Merged images of all three markers are shown in the top row. In the bottom row the channels are shifted relative to the merge to show each channel individually: left to right: AcTub, NPHP3, and PgTub. "ID no." is the identification number for an individual cilium in our SIM dataset. Note: In Figure 5A, polyglutamylated tubulin was not shown, and NPHP3 was shown in red rather than green to be consistent with colors chosen for reconstructions of GFP-INVS expressing cells.

Supplemental Figure S40. Additional SIM reconstructions of NPHP3 in WT cells expressing GFP-INVS.
As in Figure 5A, SIM IF of NPHP3 (red, AF568 secondary antibody) and GFP-INVS (green, detected with anti-GFP antibody, AF488 secondary antibody) in WT cells stably expressing GFP-INVS. Cilia were stained with anti-AcTub (blue, AF647 secondary antibody) to mark the axoneme. 20 GFP-INVS-positive cilia are shown. Merged images of all three markers are shown in the top row. In the bottom row the channels are shifted relative to the merge to show each channel individually: left to right: AcTub, GFP-INVS, and NPHP3. "ID no." is the identification number for an individual cilium in our SIM dataset.

Supplemental Figure S41. Additional SIM reconstructions of NPHP3 in INVS-KO cells rescued with GFP-INVS.
As in Figure 5A, SIM IF of NPHP3 (red, AF568 secondary antibody) and GFP-INVS (green, detected with anti-GFP antibody, AF488 secondary antibody) in INVS-KO cells rescued with GFP-INVS. Cilia were stained with anti-AcTub (blue, AF647 secondary antibody) to mark the axoneme. 20 GFP-INVS-positive cilia are shown. Merged images of all three markers are shown in the top row. In the bottom row the channels are shifted relative to the merge to show each channel individually: left to right: AcTub, GFP-INVS, and NPHP3. "ID no." is the identification number for an individual cilium in our SIM dataset.

Supplemental Figure S42. Additional SIM reconstructions of NPHP3 in ANKS6-KO cells expressing GFP-INVS.
As in Figure 5A, SIM IF of NPHP3 (red, AF568 secondary antibody) and GFP-INVS (green, detected with anti-GFP antibody, AF488 secondary antibody) in ANKS6-KO cells stably expressing GFP-INVS. Cilia were stained with anti-AcTub (blue, AF647 secondary antibody) to mark the axoneme. 20 GFP-INVS-positive cilia are shown. Merged images of all three markers are shown in the top row. In the bottom row the channels are shifted relative to the merge to show each channel individually: left to right: AcTub, GFP-INVS, and NPHP3. "ID no." is the identification number for an individual cilium in our SIM dataset. Arrows indicate cilia in which the INVc extended to the cilium tip. In these cases NPHP3 was considered to be localized in the INVc (Figure 5C).

Supplemental Figure S43. Additional SIM reconstructions of NPHP3 in NEK8-KO cells expressing GFP-INVS.
As in Figure 5A, SIM IF of NPHP3 (red, AF568 secondary antibody) and GFP-INVS (green, detected with anti-GFP antibody, AF488 secondary antibody) in NEK8-KO cells stably expressing GFP-INVS. Cilia were stained with anti-AcTub (blue, AF647 secondary antibody) to mark the axoneme. 21 GFP-INVS-positive cilia are shown. Merged images of all three markers are shown in the top row. In the bottom row the channels are shifted relative to the merge to show each channel individually: left to right: AcTub, GFP-INVS, and NPHP3. "ID no." is the identification number for an individual cilium in our SIM dataset. #1503 contains two cilia. Arrows indicate cilia in which the INVc extended to the cilium tip. In these cases NPHP3 was considered to be localized in the INVc (Figure 5C).

Supplemental Figure S44. SIM reconstructions of NPHP3 in NPHP3-KO cells expressing GFP-INVS.
SIM IF of NPHP3 (red, AF568 secondary antibody) and GFP-INVS (green, detected with anti-GFP antibody, AF488 secondary antibody) in NPHP3-KO cells stably expressing GFP-INVS. Cilia were stained with anti-AcTub (blue, AF647 secondary antibody) to mark the axoneme. 12 GFP-INVS-positive cilia are shown. Merged images of all three markers are shown in the top row. In the bottom row the channels are shifted relative to the merge to show each channel individually: left to right: AcTub, GFP-INVS, and NPHP3. "ID no." is the identification number for an individual cilium in our SIM dataset.

Supplemental Figure S45. Additional SIM reconstructions of ANKS6 in WT cells expressing GFP-INVS.
As in Supplemental Figure S35B, SIM IF of ANKS6 (red, AF568 secondary antibody) and GFP-INVS (green, detected with anti-GFP antibody, AF488 secondary antibody) in WT RPE1 cells stably expressing GFP-INVS. Cilia were stained with anti-AcTub (blue, AF647 secondary antibody) to mark the axoneme. 20 GFP-INVS-positive cilia are shown. Merged images of all three markers are shown in the top row. In the bottom row the channels are shifted relative to the merge to show each channel individually: left to right: AcTub, GFP-INVS, and ANKS6. "ID no." is the identification number for an individual cilium in our SIM dataset.

Supplemental Figure S46. Additional SIM reconstructions of ANKS6 in INVS-KO cells rescued with GFP-INVS.

As in Supplemental Figure S35C, SIM IF of ANKS6 (red, AF568 secondary antibody) and GFP-INVS (green, detected with anti-GFP antibody, AF488 secondary antibody) in INVS-KO cells rescued by stably expressing GFP-INVS. Cilia were stained with anti-AcTub (blue, AF647 secondary antibody) to mark the axoneme. 20 GFP-INVS-positive cilia are shown. Merged images of all three markers are shown in the top row. In the bottom row the channels are shifted relative to the merge to show each channel individually: left to right: AcTub, GFP-INVS, and ANKS6. "ID no." is the identification number for an individual cilium in our SIM dataset.

Supplemental Figure S47. SIM reconstructions of ANKS6 in ANKS6-KO cells expressing GFP-INVS.
SIM IF of ANKS6 (red, AF568 secondary antibody) and GFP-INVS (green, detected with anti-GFP antibody, AF488 secondary antibody) in ANKS6-KO cells stably expressing GFP-INVS. Cilia were stained with anti-AcTub (blue, AF647 secondary antibody) to mark the axoneme. 12 GFP-INVS-positive cilia are shown. Merged images of all three markers are shown in the top row. In the bottom row the channels are shifted relative to the merge to show each channel individually: left to right: AcTub, GFP-INVS, and ANKS6. "ID no." is the identification number for an individual cilium in our SIM dataset.

Supplemental Figure S48. Additional SIM reconstructions of ANKS6 in NEK8-KO cells expressing GFP-INVS.
As in Supplemental Figure S35D, SIM IF of ANKS6 (red, AF568 secondary antibody) and GFP-INVS (green, detected with anti-GFP antibody, AF488 secondary antibody) in NEK8-KO cells stably expressing GFP-INVS. Cilia were stained with anti-AcTub (blue, AF647 secondary antibody) to mark the axoneme. 20 GFP-INVS-positive cilia are shown. Merged images of all three markers are shown in the top row. In the bottom row the channels are shifted relative to the merge to show each channel individually: left to right: AcTub, GFP-INVS, and ANKS6. "ID no." is the identification number for an individual cilium in our SIM dataset.

Supplemental Figure S49. Additional SIM reconstructions of ANKS6 in NPHP3-KO cells expressing GFP-INVS.
As in Supplemental Figure S35E, SIM IF of ANKS6 (red, AF568 secondary antibody) and GFP-INVS (green, detected with anti-GFP antibody, AF488 secondary antibody) in NPHP3-KO cells stably expressing GFP-INVS. Cilia were stained with anti-AcTub (blue, AF647 secondary antibody) to mark the axoneme. 20 GFP-INVS-positive cilia are shown. Merged images of all three markers are shown in the top row. In the bottom row the channels are shifted relative to the merge to show each channel individually: left to right: AcTub, GFP-INVS, and ANKS6. "ID no." is the identification number for an individual cilium in our SIM dataset.

Supplemental Figure S50. DLM of ANKS6 INVc localization in NEK8-KO cells rescued with kinase dead (K33M) or JCK GFP-NEK8 alleles.
(A) Schematic illustrating the coloring and relative positioning of fluorescent markers in the images in B and C. (B) DLM IF of ANKS6 (red) in NEK8-KO cell lines stably expressing GFP-mNEK8 (WT), GFP-mNEK8-K33M, and GFP-mNEK8-JCK. GFP-NEK8 is detected by native GFP fluorescence. Acetylated tubulin marks the axoneme. Images on the left (B-C) show only the ciliary marker (blue, AcTub) and ANKS6 (red) as GFP-NEK8 has non-ciliary localization in some fields which can obscure cilia in these figures. ANKS6 with GFP-NEK8 (green) in the second set of panels (right, B'-C'). (C) DLM IF of ANKS6 (red) in NEK8-KO cells stably

expressing GFP-INVS, to demonstrate that GFP-NEK8 mutants (B) rescue ANKS6 INVc localization in NEK8-KO cells more fully than GFP-INVS. (D) Quantification of ciliary ANKS6 densities for the samples shown in B and C. (E) Quantification of ciliary GFP densities for the samples shown in B and C.

Supplemental Figure S51. NPHP3 INVc localization in NEK8-KO cells rescued with kinase dead (K33M) or JCK GFP-NEK8 alleles.
(A) Schematic illustrating the coloring and relative positioning of fluorescent markers in the images shown in B and C. (B) DLM IF of NPHP3 (red) in NEK8-KO cell lines stably expressing GFP-mNEK8 (WT), GFP-mNEK8-K33M, and GFP-mNEK8-JCK. GFP-NEK8 detected by native GFP fluorescence. Acetylated tubulin marks the axoneme. B) Images on the left (B-C) show only the ciliary marker (blue, AcTub) and NPHP3 (red) as GFP-NEK8 has non-ciliary localization in some fields which can obscure cilia in these figures. NPHP3 with GFP-NEK8 (green) are shown in the second set of panels (right, B'-C'). (C) DLM IF of NPHP3 (red) in NEK8-KO cells stably expressing GFP-INVS, to demonstrate that GFP-NEK8 mutants (B) rescue NPHP3 INVc localization in NEK8-KO cells more fully than GFP-INVS. (D) Quantification of ciliary NPHP3 densities for the samples in B and C. (E) Quantification of cilium length for the samples in B and C and Supplemental Figure S50B-C compared with WT RPE1 cells. Median lengths were: WT, 4.0 µm (Stdev 1.6 µm, n = 482); NEK8-KO, 3.7 µm (Stdev 1.5 µm, n = 363); NEK8-KO GFP-NEK8-WT rescue, 4.7 µm (Stdev 1.4 µm, n = 320); NEK8-KO GFP-NEK8-K33M rescue, 4.5 µm (Stdev 1.3 µm, n = 358); NEK8-KO GFP-NEK8-JCK rescue, 4.6 µm (Stdev 1.4 µm, n = 362); NEK8-KO GFP-INVS, 4.2 µm (Stdev 1.7 µm, n = 531). Cilia in the renal tubules of LPK (NEK8 mutant) rats (Mccooke et al. 2012) and JCK mice (Smith et al. 2006; Sohara et al. 2008) with cystic kidneys, and yet the JCK mutation does not affect cilia length in RPE1 cells.

Supplemental Figure S52. SIM reconstructions of the INVc in NEK8-KO cells rescued with kinase dead (K33M) or JCK GFP-NEK8 alleles.
(A) SIM IF of ANKS6 or NPHP3 (red, AF568 secondary) in NEK8-KO cell lines stably expressing GFP-mNEK8 (WT), GFP-mNEK8-K33M, and GFP-mNEK8-JCK. GFP-NEK8 detected by indirect IF with anti-GFP primary antibody (green, AF488 secondary). AcTub (blue, AF647 secondary) marks the axoneme. Additional images are shown for each sample in Supplemental Figures S53-S58. (B) Schematic illustrating the coloring and relative positioning of fluorescent markers in the SIM reconstructions in A. (C) Quantification of the percent GFP-positive cilia with ANKS6 or NPHP3 properly localized in the INVc measured by SIM.

Supplemental Figure S53. Additional SIM reconstructions of ANKS6 in NEK8-KO rescued with GFP-NEK8-WT.
As in Supplemental Figure S52, SIM IF of ANKS6 (red, AF568 secondary antibody) and GFP-NEK8 (green, detected with anti-GFP antibody, AF488 secondary antibody) in NEK8-KO cells rescued by stably expressing WT GFP-NEK8. Cilia were stained with anti-AcTub (blue, AF647 secondary antibody) to mark the axoneme. 20 GFP-NEK8-positive cilia are shown. Merged images of all three markers are shown in the top row. In the bottom row the channels are shifted relative to the merge to show each channel individually: left to right: AcTub, GFP-NEK8, and ANKS6. "ID no." is the identification number for an individual cilium in our SIM dataset.

Supplemental Figure S54. Additional SIM reconstructions of ANKS6 in NEK8-KO rescued with GFP-NEK8-K33M.
As in Supplemental Figure S52, SIM IF of ANKS6 (red, AF568 secondary antibody) and GFP-NEK8-K33M (green, detected with anti-GFP antibody, AF488 secondary antibody) in NEK8-KO cells rescued by stably expressing the kinase dead GFP-NEK8-K33M allele. Cilia were stained with anti-AcTub (blue, AF647 secondary antibody) to mark the axoneme. 20 GFP-NEK8-positive cilia are shown. Merged images of all three markers are shown in the top row. In the bottom row the channels are shifted relative to the merge to show each channel individually: left to right: AcTub, GFP-NEK8, and ANKS6. "ID no." is the identification number for an individual cilium in our SIM dataset.

Supplemental Figure S55. Additional SIM reconstructions of ANKS6 in NEK8-KO cells rescued with GFP-NEK8-JCK.
As in Supplemental Figure S52, SIM IF of ANKS6 (red, AF568 secondary antibody) and GFP-NEK8-G448V (green, detected with anti-GFP antibody, AF488 secondary antibody) in NEK8-KO cells rescued by stably expressing the JCK mutant GFP-NEK8-G448V allele. Cilia were stained with anti-AcTub (blue, AF647 secondary antibody) to mark the axoneme. 20 GFP-NEK8-positive cilia are shown. Merged images of all three markers are shown in the top row. On the bottom row the channels are shifted relative to the merge to show each channel individually: left to right: AcTub, GFP-NEK8, and ANKS6. "ID no." is the identification number for an individual cilium in our SIM dataset.

Supplemental Figure S56. Additional SIM reconstructions of NPHP3 in NEK8-KO cells rescued with GFP-NEK8-WT.
As in Supplemental Figure S52, SIM IF of NPHP3 (red, AF568 secondary antibody) and GFP-NEK8 (green, detected with anti-GFP antibody, AF488 secondary antibody) in NEK8-KO cells rescued by stably expressing WT GFP-NEK8. Cilia were stained with anti-AcTub (blue, AF647 secondary antibody) to mark the axoneme. 20 GFP-NEK8-positive cilia are shown. Merged images of all three markers are shown in the top row. In the bottom row the channels are shifted relative to the merge to show each channel individually: left to right: AcTub, GFP-NEK8, and NPHP3. "ID no." is the identification number for an individual cilium in our SIM dataset.

Supplemental Figure S57. Additional SIM reconstructions of NPHP3 in NEK8-KO cells rescued with GFP-NEK8-K33M.
As in Supplemental Figure S52, SIM IF of NPHP3 (red, AF568 secondary antibody) and GFP-NEK8-K33M (green, detected with anti-GFP antibody, AF488 secondary antibody) in NEK8-KO cells rescued by stably expressing the kinase dead GFP-NEK8-K33M allele. Cilia were stained with anti-AcTub (blue, AF647 secondary antibody) to mark the axoneme. 20 GFP-NEK8-positive cilia are shown. Merged images of all three markers are shown in the top row. In the bottom row the channels are shifted relative to the merge to show each channel individually: left to right: AcTub, GFP-NEK8, and NPHP3. "ID no." is the identification number for an individual cilium in our SIM dataset.

Supplemental Figure S58. Additional SIM reconstructions of NPHP3 in NEK8-KO cells rescued with GFP-NEK8-JCK.
As in Supplemental Figure S52, SIM IF of NPHP3 (red, AF568 secondary antibody) and GFP-NEK8-G448V (green, detected with anti-GFP antibody, AF488 secondary antibody) in NEK8-

KO cells rescued by stably expressing the JCK mutant GFP-NEK8-G448V allele. Cilia were stained with anti-AcTub (blue, AF647 secondary antibody) to mark the axoneme. 20 GFP-NEK8-positive cilia are shown. Merged images of all three markers are shown in the top row. In the bottom row the channels are shifted relative to the merge to show each channel individually: left to right: AcTub, GFP-NEK8, and NPHP3. "ID no." is the identification number for an individual cilium in our SIM dataset.

Supplemental Figure S59. A fibrilloid structure provides new insights into the observed morphological variation in the INVc.
(A) INVc (green) length is determined by the net length of its fibrilloid substructure. Variation in INVc length could reflect cilium to cilium differences in fibrilloid length or relative positioning to form either elongated or compact structures. Axoneme shown in magenta. (B) INVc asymmetry observed in some SIM reconstructions of the INVc could be caused by the non-uniform distribution of fibrilloids around the axoneme. A hypothetical INVc (green) composed of 2 fibrilloids (medium-low density) is diagrammed here relative to the axoneme (magenta) alongside expected results from imaging such a compartment by 3D SM SR microscopy, by SIM, or by DLM. (C) Observed variations in INVc protein density (top) could be determined by differences in fibrilloid number and packing density (bottom) or (D) the density of INVc proteins within individual fibrilloids. Compartments with higher numbers of fibrilloids would be expected to contain a higher density of the INVc proteins of which the fibrilloids are composed (C). Based on the reconstructions in this study, fibrilloid packing and subfibrilloid density did not vary as much as fibrilloid number. Changes in fibrilloid number are likely the primary driver of variation in INVc density. (D) Possible models of fibrilloid substructure: I. Continuous polymers composed of multiple INVc protein (heteropolymers) or just one self-associating INVc protein (homopolymer), which would most likely be INVS as shown here. II. Discontinuous structures which are actually templated by an unidentified factor upstream of INVc assembly.

Supplemental Figure S1. Workflow for quantitative analysis of cilia and INVcs in RPE1 cells measured by DLM.

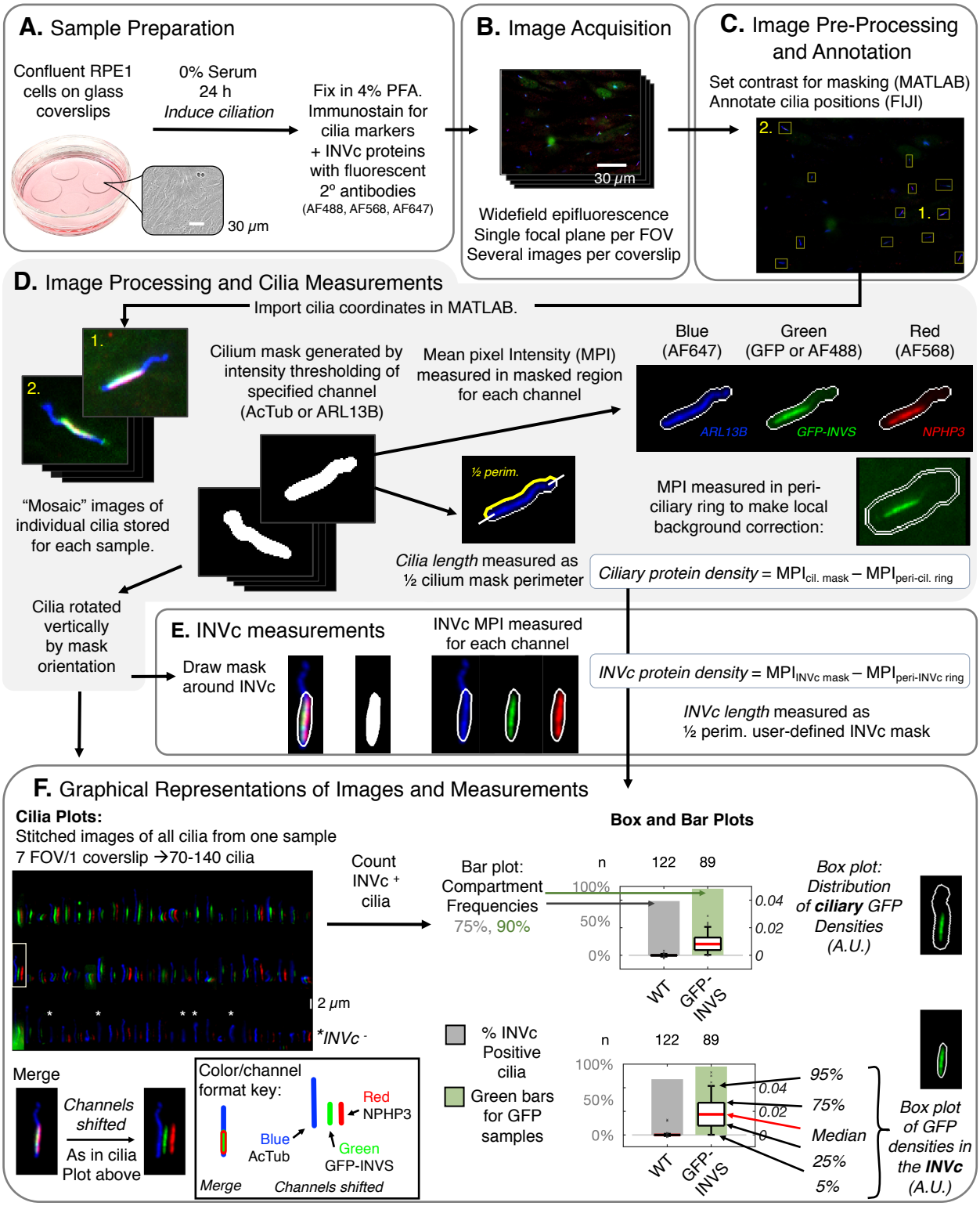

Supplemental Figure S2. Definition of morphological features and measurements of the INVc.

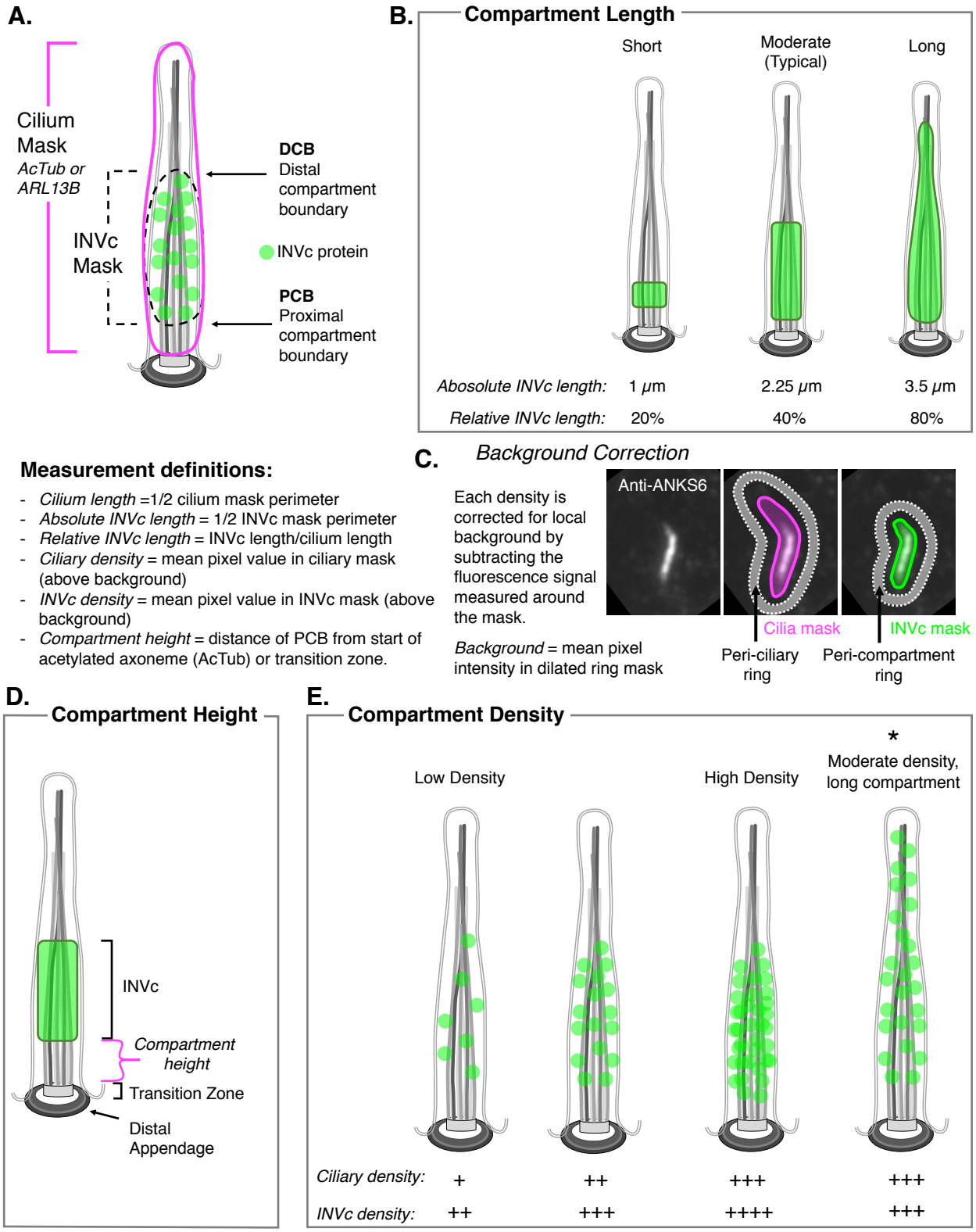

Supplemental Figure S3. DLM images of 100 cilia stained with anti-INVS representing variation in INVc length and density in RPE1 cells; and cilia and sub-compartment masks.

A.

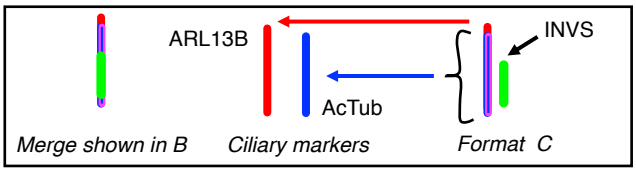

B.

100 cilia sorted by cilium length

DLM

▲ = INVc negative (16/100 cilia)

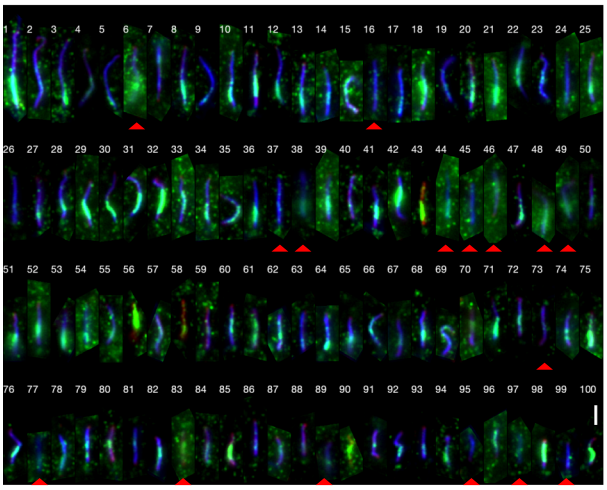

2 μm

C.

INVS (green channel) shifted 600 nm to the right demonstrates relative compartment length compared to cilium length (AcTub and ARL13B)

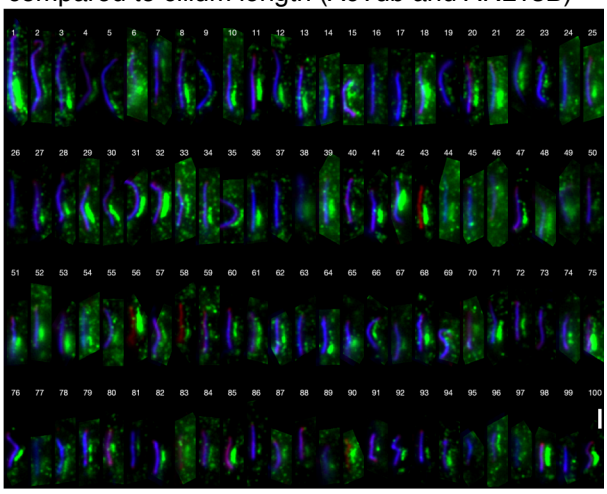

2 μm

D.

Cilium region masked by thresholding ciliary markers AcTub and ARL13B (sum of red and blue channels)

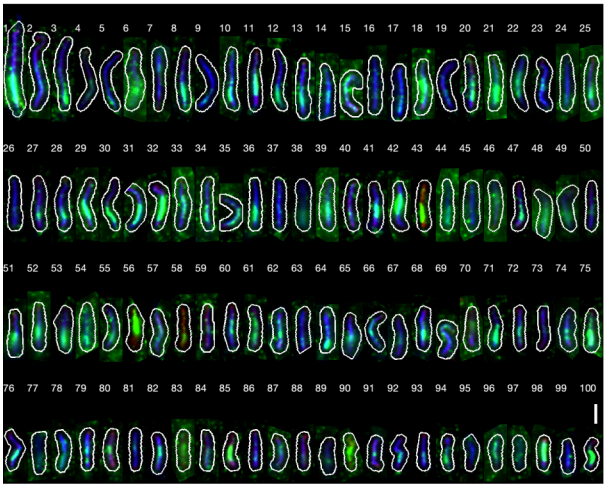

2 μm

E.

Sub-compartment region (INVc) masked by user defined INVS positive region (green channel)

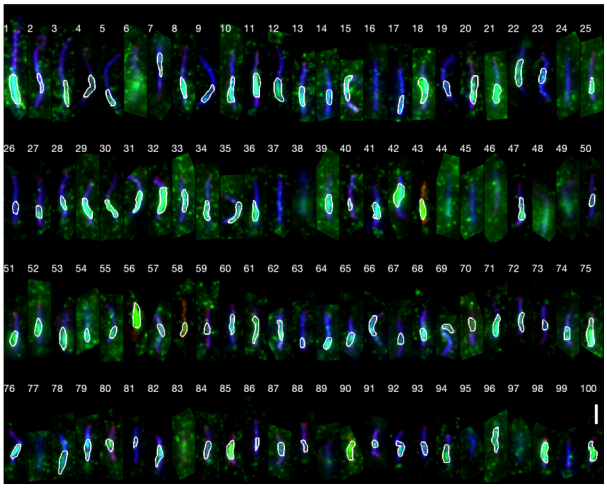

2 μm

Supplemental Figure S4. Localization of GFP-pINVc expressed in RPE1 cells.

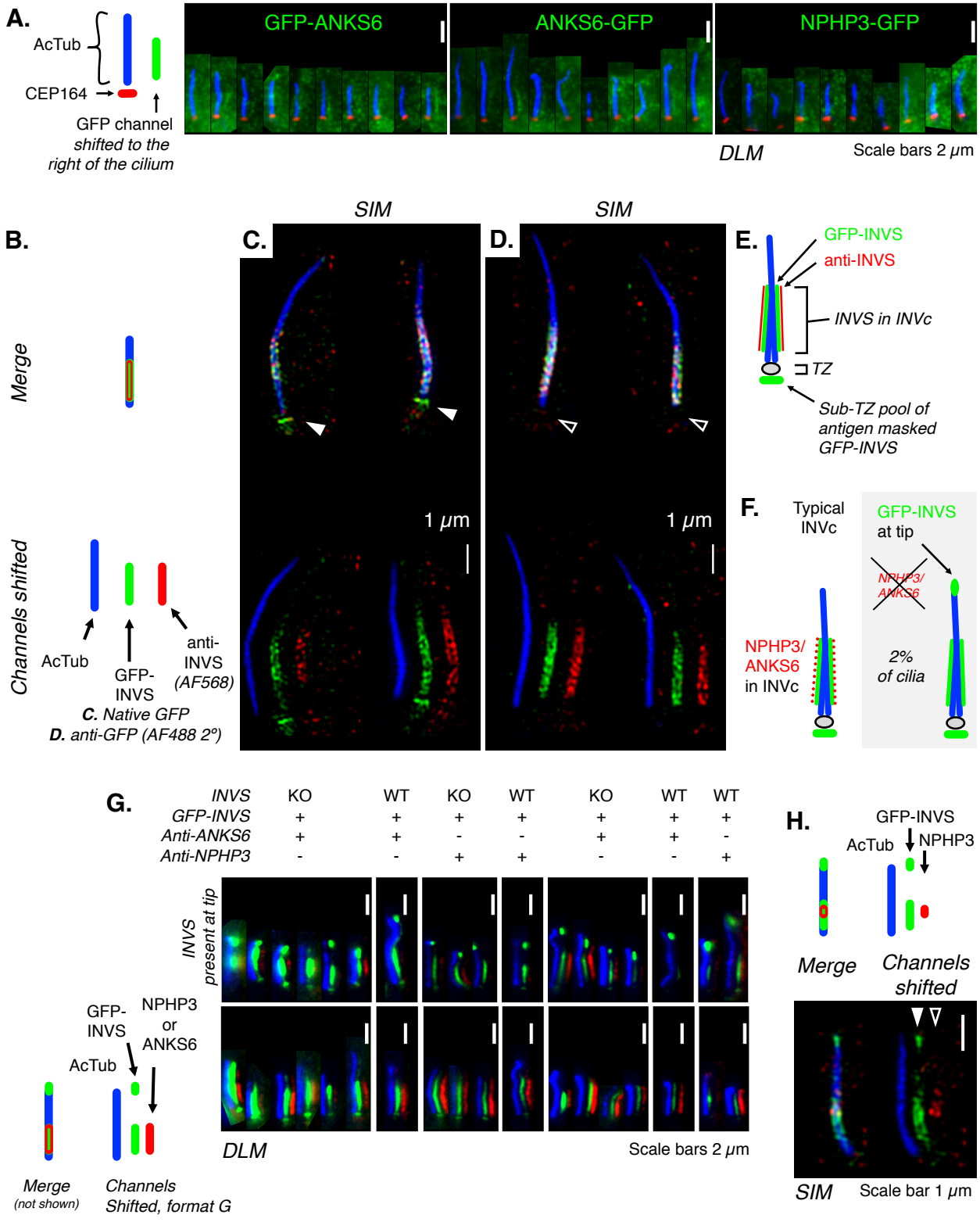

Supplemental Figure S5. INVc length does not correlate with cilium length or ciliary pocket depth.

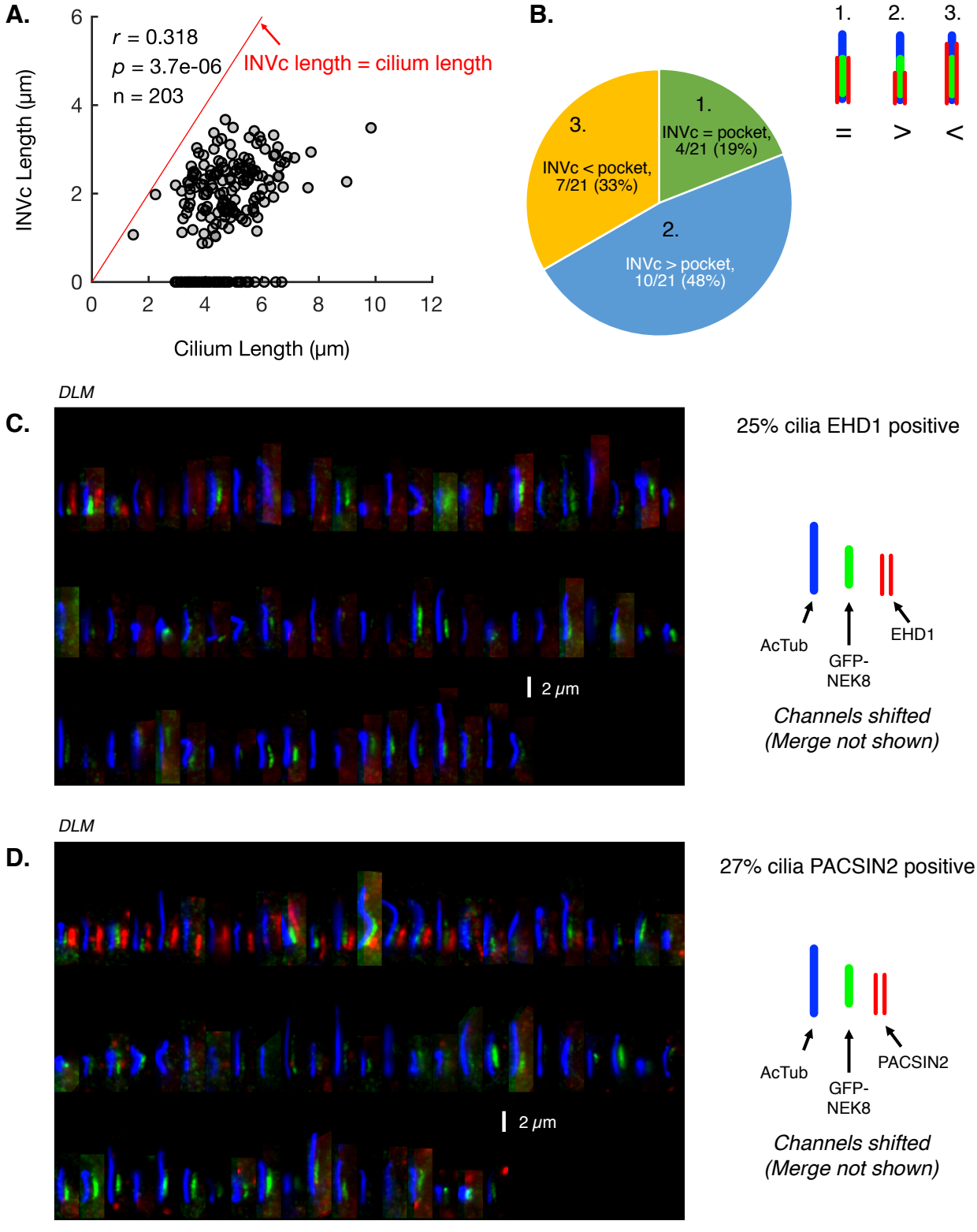

Supplemental Figure S6. SIM of the INVc and ciliary pocket markers.

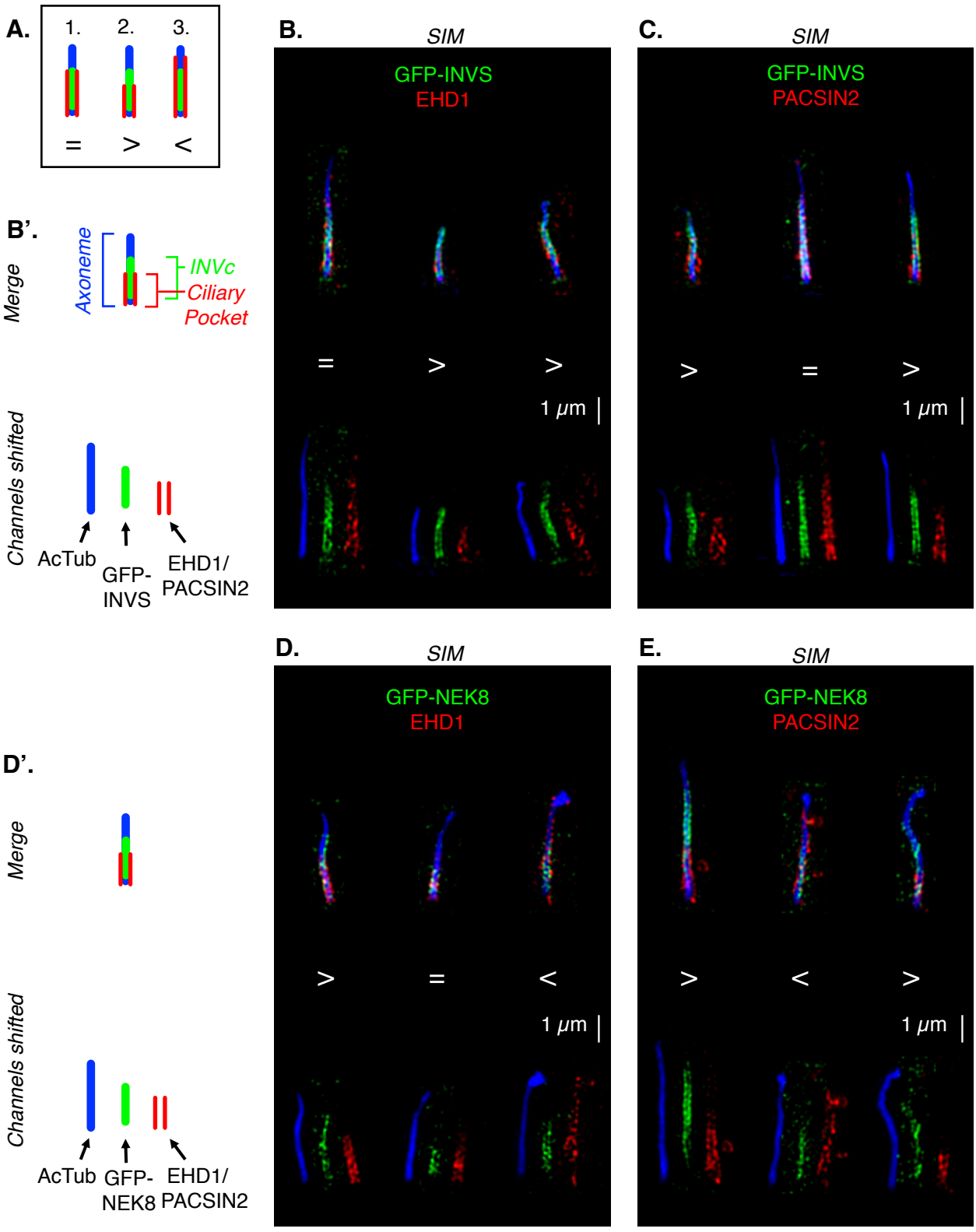

Supplemental Figure S7. The length of the INVc is not correlated with the length of the polyglutamylated region of the axoneme.

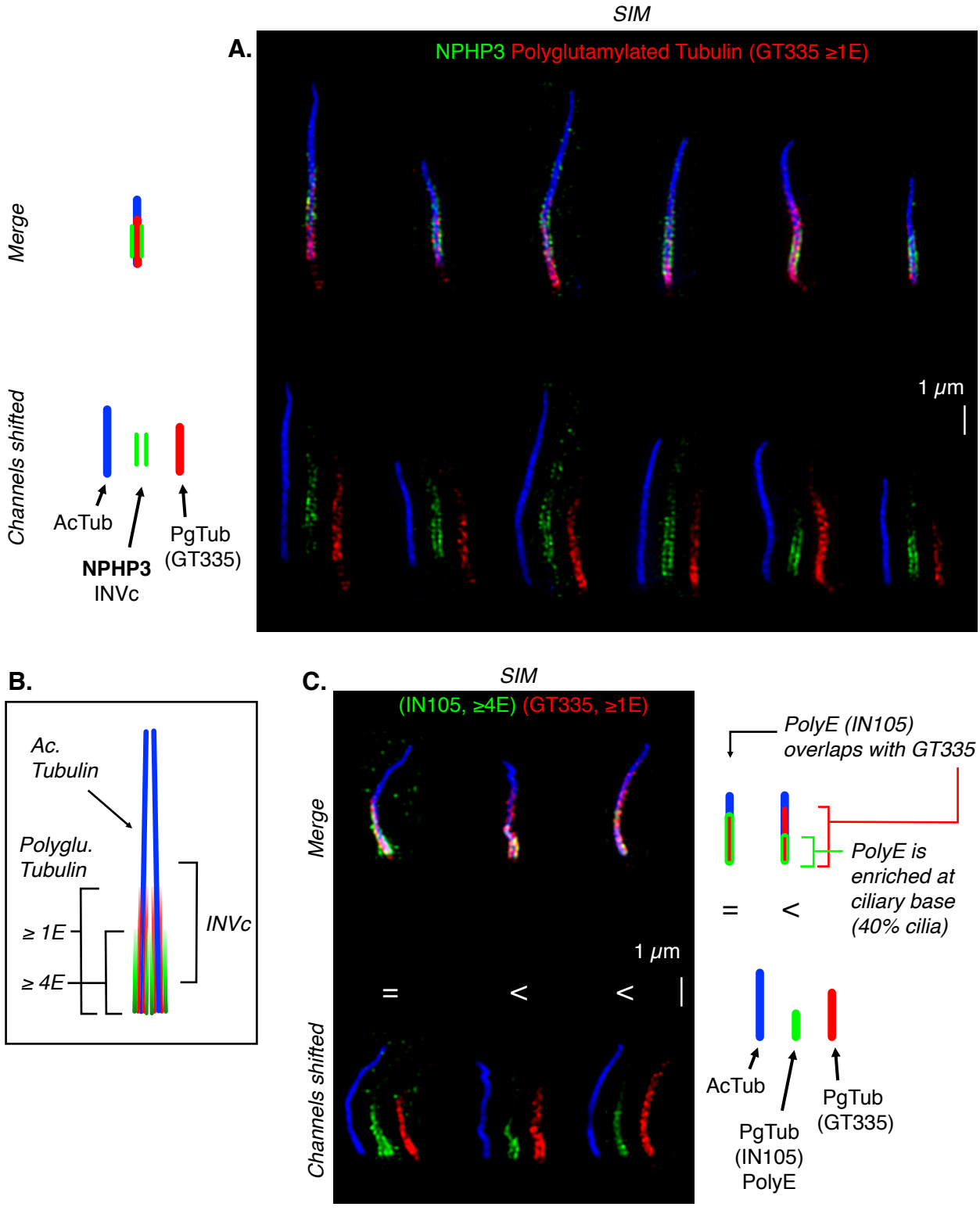

Supplemental Figure S8. The INVc does not start directly above the transition zone (TZ).

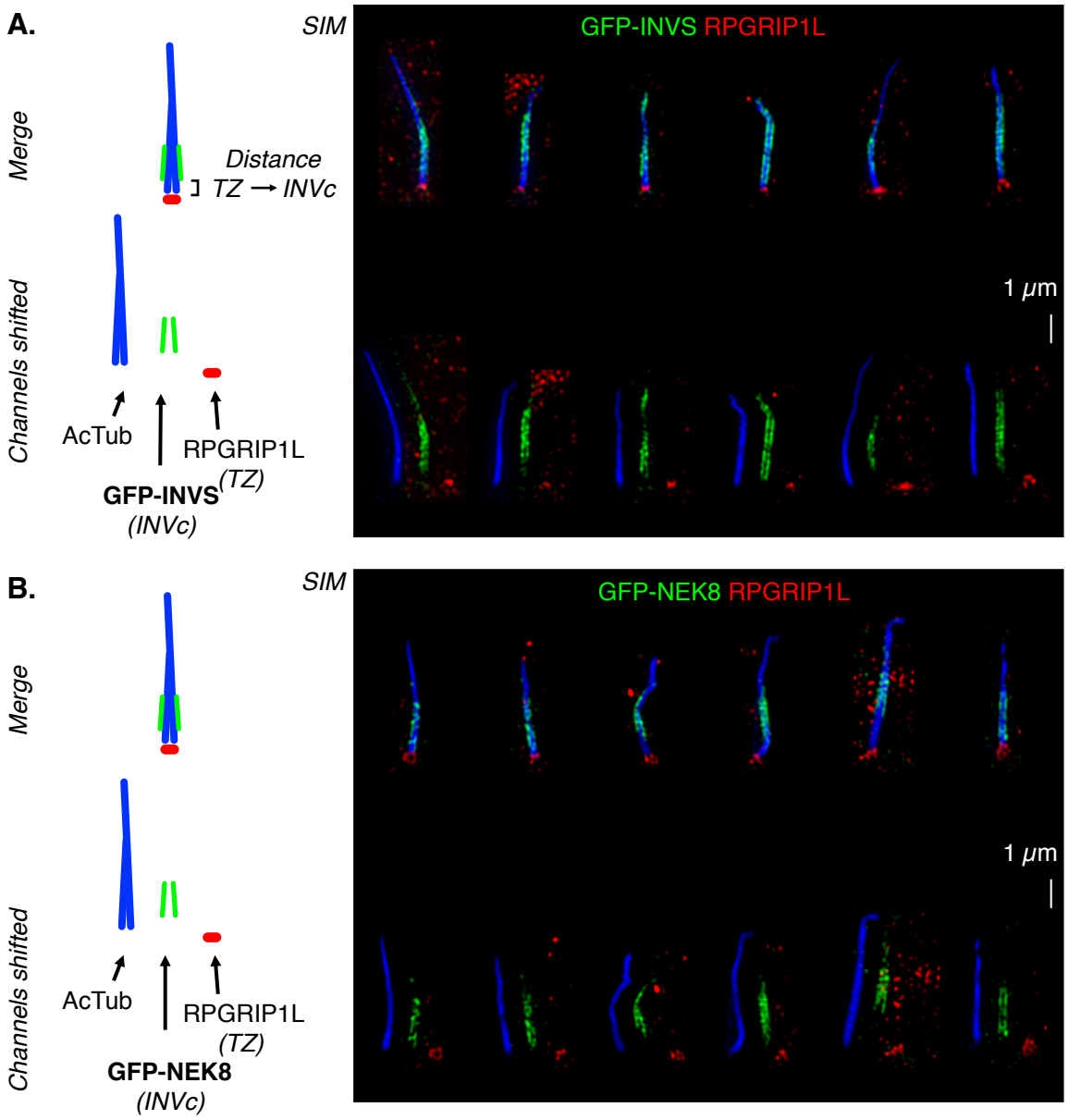

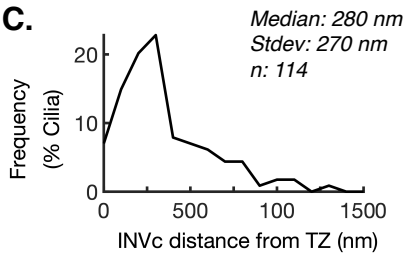

D.

(SIM) Distances μm	(a)	(b) Cilium length	(a)/(b)	(c)	(d)
Median	2.4	4.5	55%	0.280	1.5
Interquartile range	2-2.8	3.6-5	48-65%	0.160-0.490	1-2
Range	1 3.6	1-6.4	30-100%	0-1.2	0-3.6

(e) Compartment diameter: 280 nm (SIM); ~200 nm (SM SR)
SIM: 114 cilia, SM SR: 23

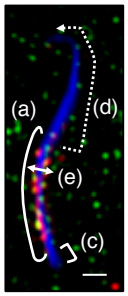

Supplemental Figure S9. Co-localization of the INVc with IFT.

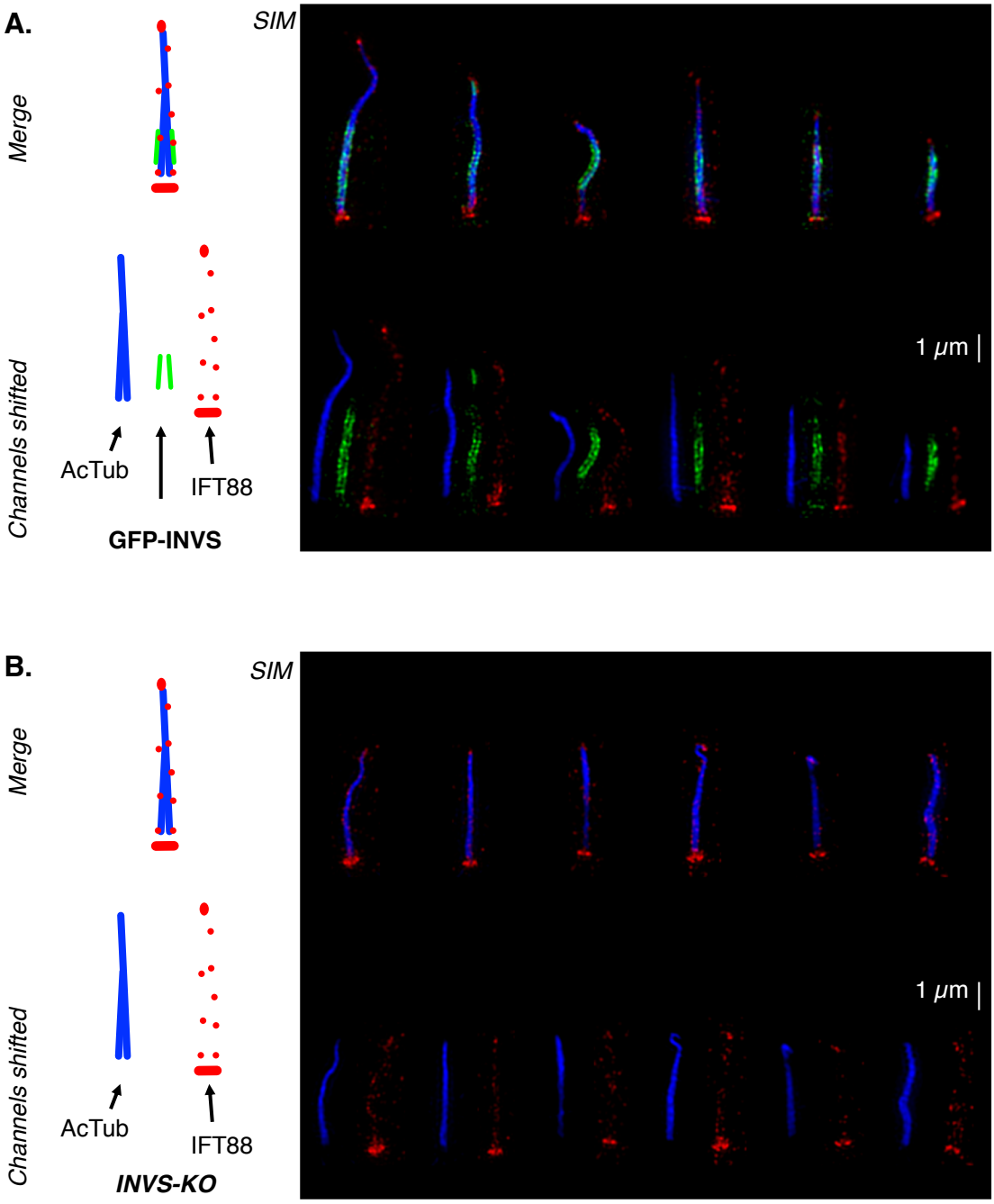

Supplemental Figure S10. Co-localization of the INVc with ciliary membrane proteins.

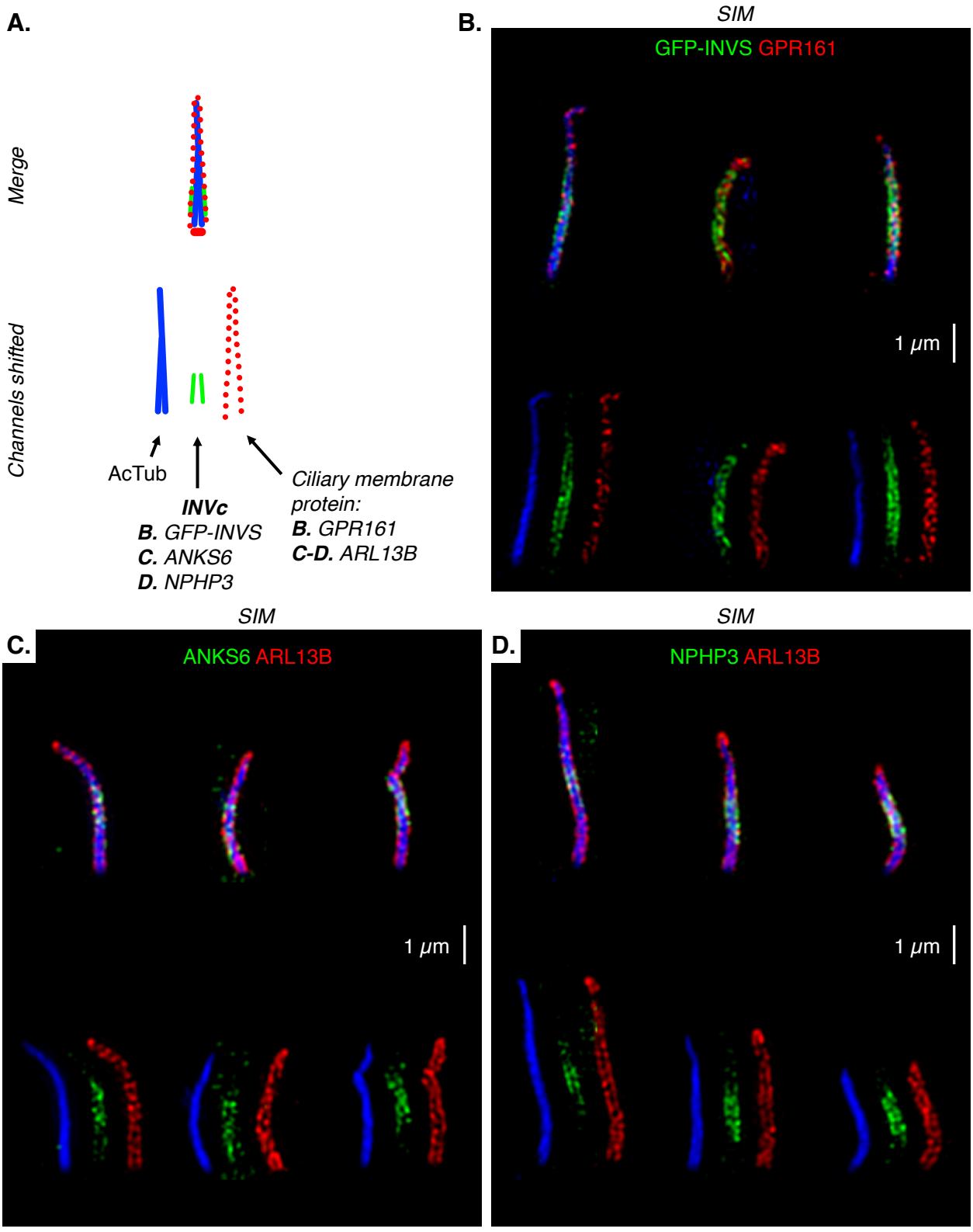

Supplemental Figure S11. INVc length and density in INVcs containing endogenous INVS and GFP-INVS.

A.

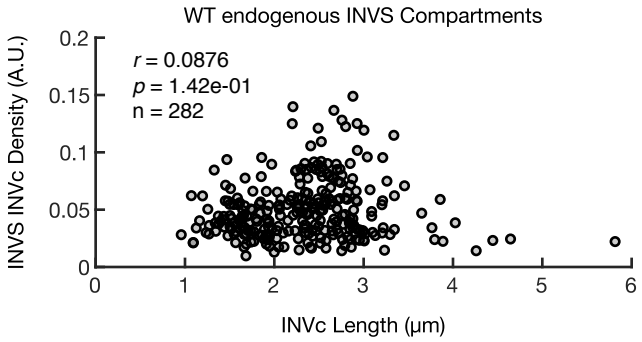

B.

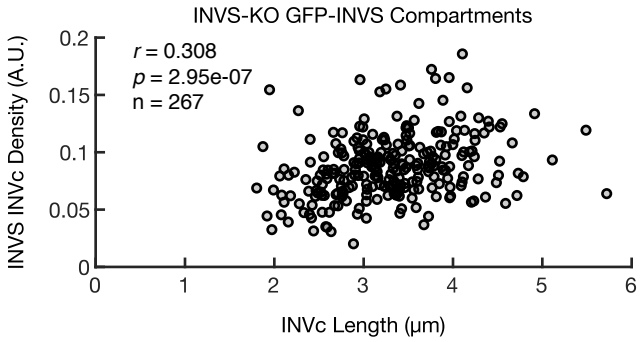

C.

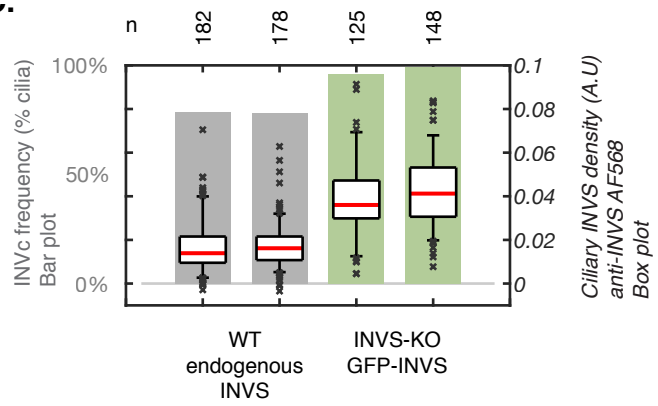

Supplemental Figure S12. Additional SIM reconstructions of GFP-NEK8 and INVS in WT cells.

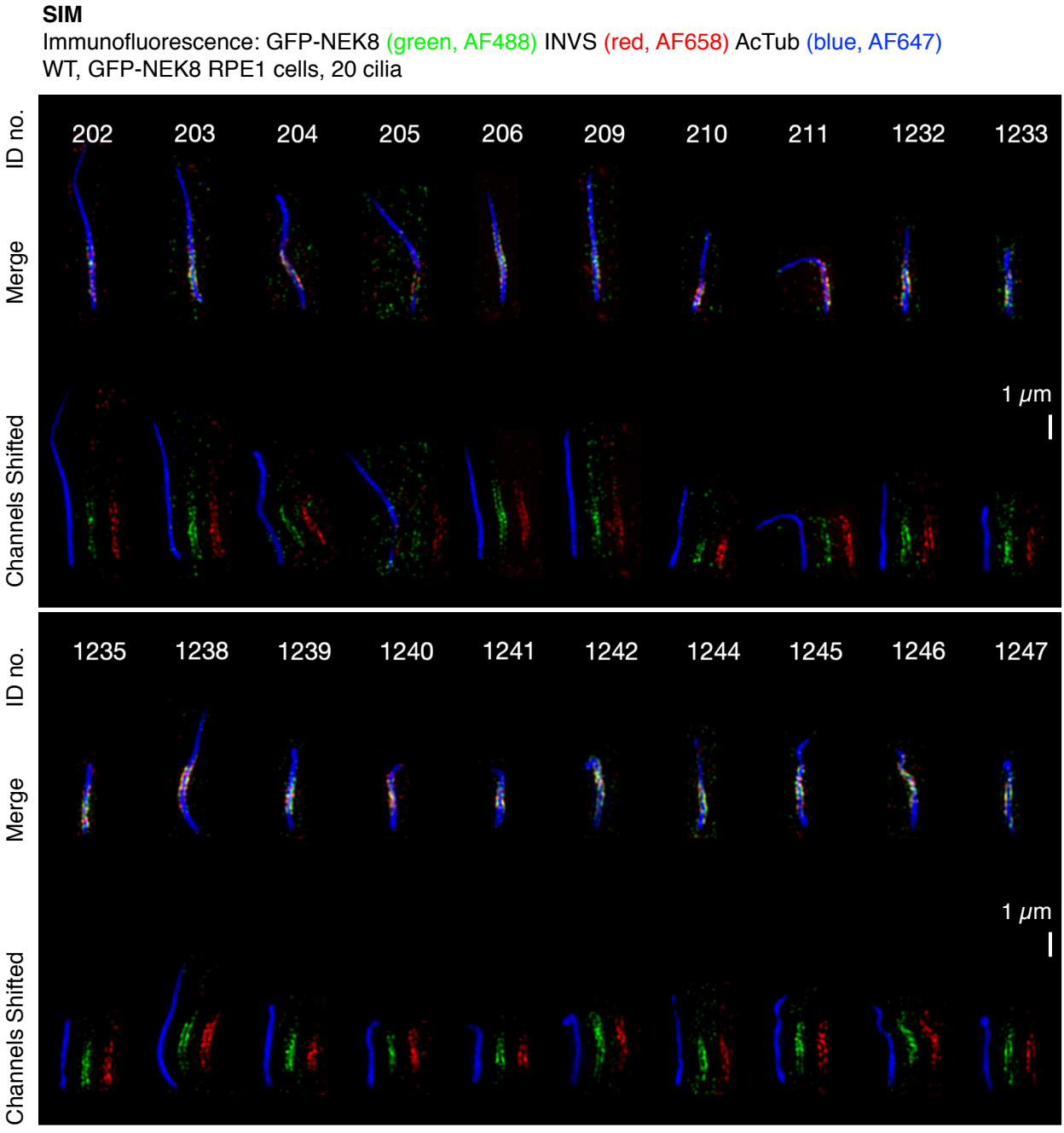

Supplemental Figure S13. Additional SIM reconstructions of GFP-NEK8 and ANKS6 in WT cells.

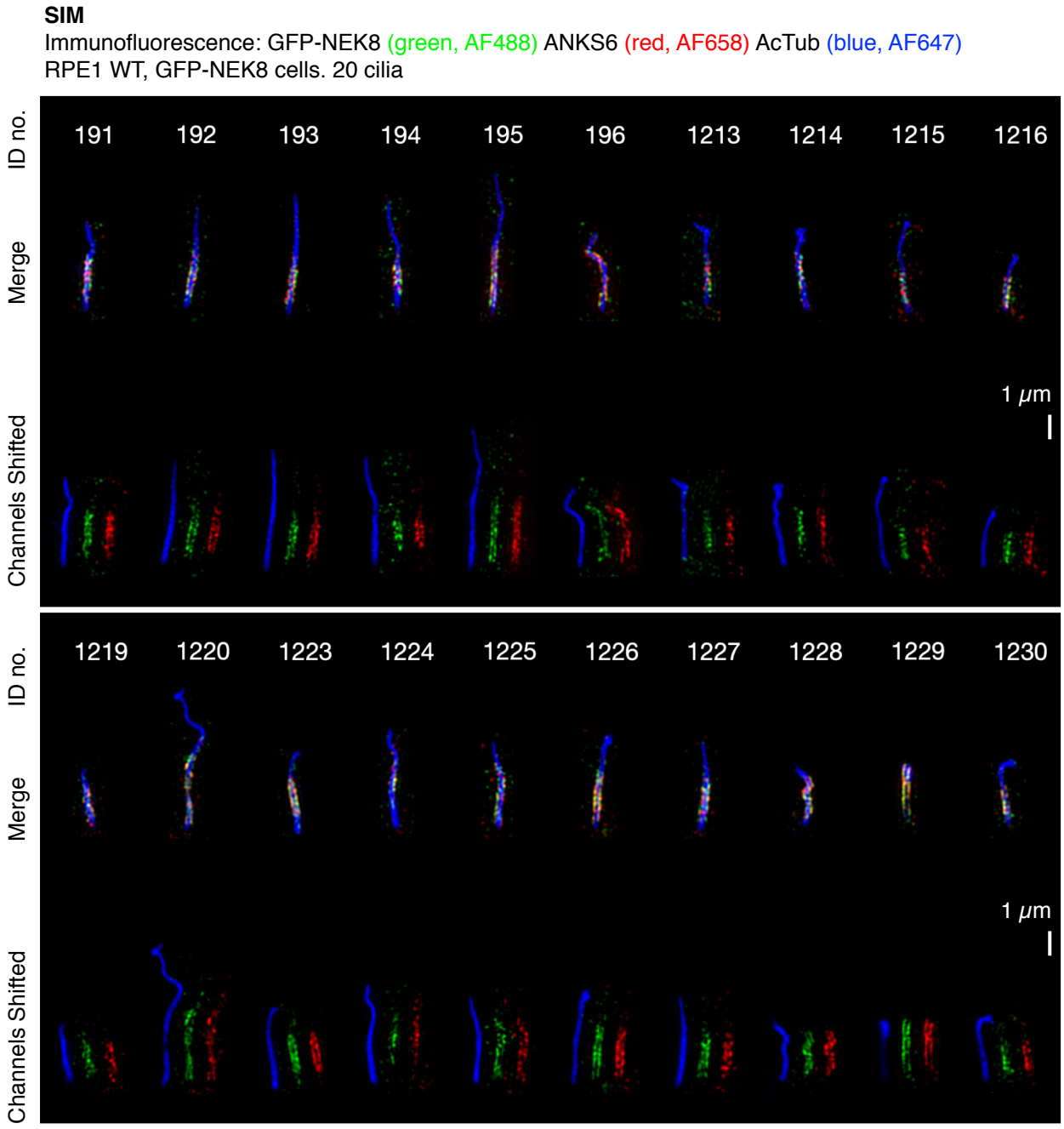

Supplemental Figure S14. Additional SIM reconstructions of GFP-NEK8 and NPHP3 in WT cells.

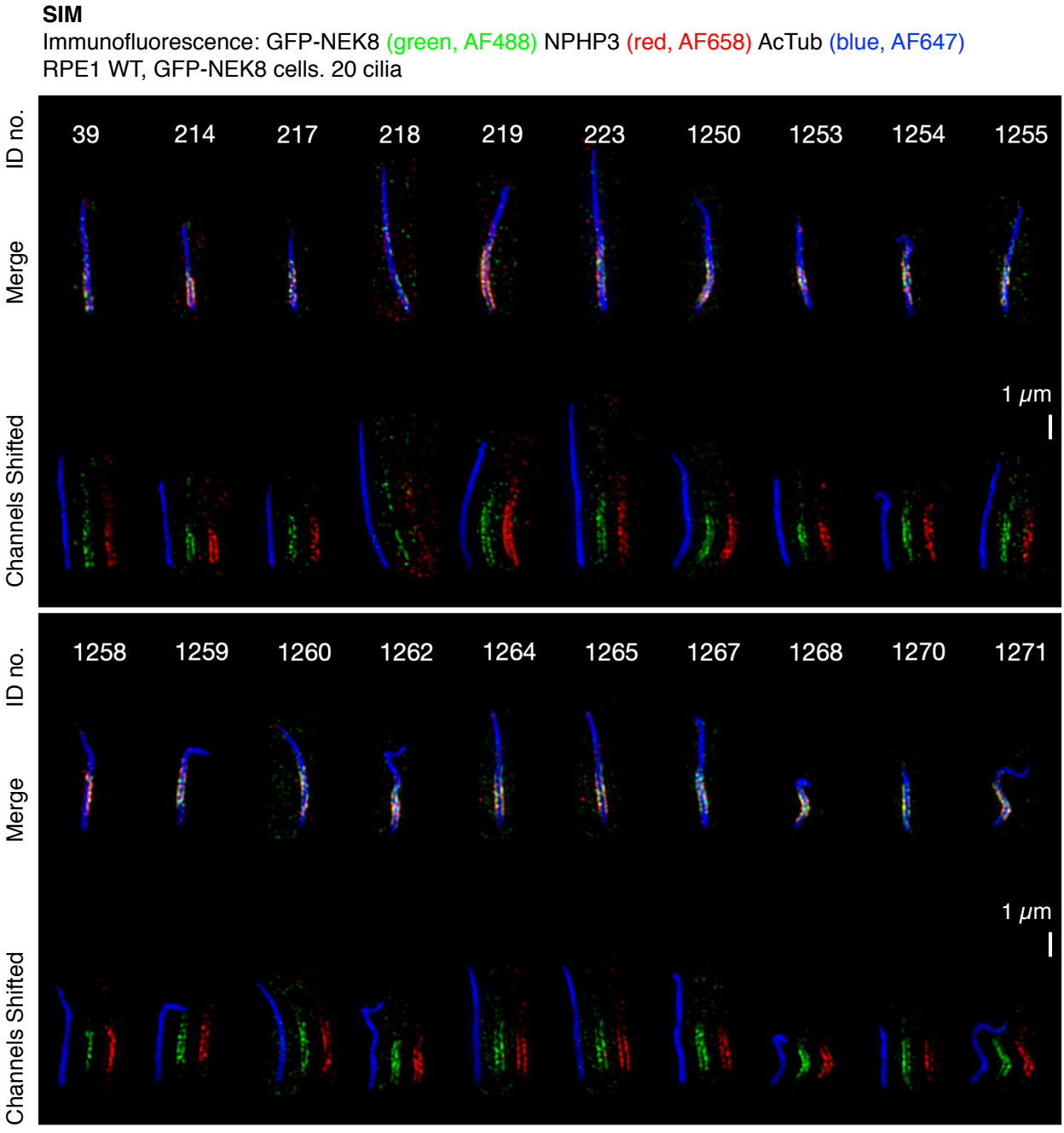

Supplemental Figure S15. Expected and observed geometries of ciliary proteins measured by SIM.

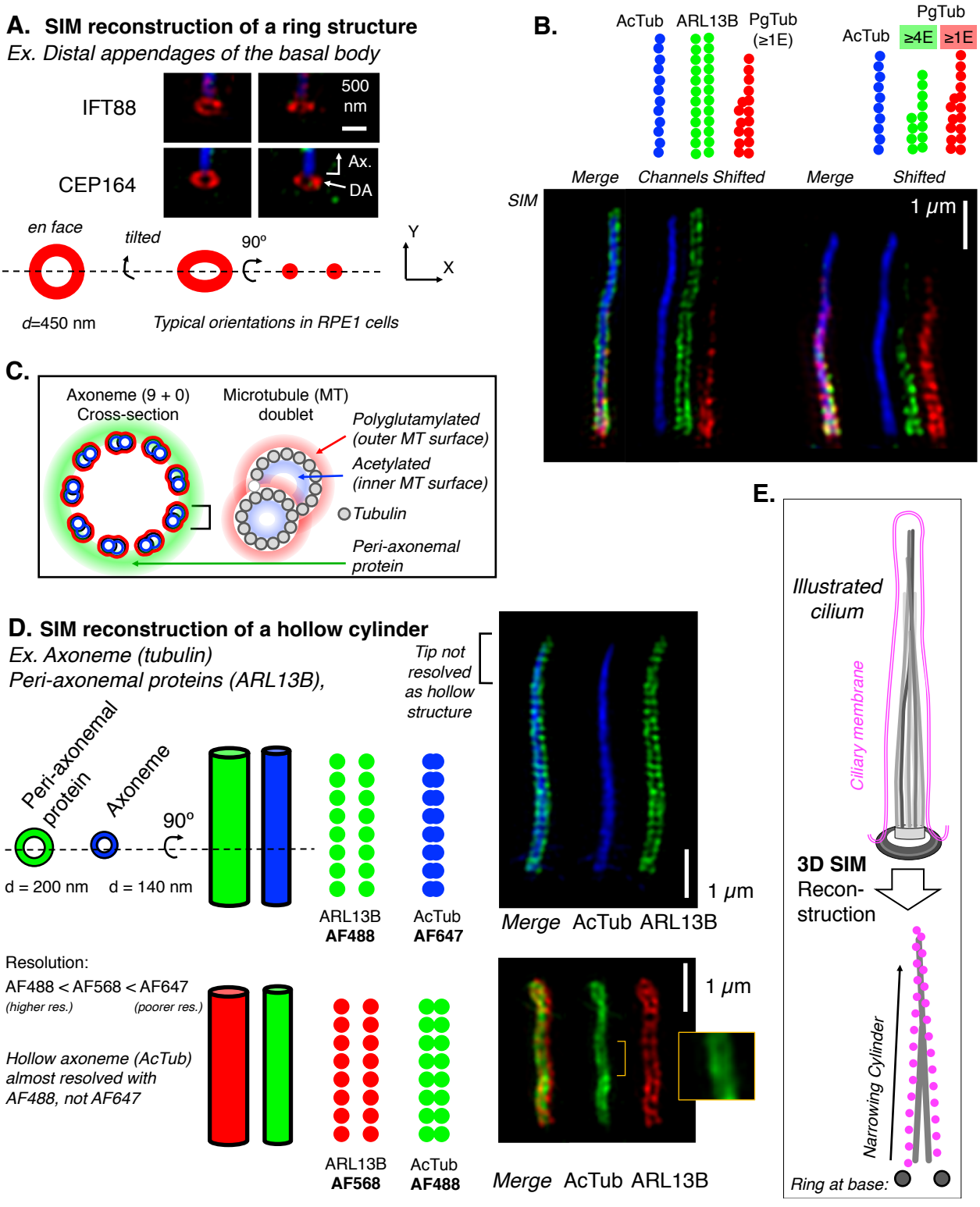

Supplemental Figure S16. The INVc is asymmetric in some cilia measured by SIM.

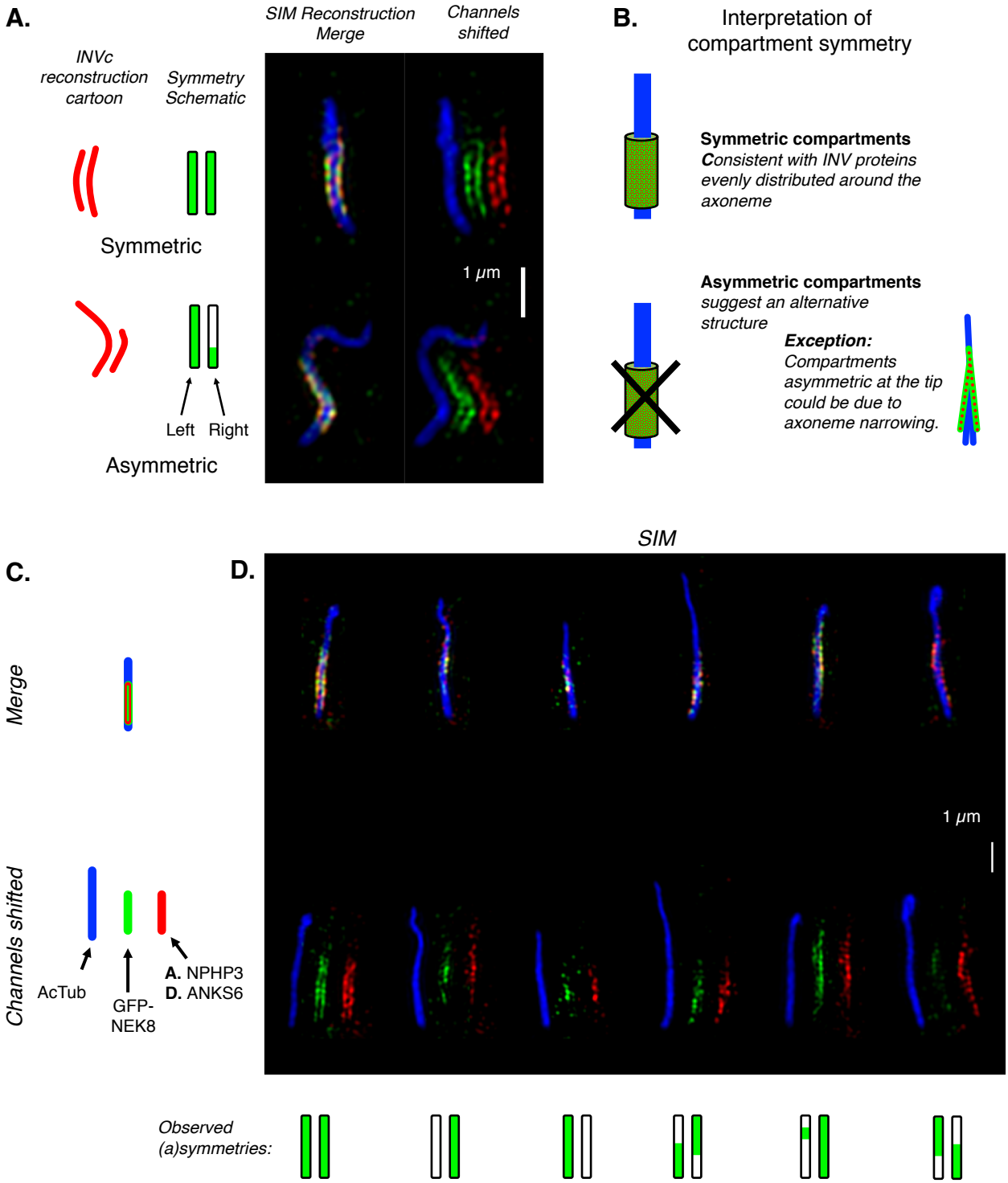

Supplemental Figure S17. Asymmetries are more likely to be detected by SIM in low density compartments.

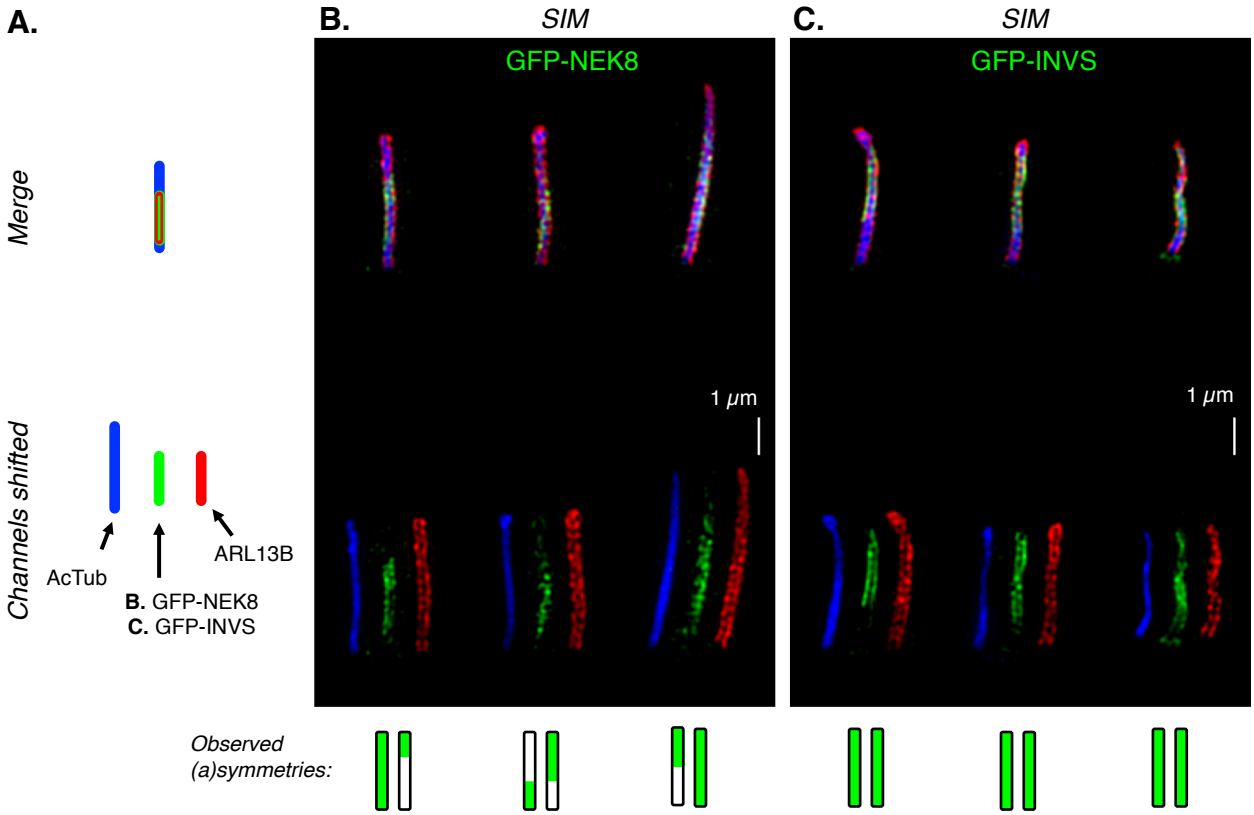

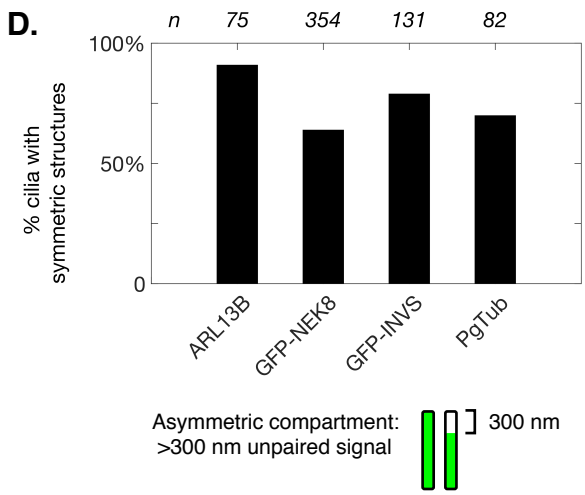

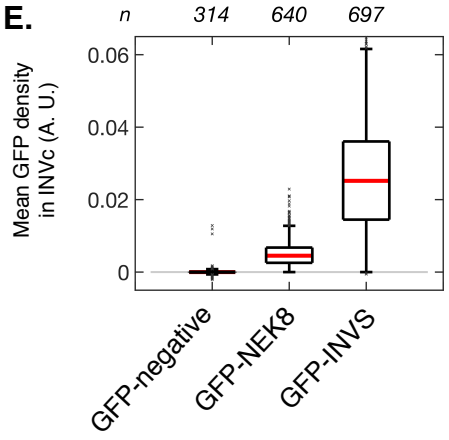

Supplemental Figure S18. 3D SM SR reconstruction statistics for two-color NPHP3 and AcTub and single-color ARL13B experiments.

A.

NPHP3
Two-Color
AF647

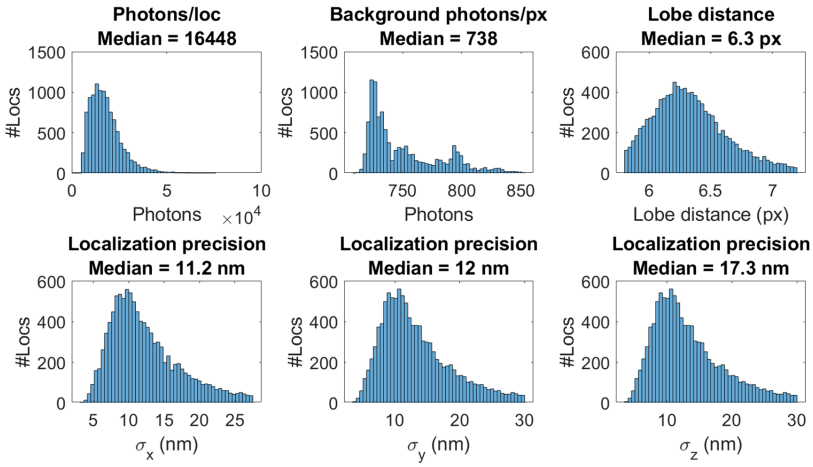

B.

AcTub
Two-Color
CF568

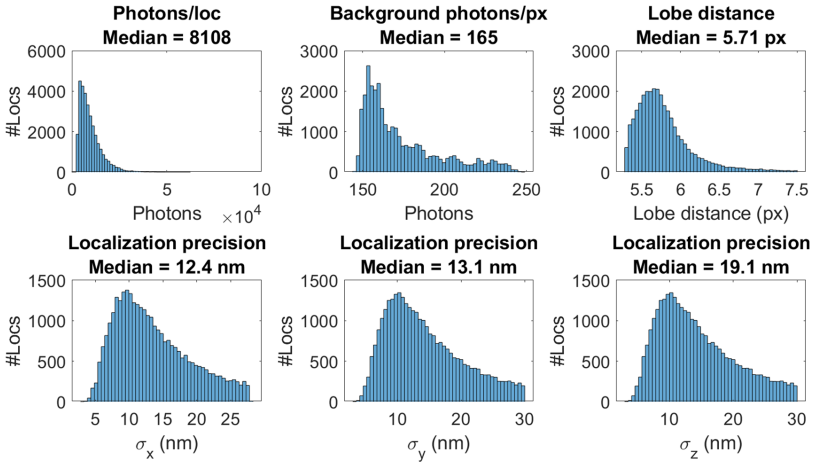

C.

ARL13B
Single-Color
AF647

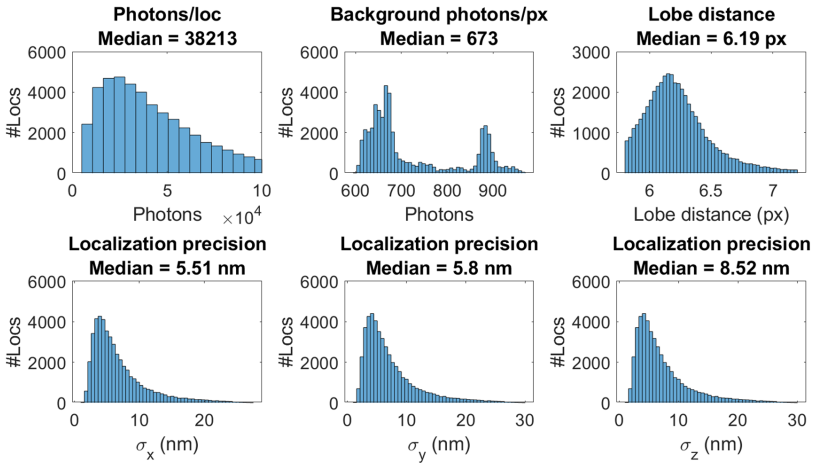

Supplemental Figure S19. 3D SM SR reconstruction statistics for single-color INVS, ANKS6, and NPHP3 experiments.

A.

INVS
Single-Color
AF647

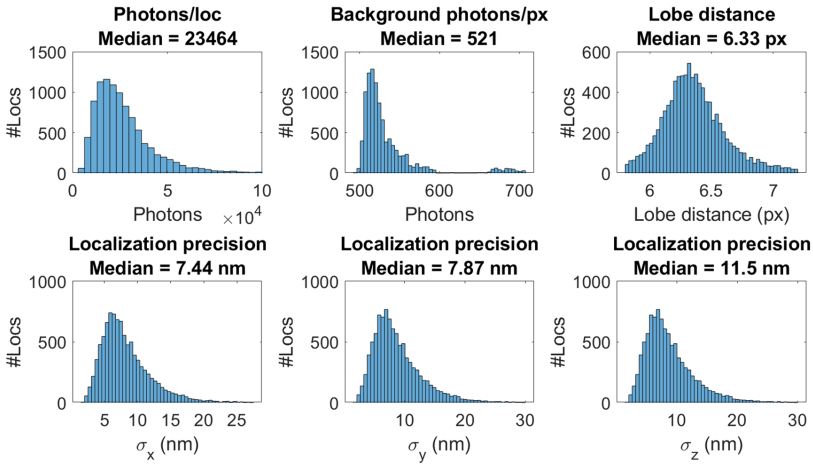

B.

ANKS6
Single-Color
AF647

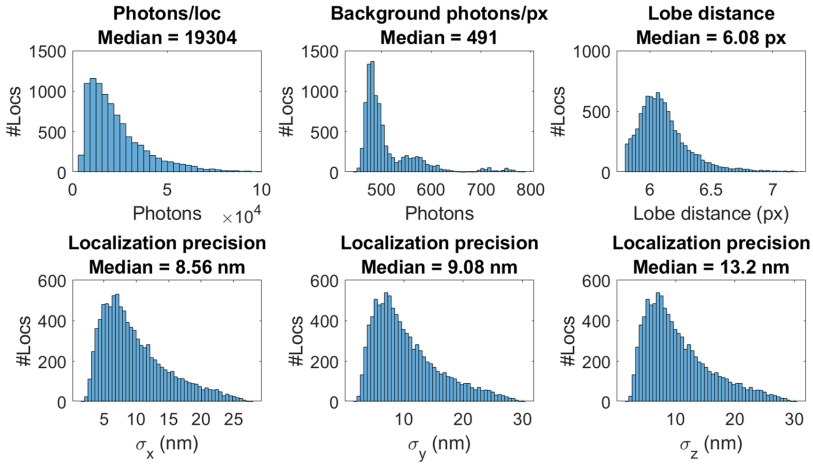

C.

NPHP3
Single-Color
AF647

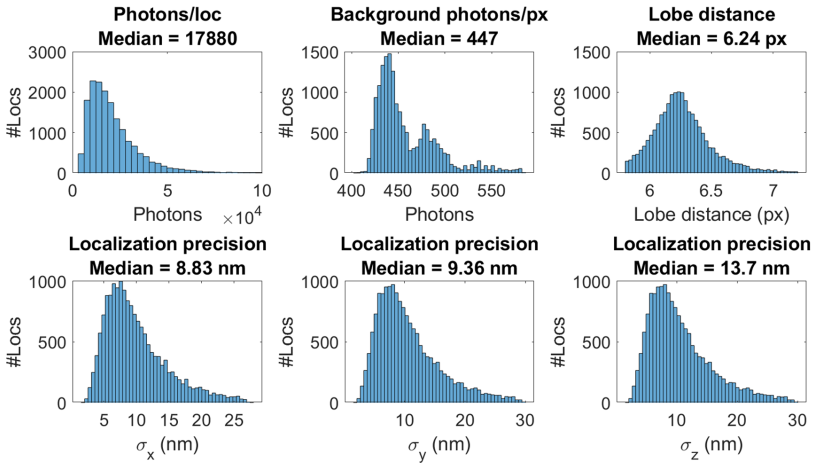

Supplemental Figure S20. DLM images of 3D SM SR labeling controls.

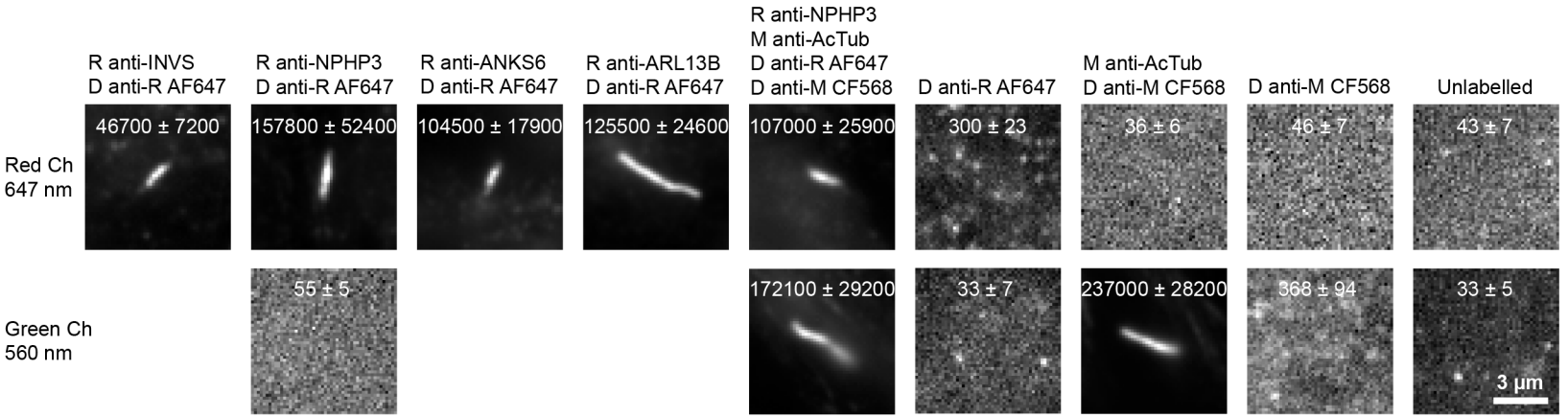

Supplemental Figure S21. Additional 3D SM SR reconstructions and fibrilloid measurements.

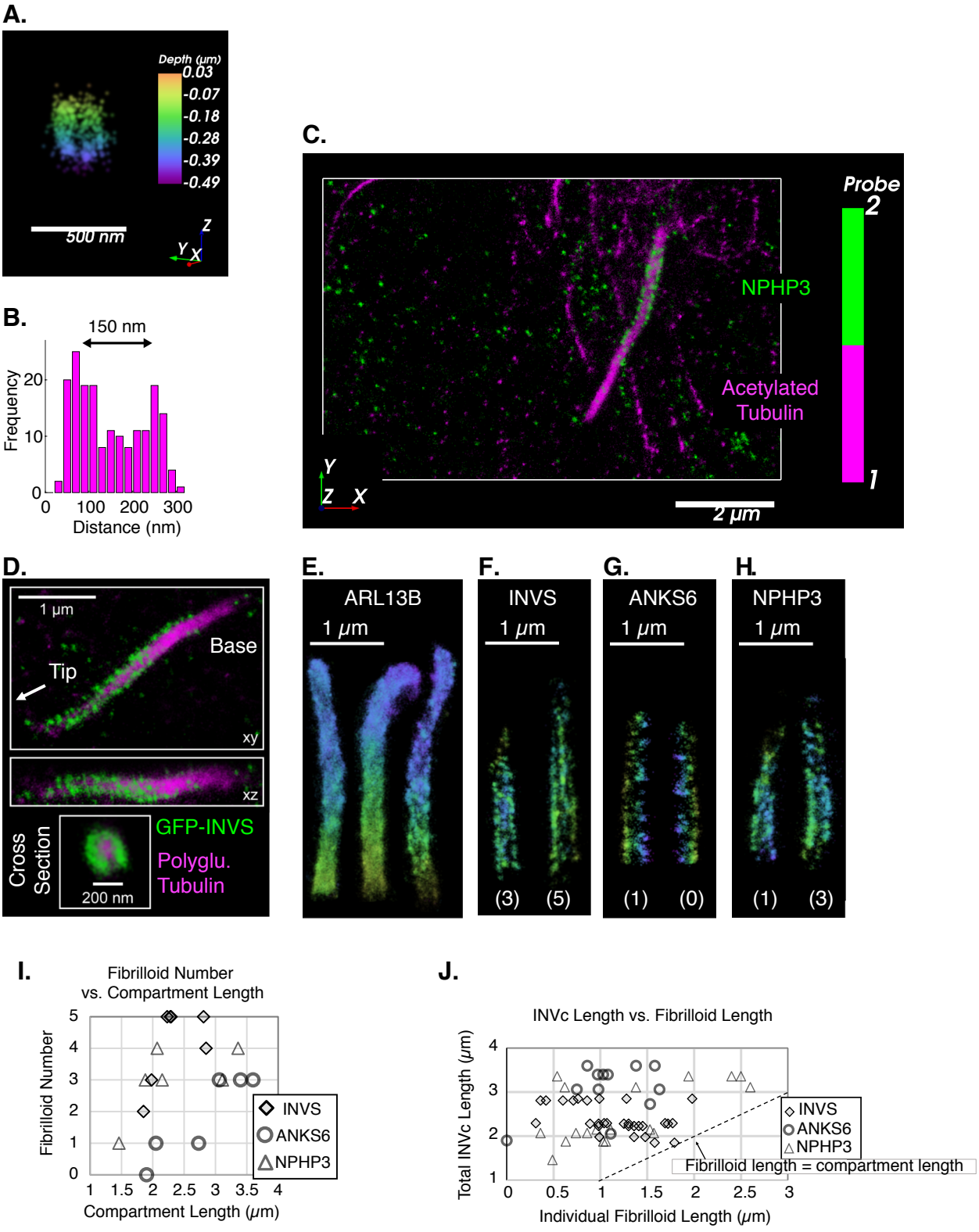

Supplemental Figure S22. Artificially sparse reconstructions of ARL13B.

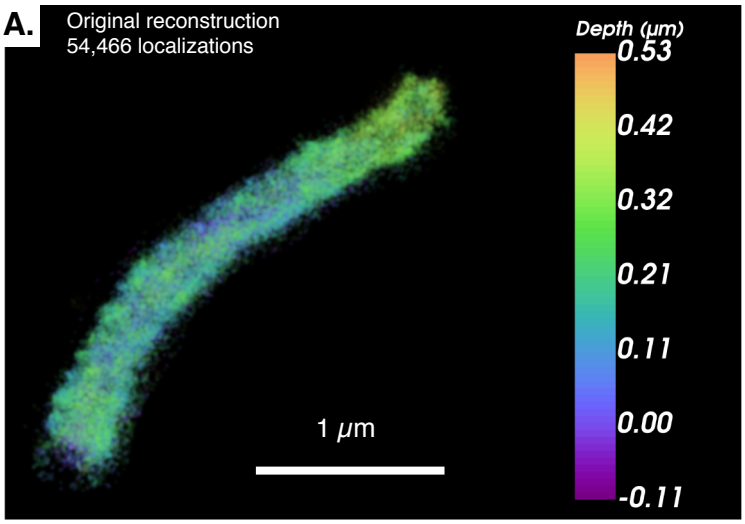

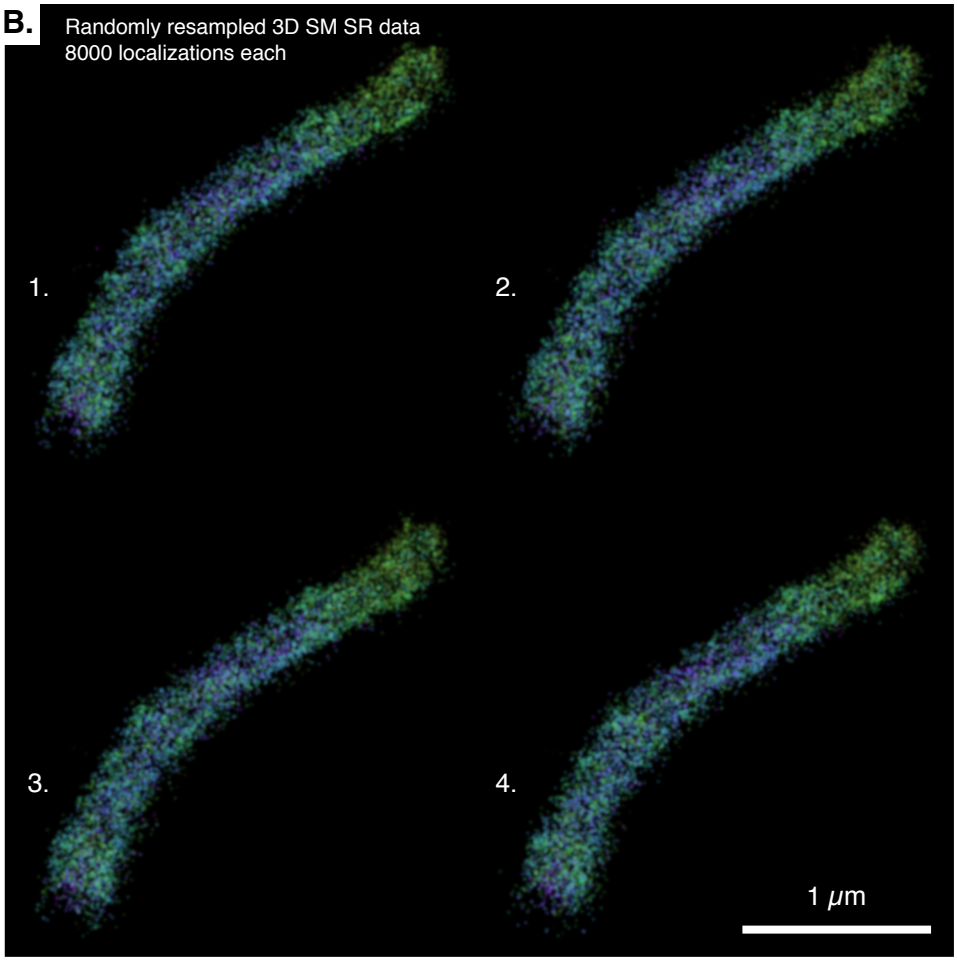

Supplemental Figure S23. Knockout cell line generation and validation of INVS-KO.

A.

1. Transduce Cas9 cells with guide RNA to edit GOI

RPE1 Cas9-BFP cells

Lentiviral infection with:
pMCB306+sgRNA #1
pMCB306+sgRNA #2
pMCB306+sgRNA #3

Select in puromycin

2. Choose most efficient guide

Extract gDNA, PCR with primers flanking guide site*, Analyze sequence by TIDE

3. Guide cassette removal

AV-cre → Single cell sort GFP neg. cells

4. Select knockout clones

Expand → Genotype by TIDE (**C**)

Phenotype by IF

Mix single cell clones to generate final superclonal KO cell line
Validate by IF (**G**)
If possible, rescue (**S31**)

B.

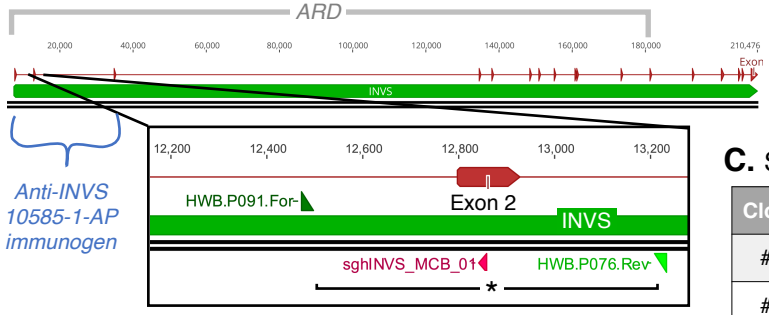

C. Single cell clone TIDE results (INVS)

Clone	Copy 1	Copy 2
#1	~100 bp deletion*	~100 bp deletion*
#2	7 bp deletion	7 bp deletion
#3	95 bp deletion	1 bp insertion
#4	4 bp insertion	1 bp insertion

*Detected by band shift in gel, not by TIDE

D.

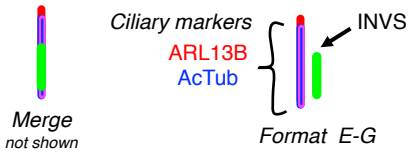

E. DLM WT

E'. *INVS contrast adjusted (green channel only)*

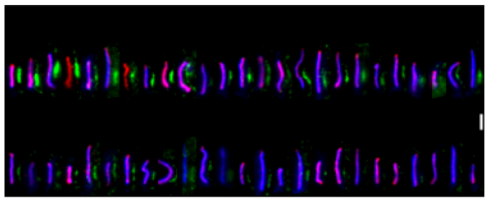

F. WT Cas9-BFP

F'.

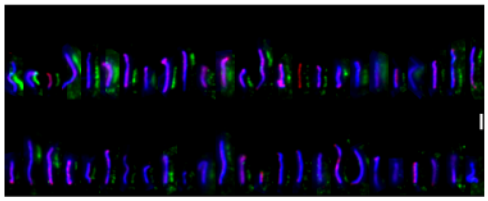

G. INVS-KO (Cas9-BFP)

G'.

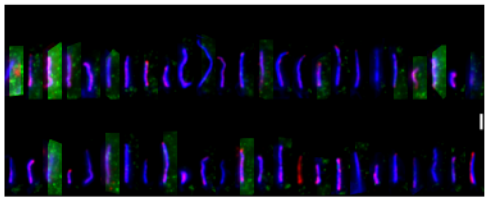

▲▲ Non-specific basal body staining

Scale bars 2 μm

Supplemental Figure S24. NEK8-KO genotyping by TIDE and validation of ANKS6-KO cell line by IF.

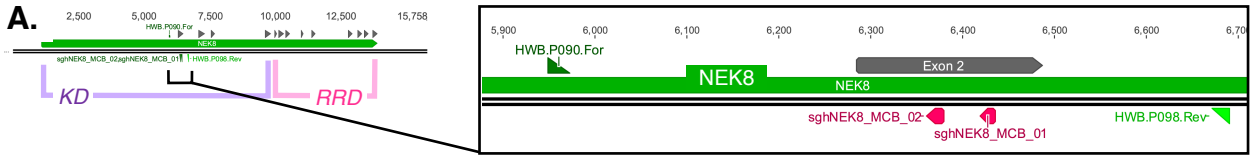

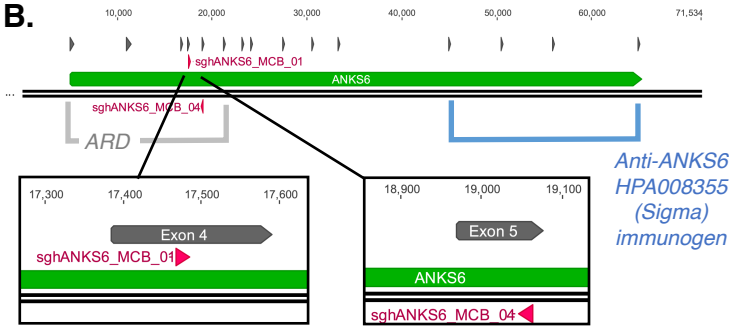

C. Single cell clone TIDE results (NEK8)

Clone (guide)	Copy 1	Copy 2
#1 (1)	4 bp deletion	8 bp deletion
#2 (1)	2 bp deletion	7 bp deletion
#3 (1)	4 bp deletion	4 bp deletion
#4 (1)	1 bp insertion	5 bp deletion
#5 (2)	4 bp deletion	4 bp deletion
#6 (2)	8 bp insertion	8 bp deletion
#7 (2)	8 bp deletion	8 bp deletion

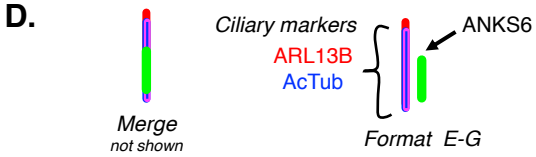

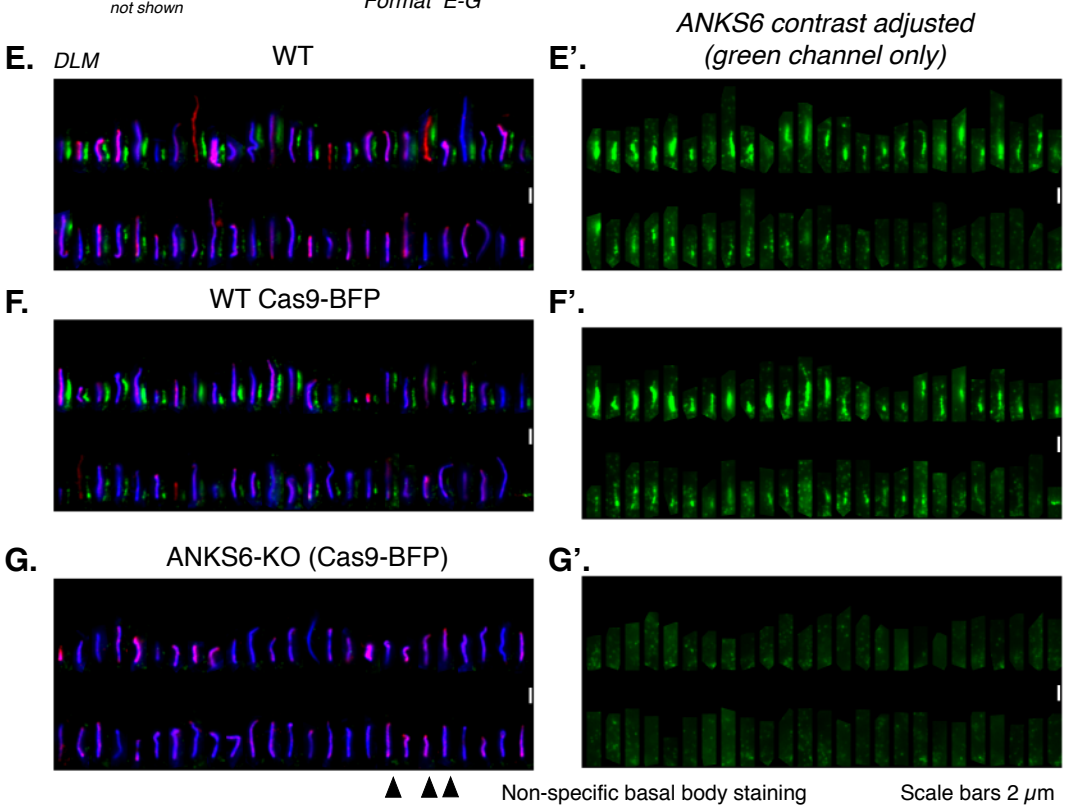

Supplemental Figure S25. Validation of NPHP3-KO cell line by IF.

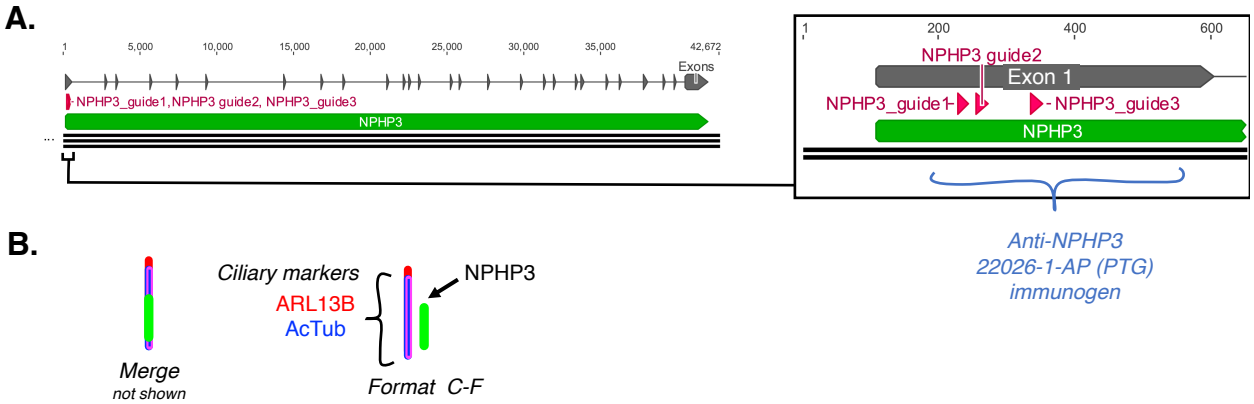

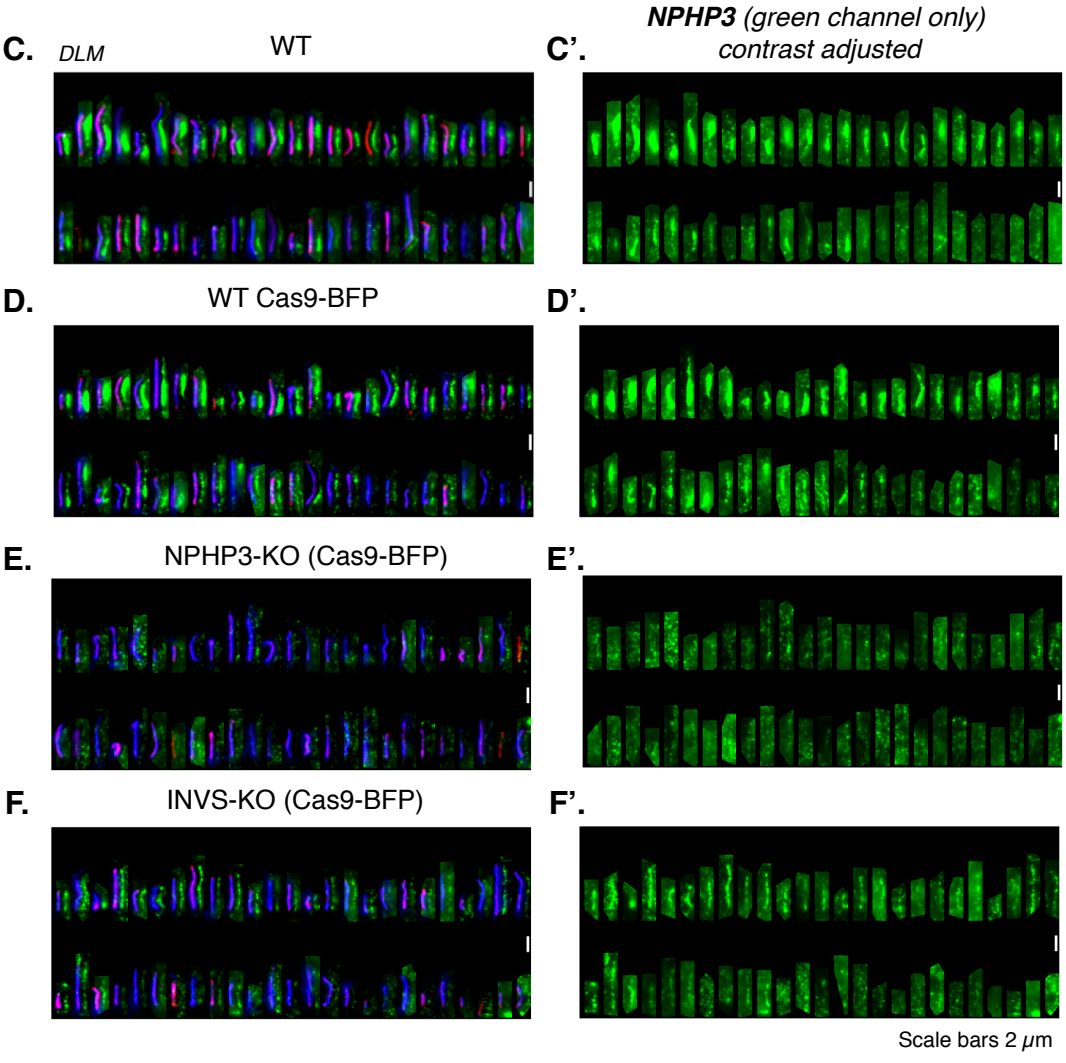

Scale bars 2 μm

Supplemental Figure S26. Validation of ANKS6-KO and NPHP3-KO cell lines by immunoblot.

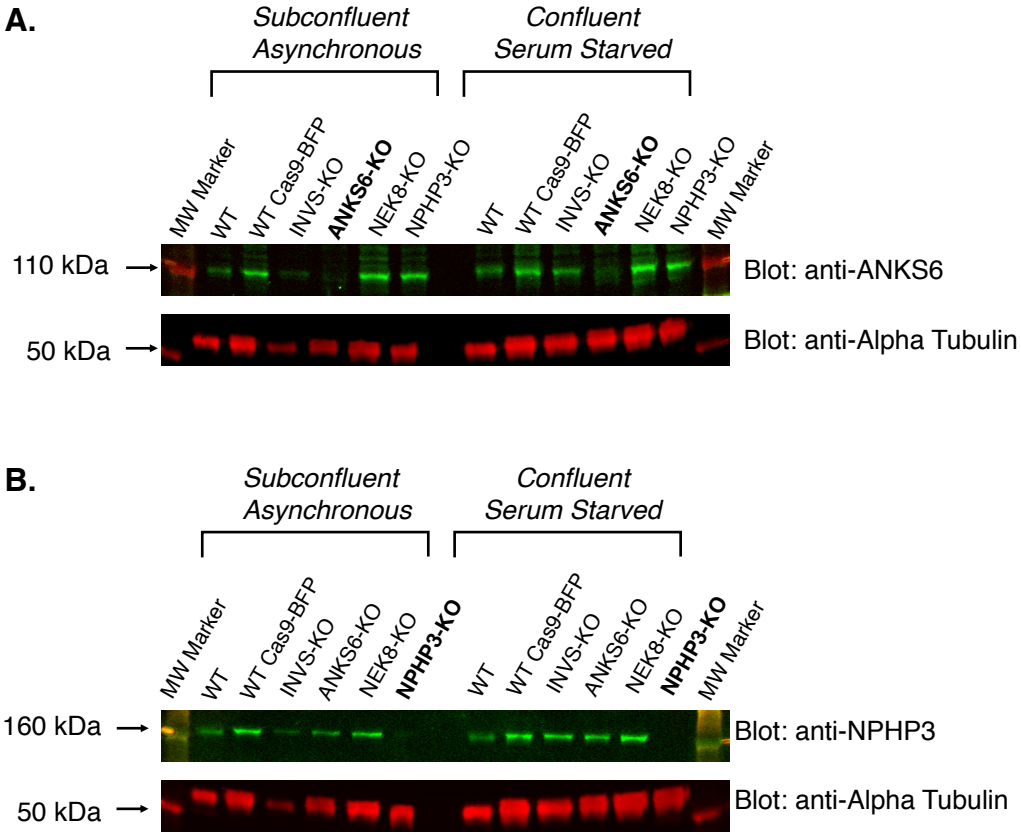

Supplemental Figure S27. gINVc-KO lines do not have ciliation or cilia length defects.

A.

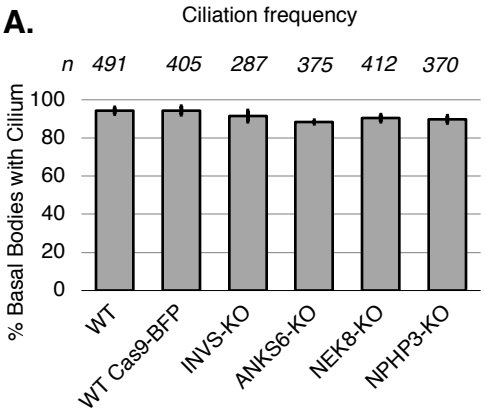

B.

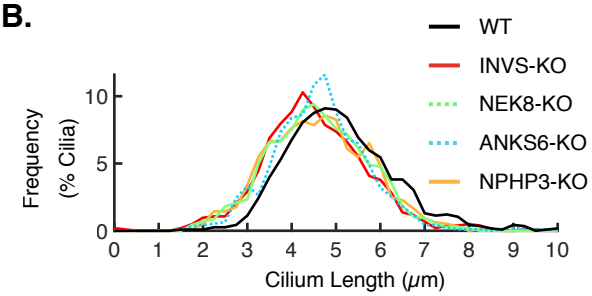

Cell Line	Mean cilium length (μm)	Standard Dev. (μm)	n
WT	5.00	1.20	577
INVS-KO	4.41	1.16	515
ANKS6-KO	4.52	1.09	470
NEK8-KO	4.47	1.10	579
NPHP3-KO	4.48	1.14	484

C.

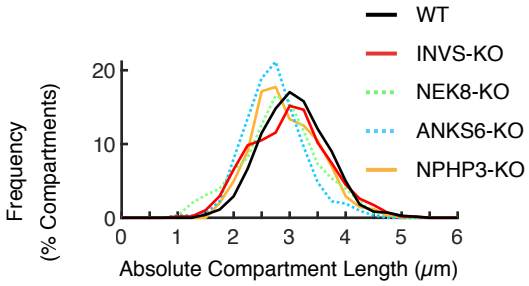

Cell Line	Mean INVc length (μm)	Standard Dev. (μm)	n
WT GFP-INVS	2.86	0.68	290
INVS-KO GFP-INVS	2.95	0.57	362
ANKS6-KO GFP-INVS	2.61	0.68	156
NEK8-KO GFP-INVS	2.69	0.67	178
NPHP3-KO GFP-INVS	2.81	0.68	172

Supplemental Figure S28. Summary of T-test results for significant differences in ciliary pINVc density in WT and gINVc-KO cells.

A. INVS

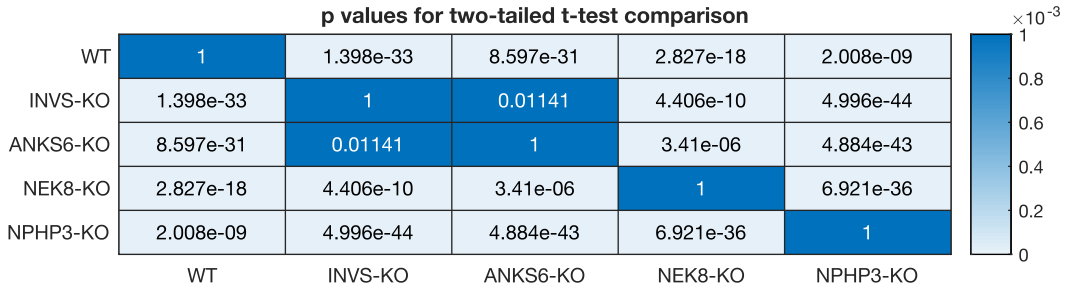

B. ANKS6

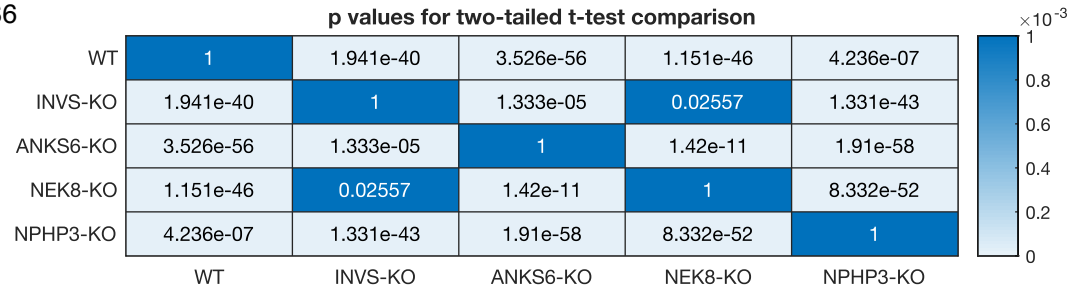

C. NPHP3

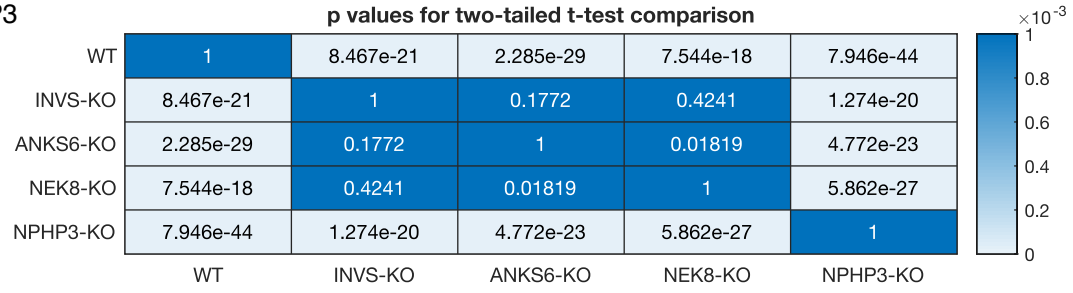

D. GFP-NEK8

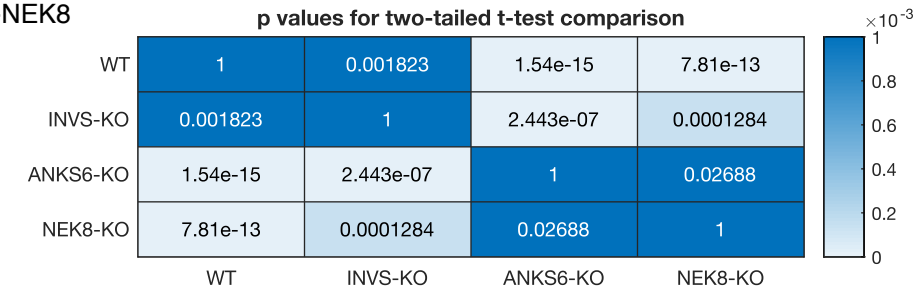

E. GFP-INVS

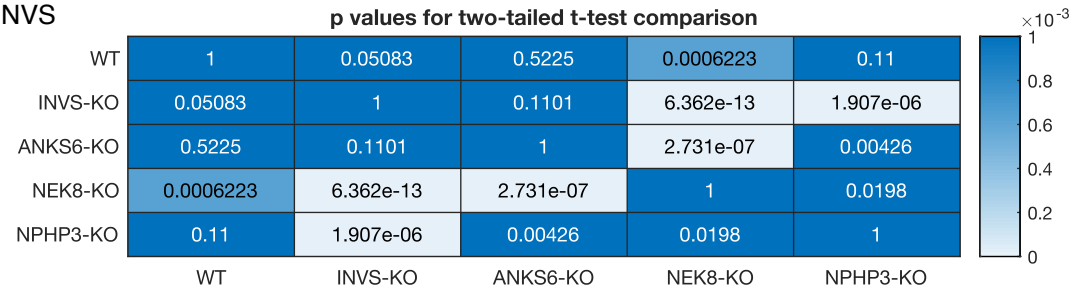

Supplemental Figure S29. Validation of GFP-INVS and GFP-NEK8 cell lines by immunoblot.

A.

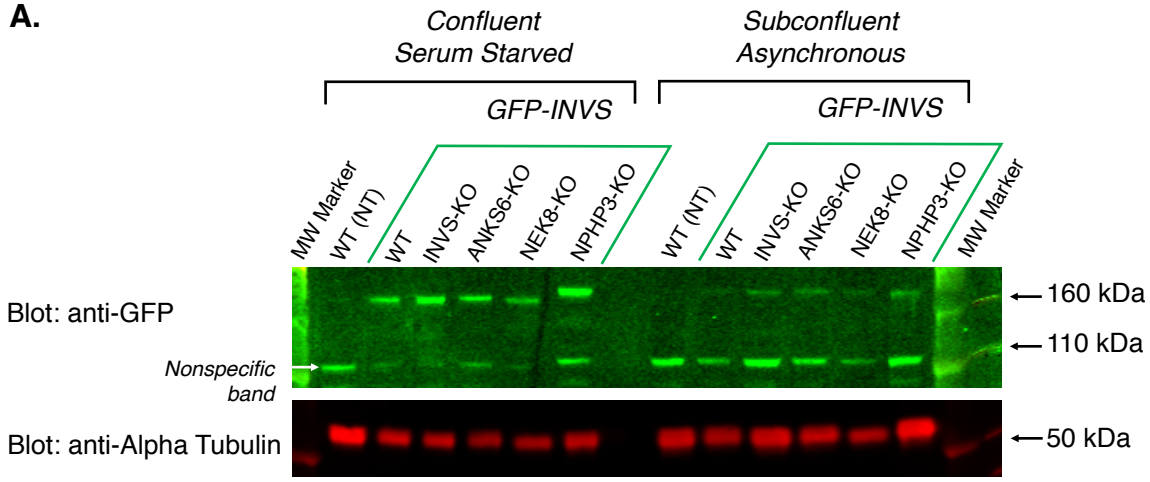

B.

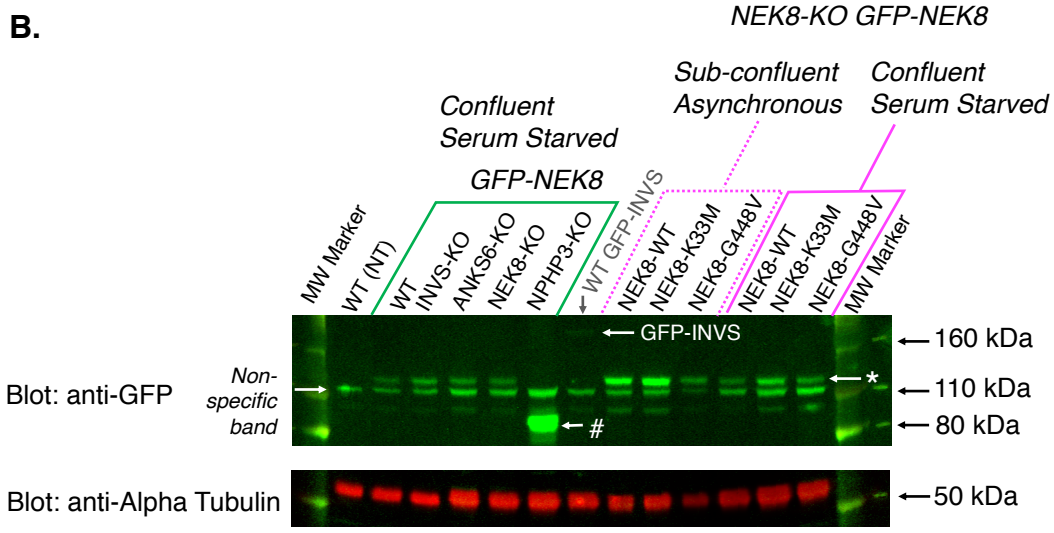

Supplemental Figure S30. Rescue of NEK8-KO cells with GFP-NEK8.

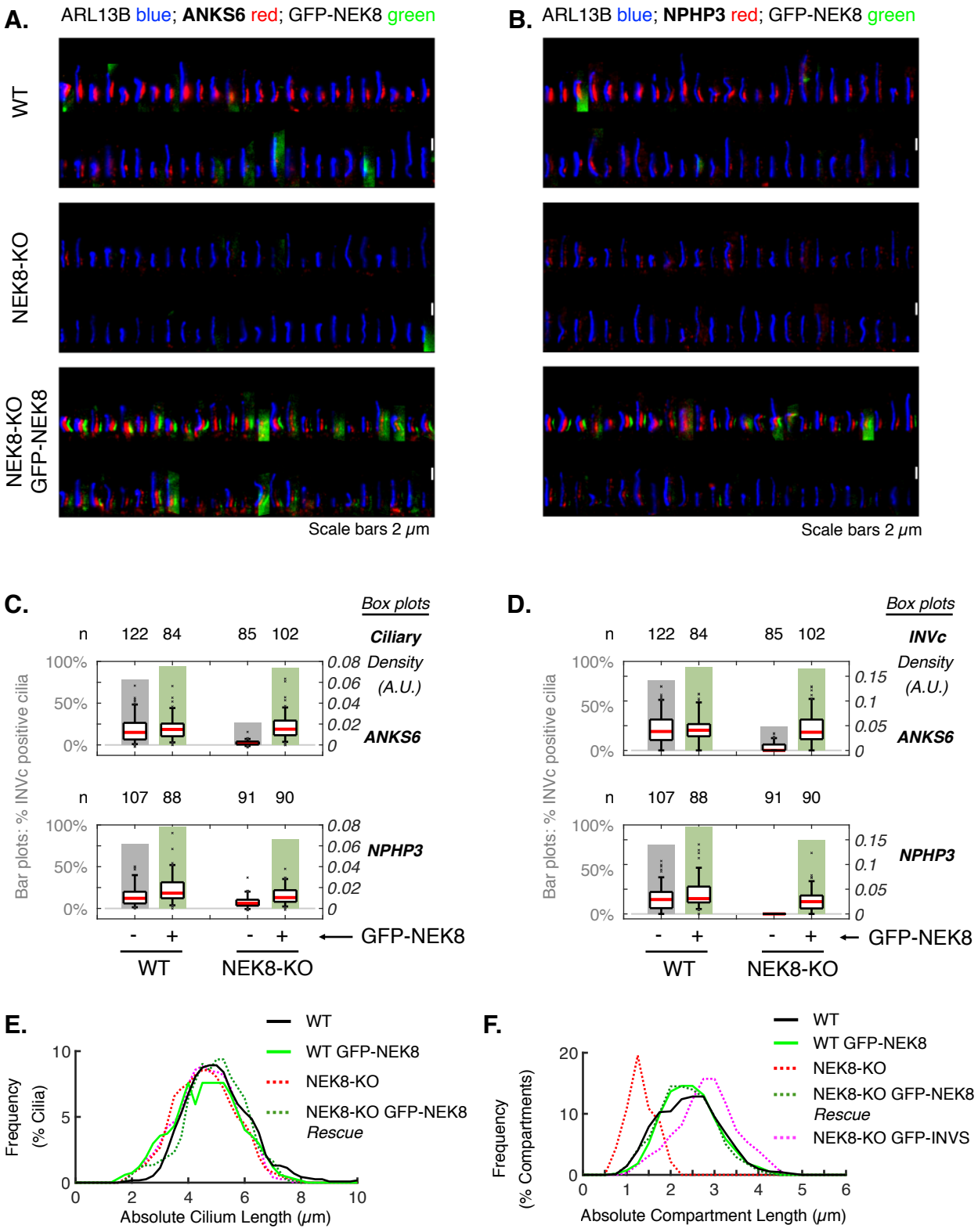

Supplemental Figure S31. Rescue of INVS-KO cells with GFP-INVS.

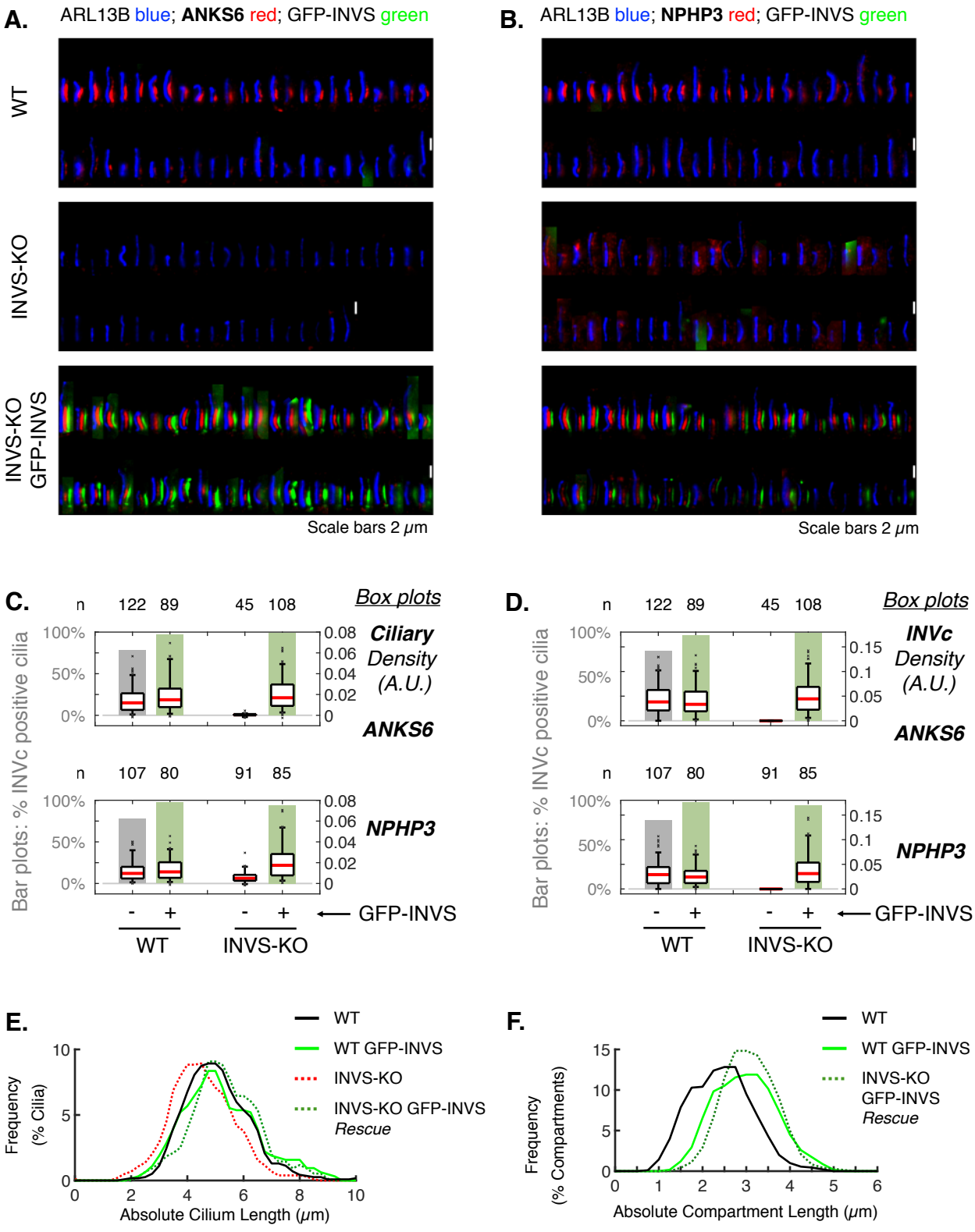

Supplemental Figure S32. Additional DLM images of ANKS6 localization and INVc-specific density measurements of ANKS6 and NPHP3 in gINVc-KO cell lines expressing GFP-INVS.

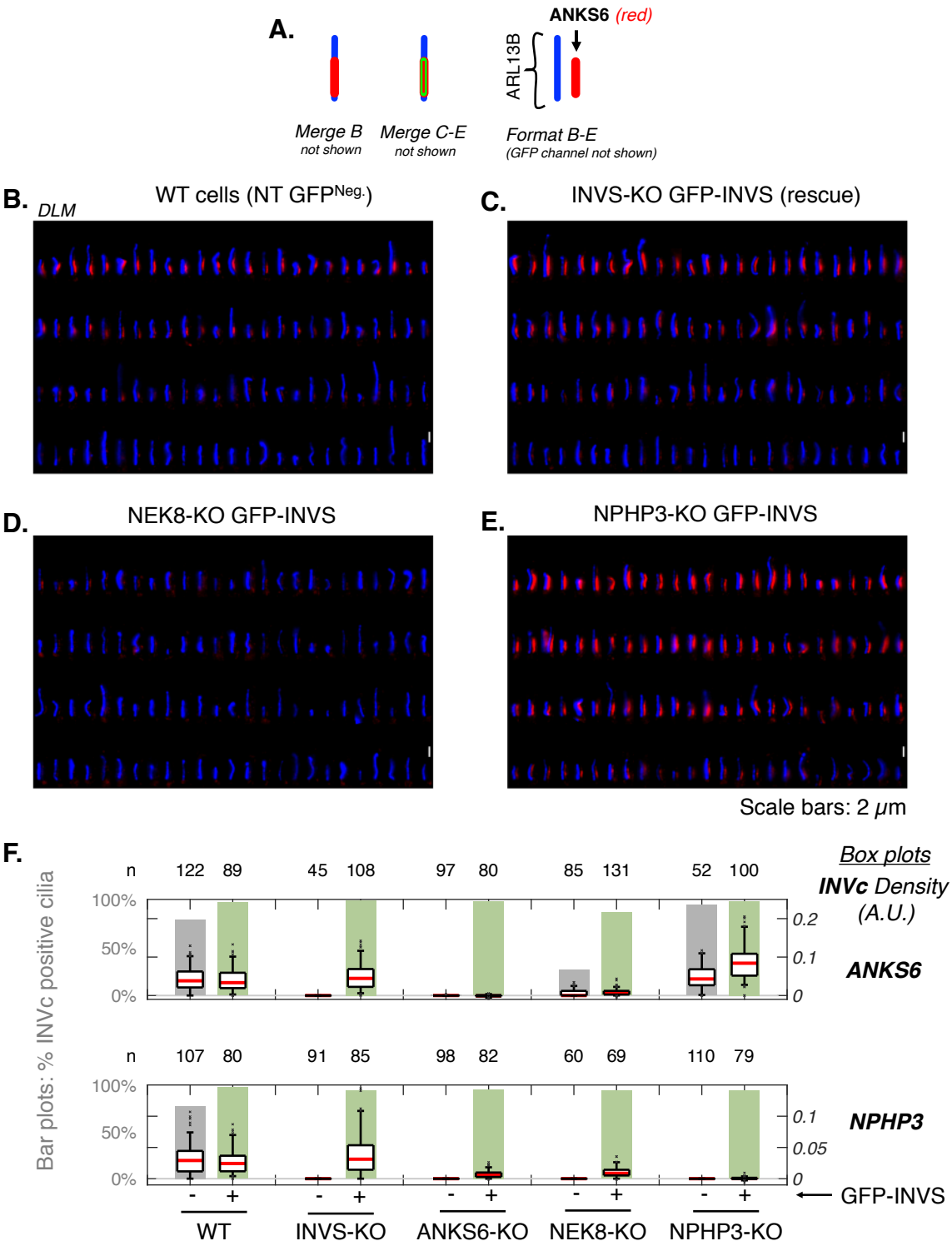

Supplemental Figure S33. Additional DLM images of NPHP3 localization in gINVc-KO cell lines expressing GFP-INVS.

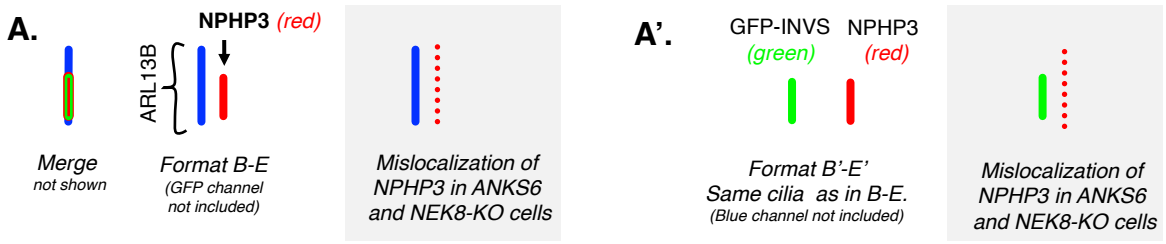

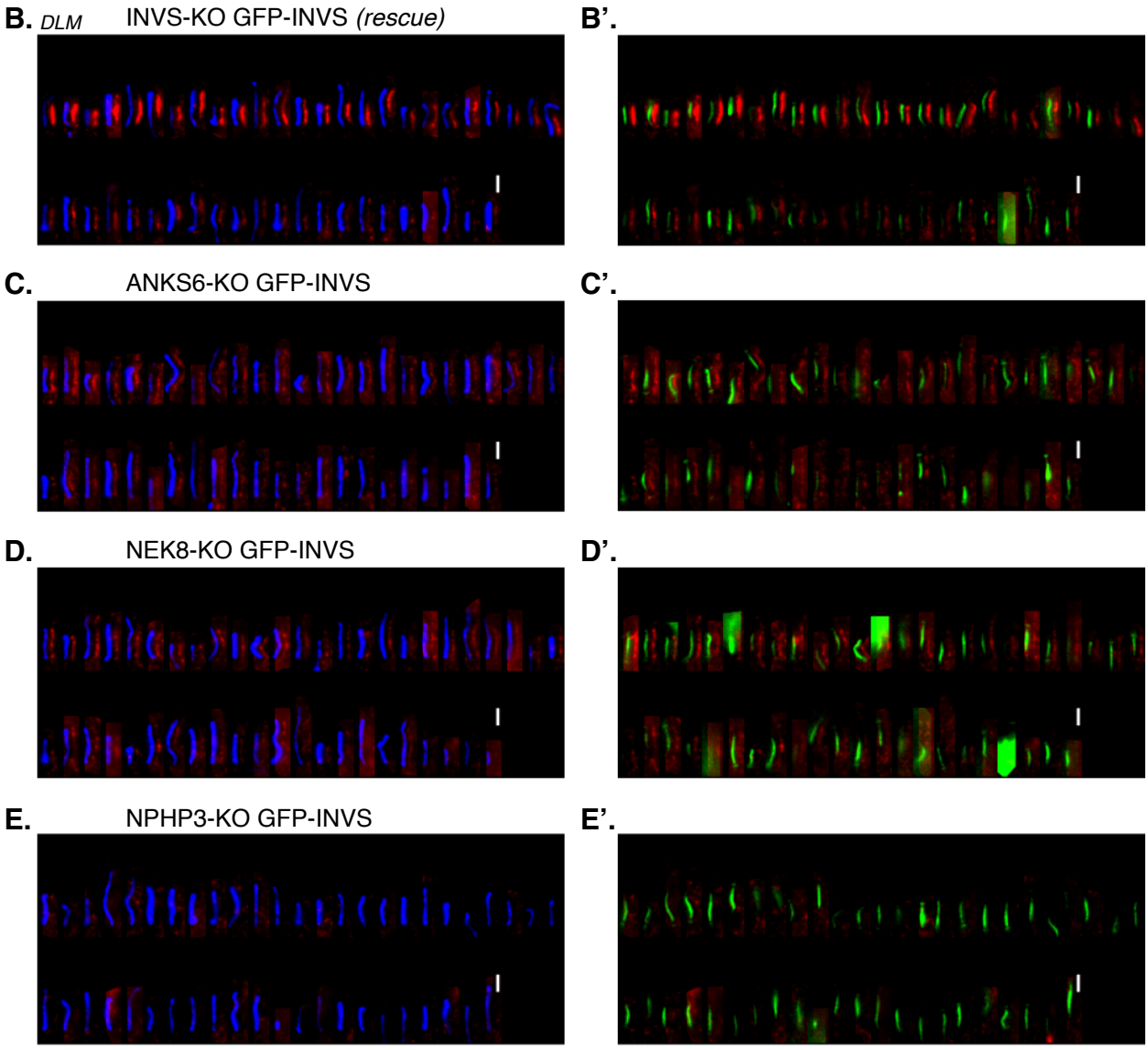

Scale bars: 2 μm

Supplemental Figure S34. Summary of T-test results for significant differences in ciliary ANKS6 and NPHP3 density in cell lines expressing GFP-INVS.

A. ANKS6 ciliary density

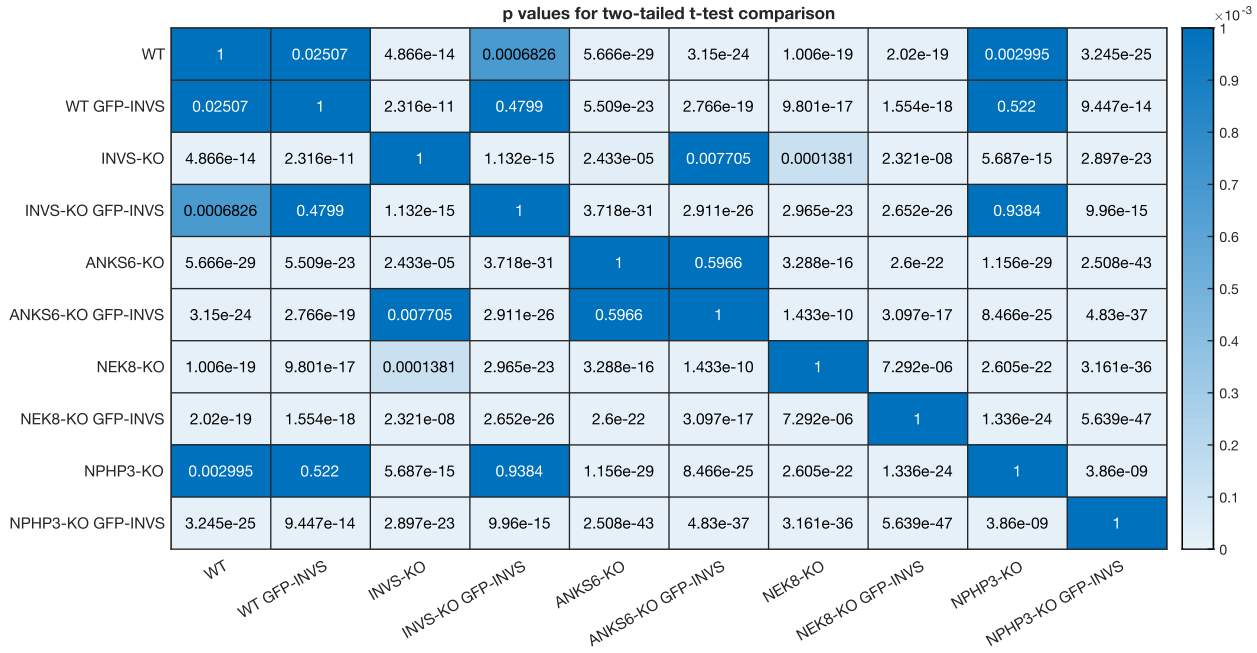

B. NPHP3 ciliary density

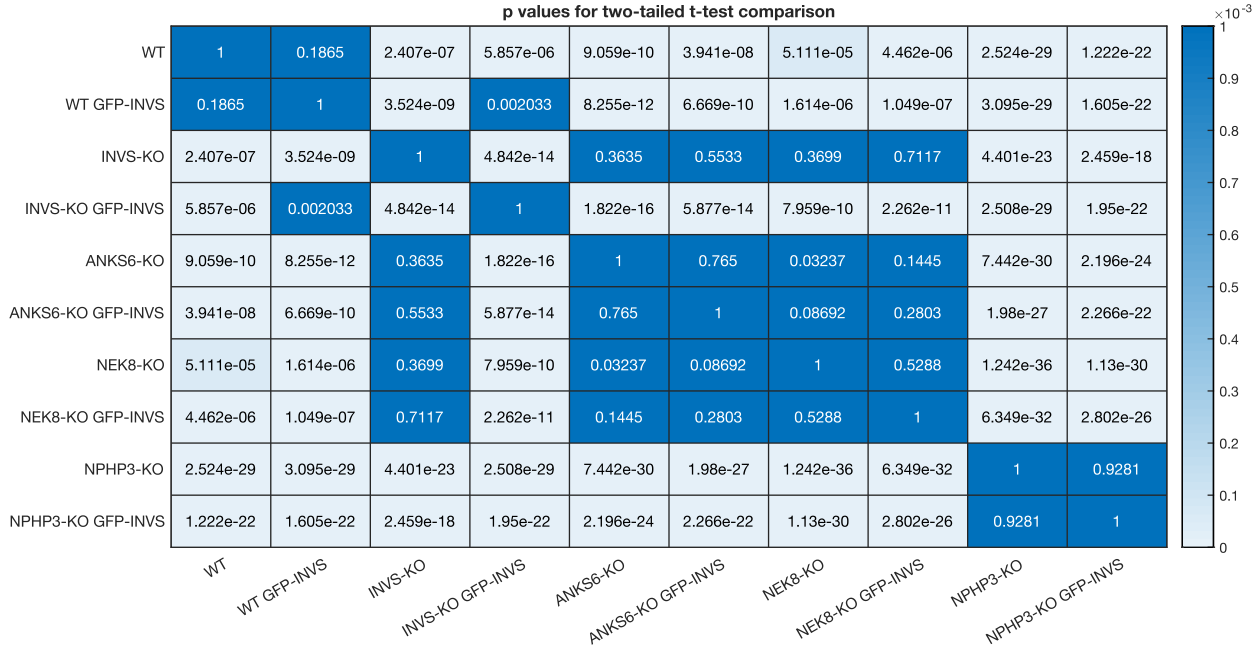

Supplemental Figure S35. Summary of ANKS6 localization in WT, INVS-KO, NEK8-KO, and NPHP3-KO cell lines expressing GFP-INVS.

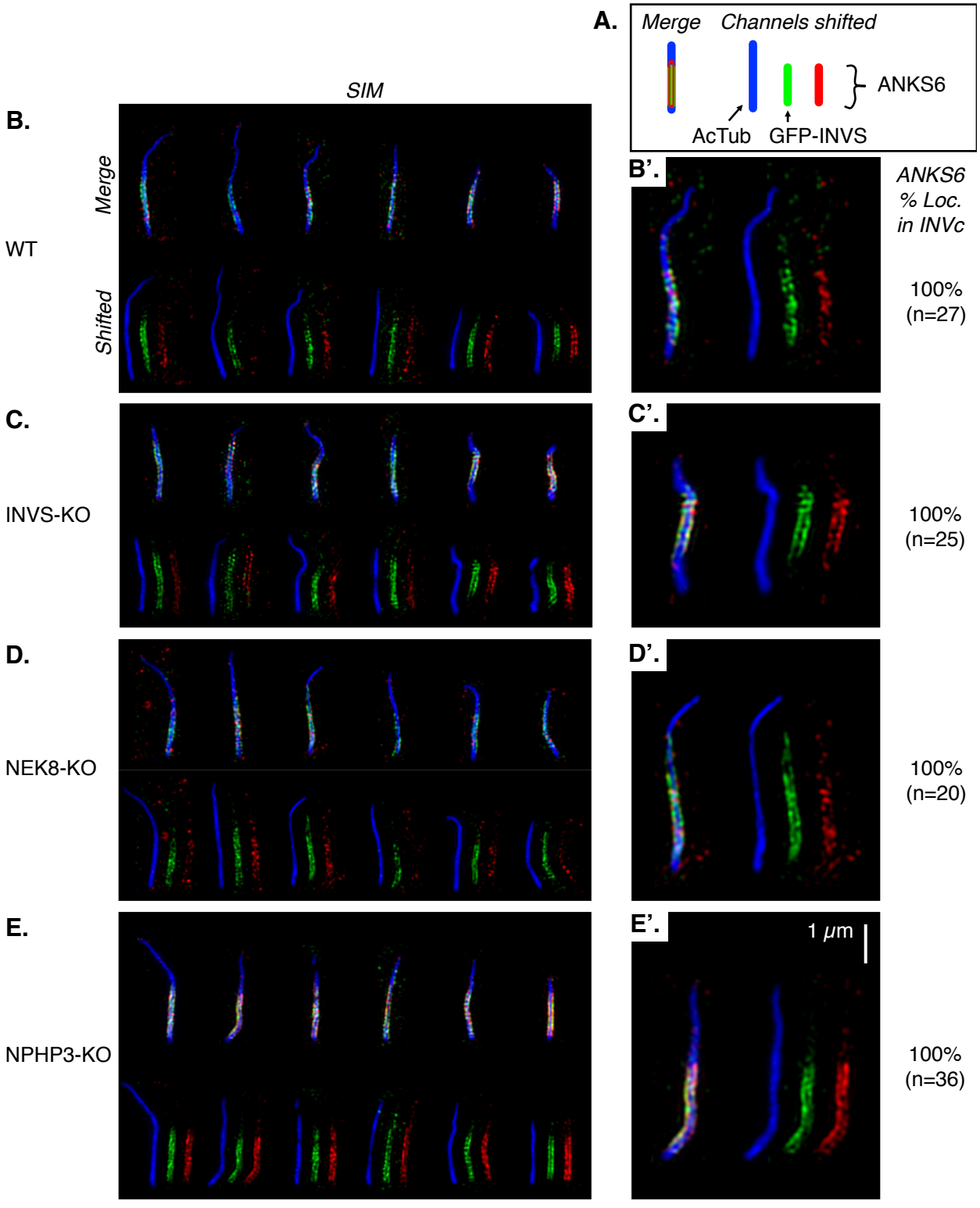

Supplemental Figure S36. Correlation of GFP-NEK8 and GFP-INVS with ANKS6 and NPHP3 in NEK8-KO and INVS-KO cell lines rescued with GFP fusion proteins.

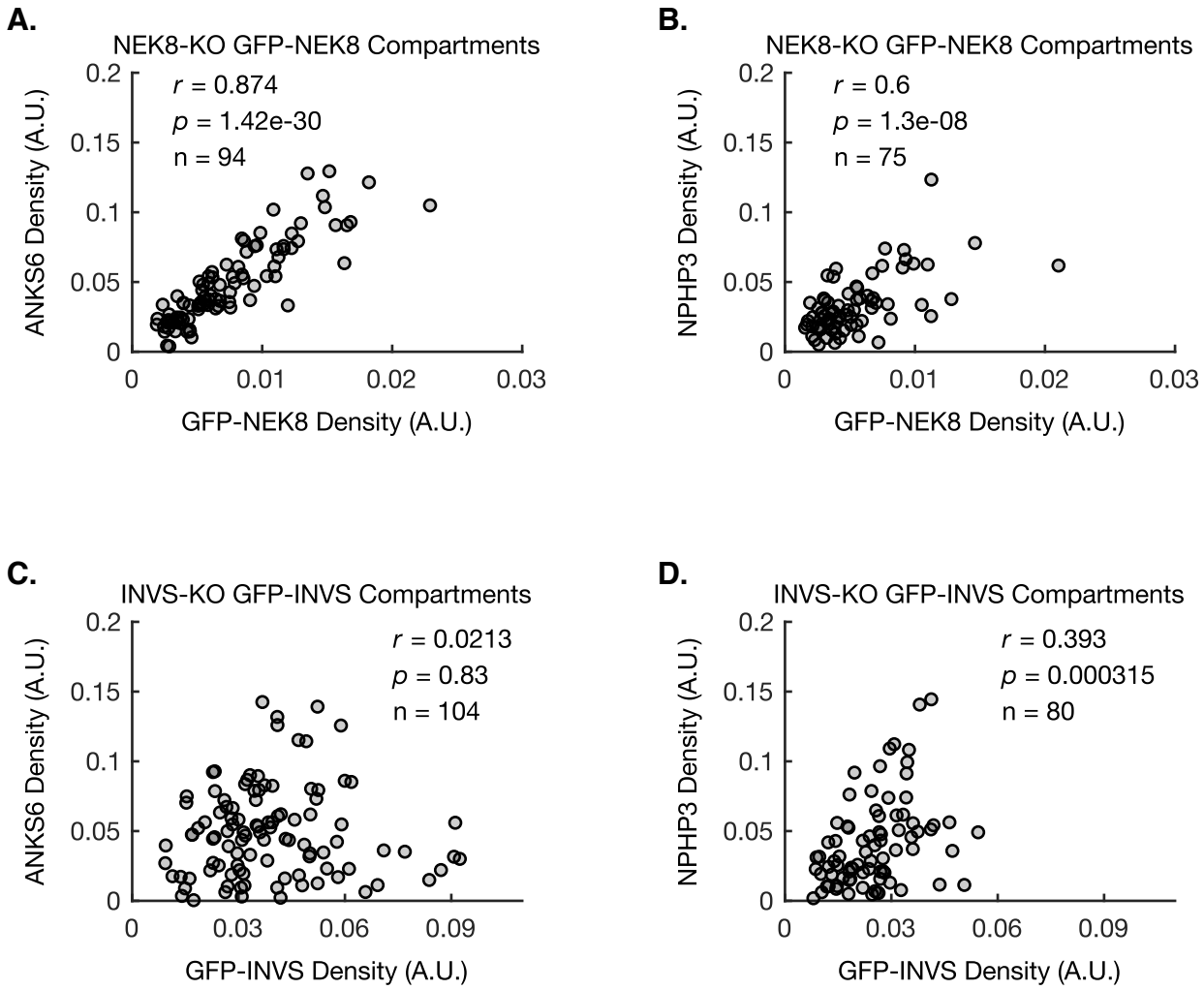

Supplemental Figure S37. SIM reconstructions of NPHP3(1-200) in WT cells.

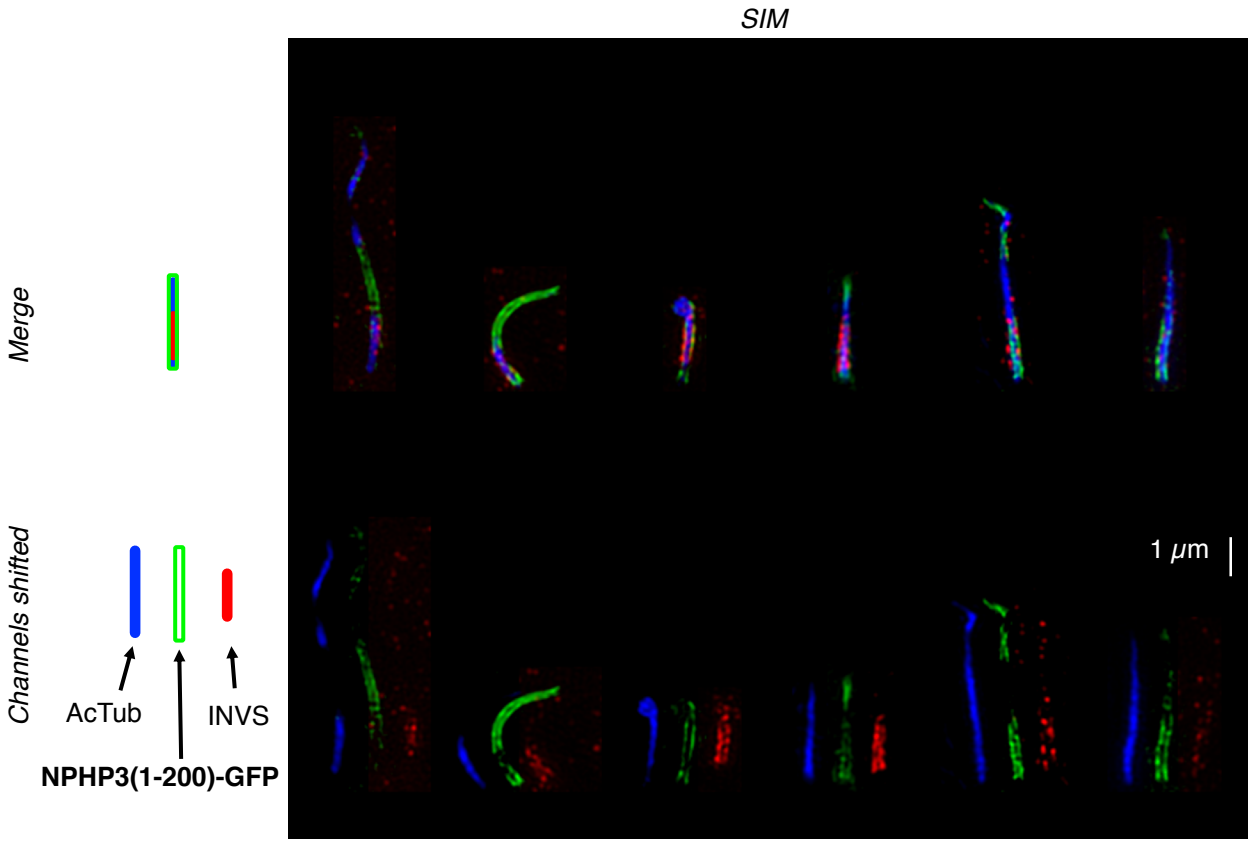

Supplemental Figure S38. Additional SIM reconstructions of NPHP3 in WT cells.

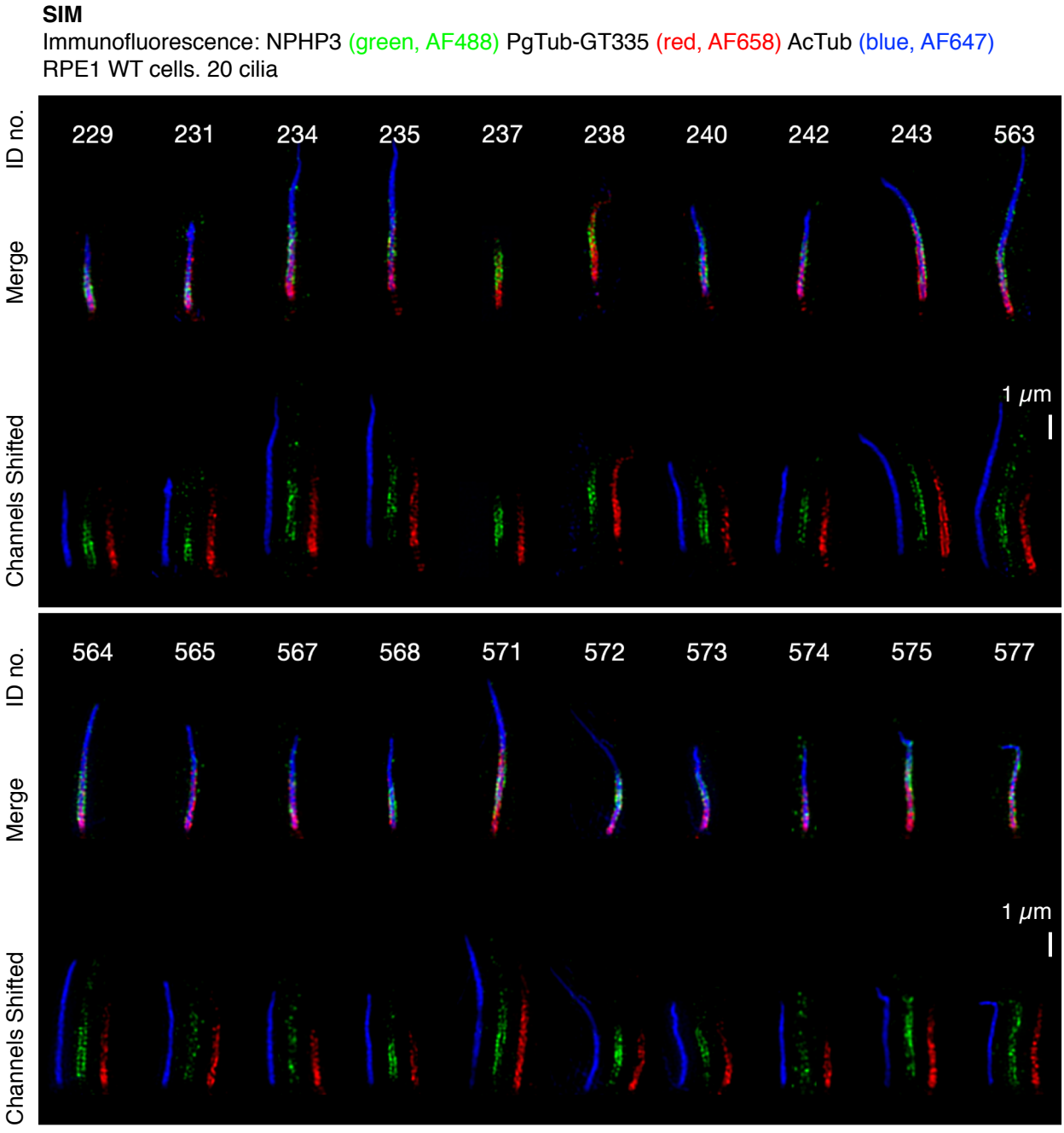

Supplemental Figure S39. Additional SIM reconstructions of NPHP3 in INVS-KO cells.

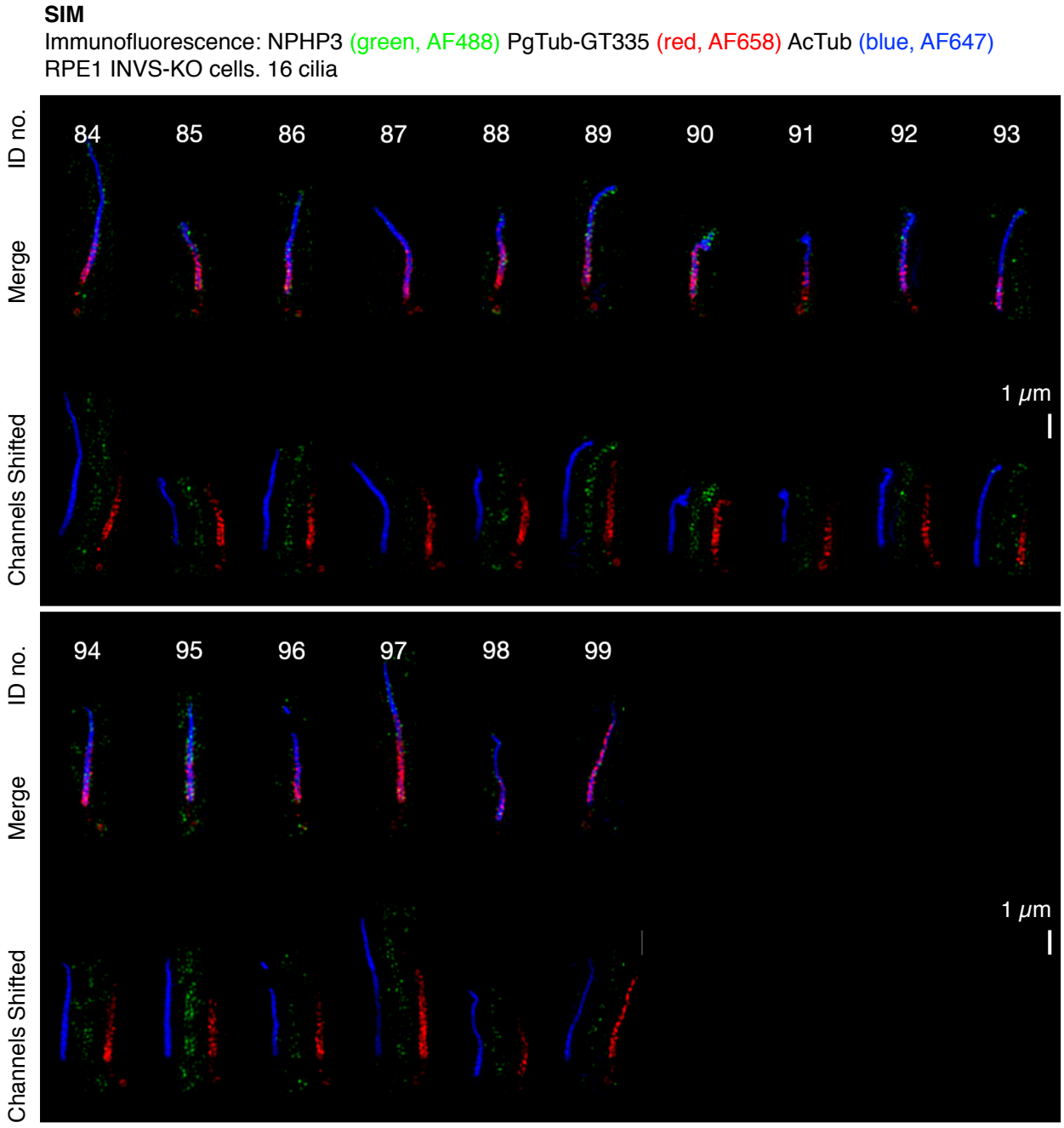

Supplemental Figure S40. Additional SIM reconstructions of NPHP3 in WT cells expressing GFP-INVS.

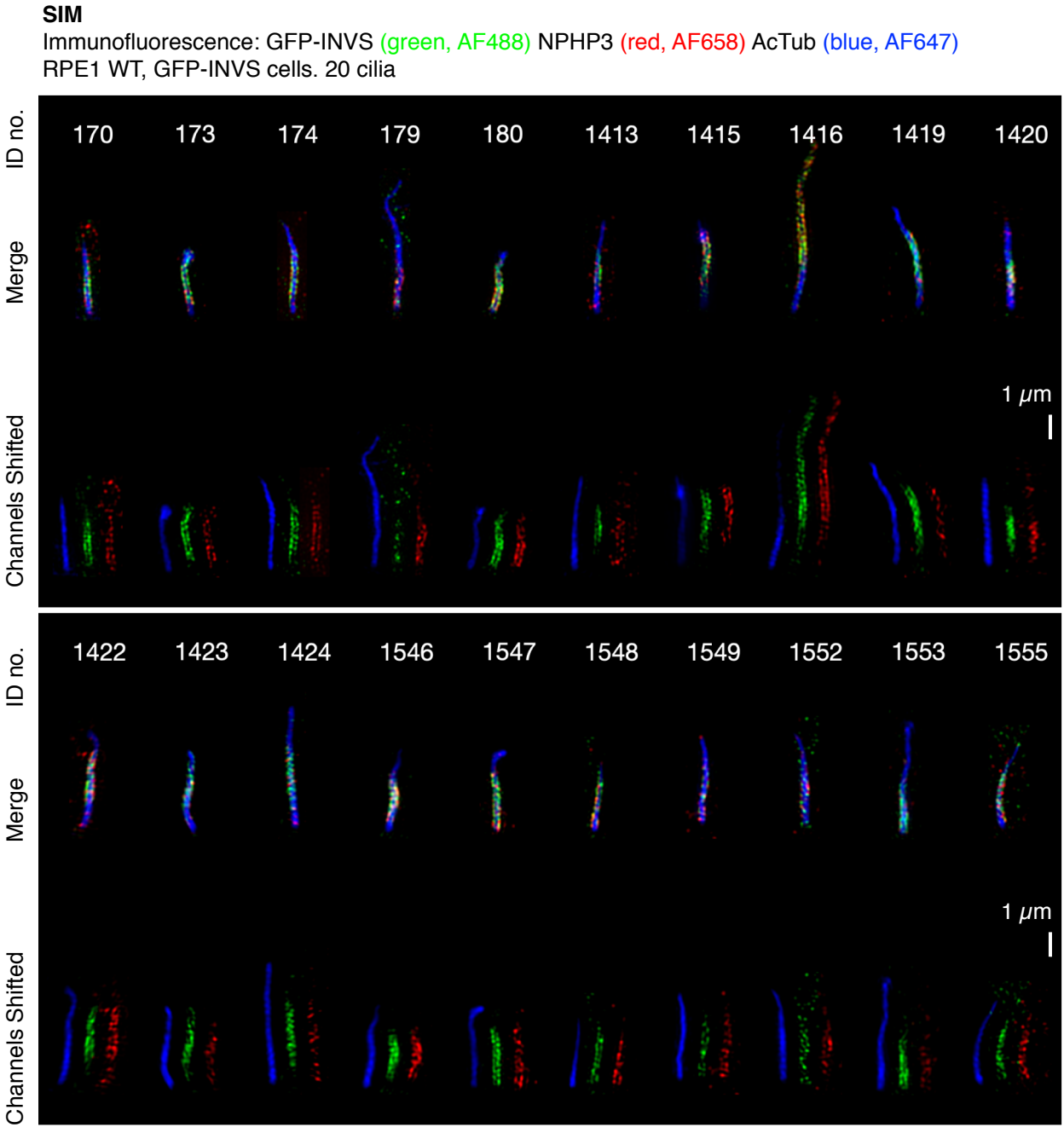

Supplemental Figure S41. Additional SIM reconstructions of NPHP3 in INVS-KO cells rescued with GFP-INVS.

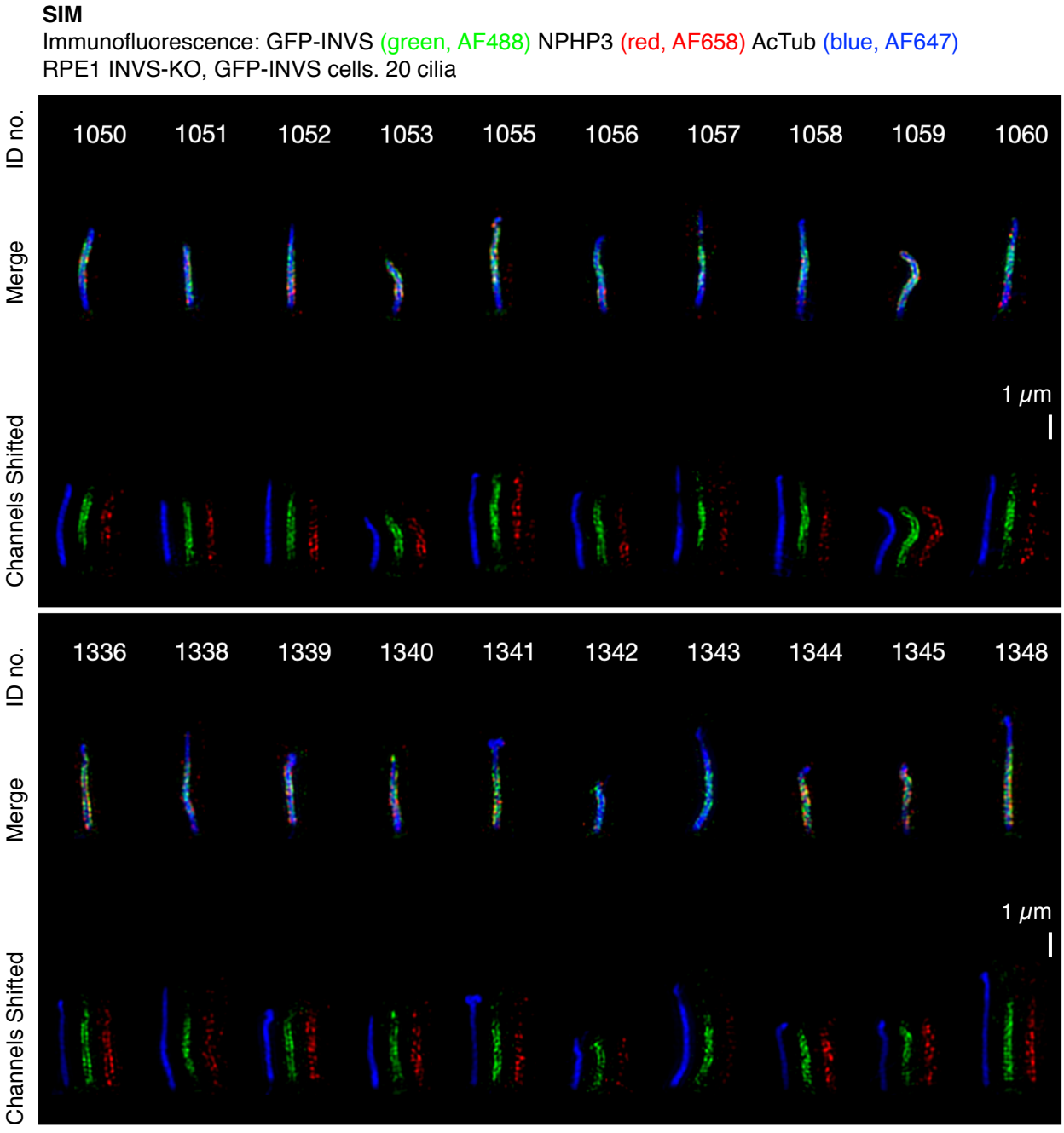

Supplemental Figure S42. Additional SIM reconstructions of NPHP3 in NEK8-KO cells expressing GFP-INVS.

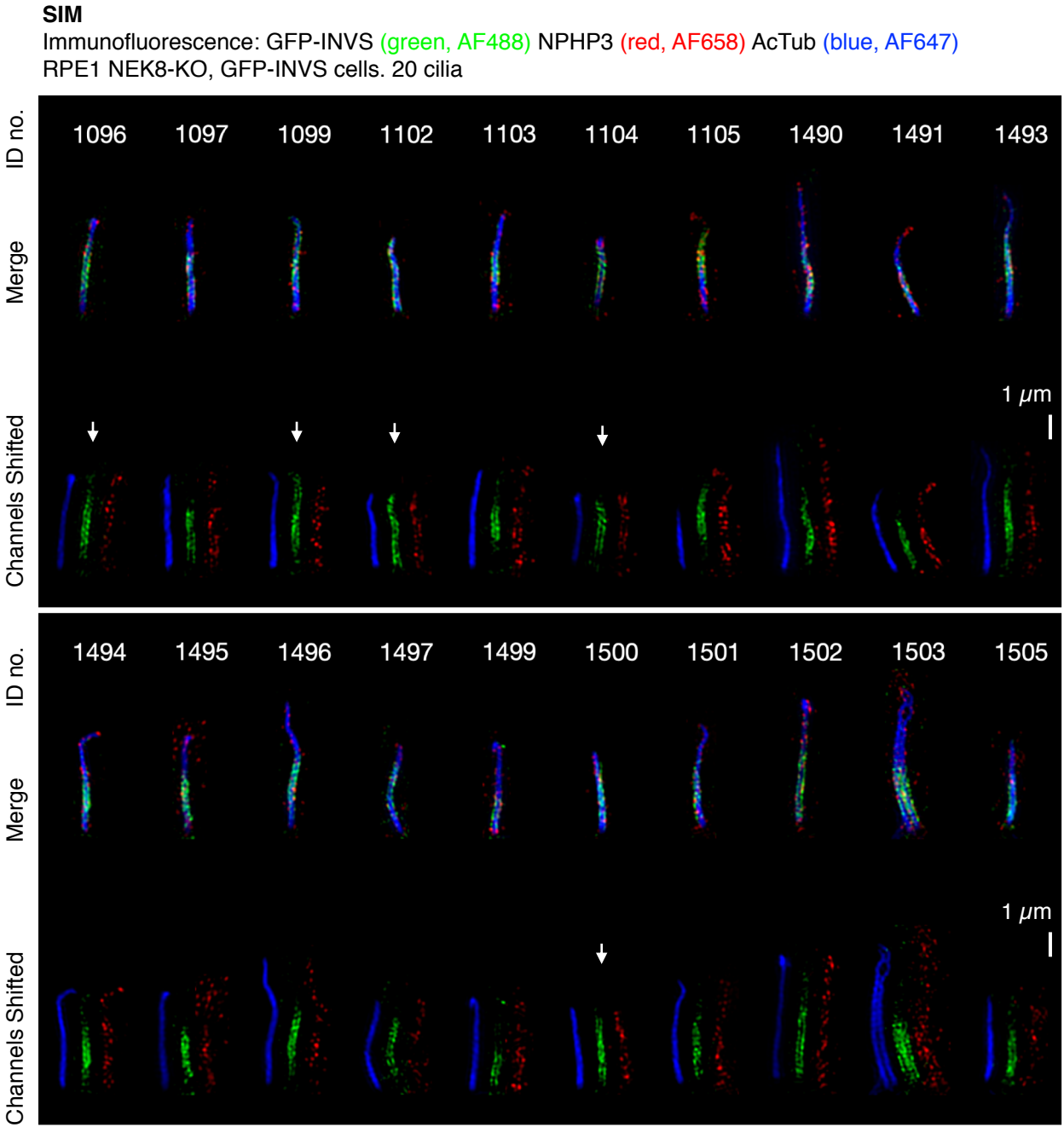

Supplemental Figure S43. Additional SIM reconstructions of NPHP3 in ANKS6-KO cells expressing GFP-INVS.

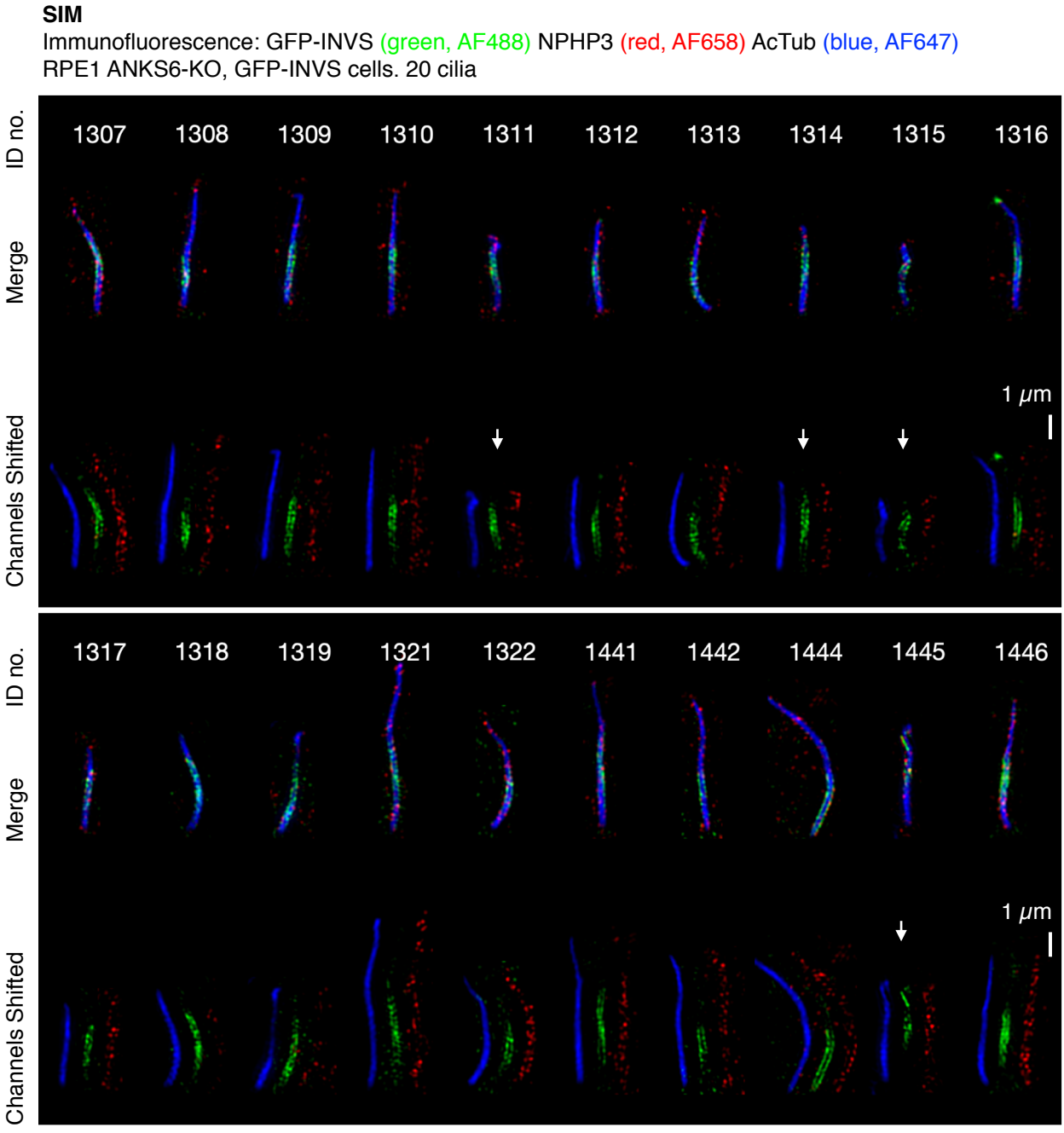

Supplemental Figure S44. SIM reconstructions of NPHP3 in NPHP3-KO cells expressing GFP-INVS.

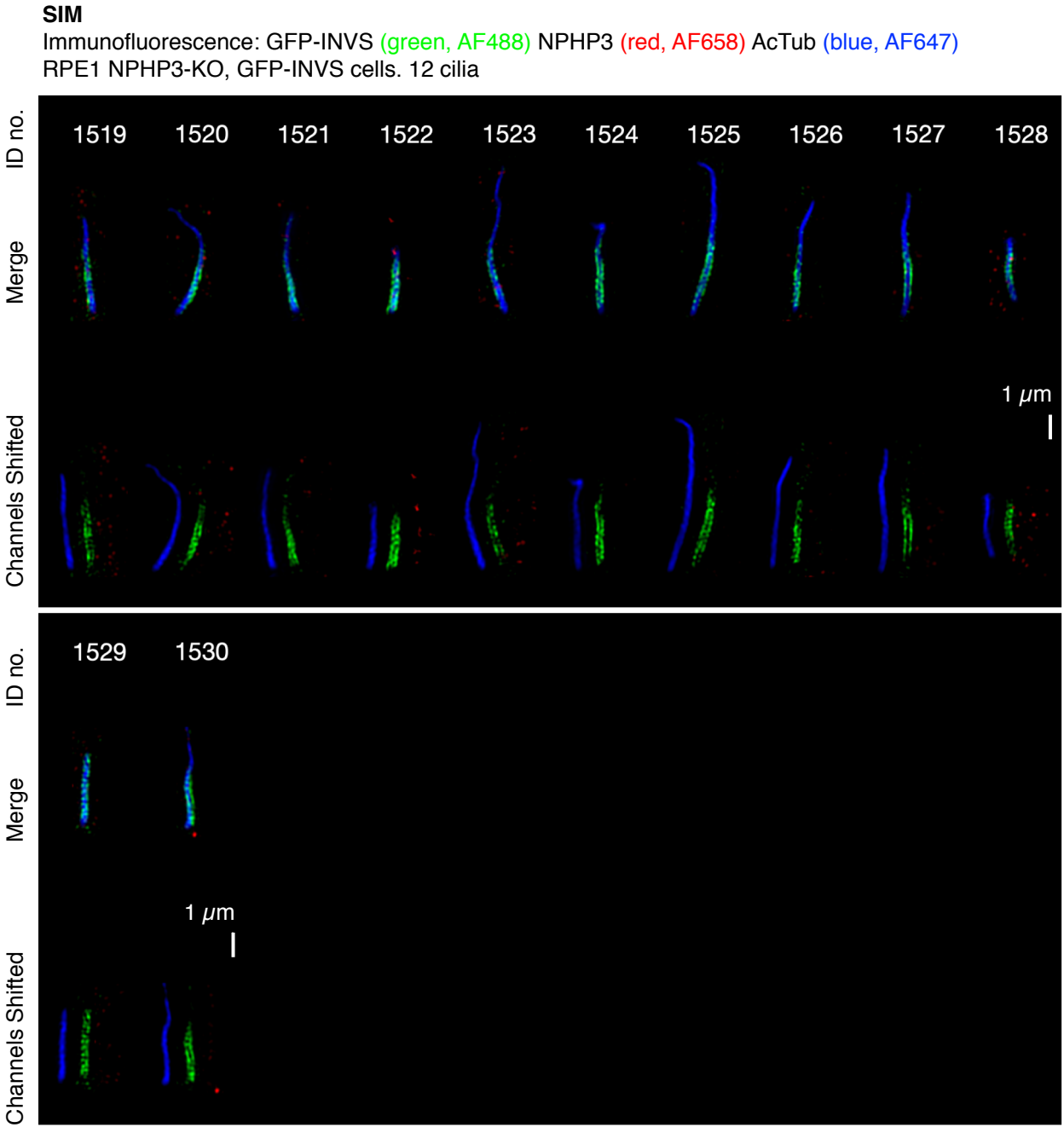

Supplemental Figure S45. Additional SIM reconstructions of ANKS6 in WT cells expressing GFP-INVS.

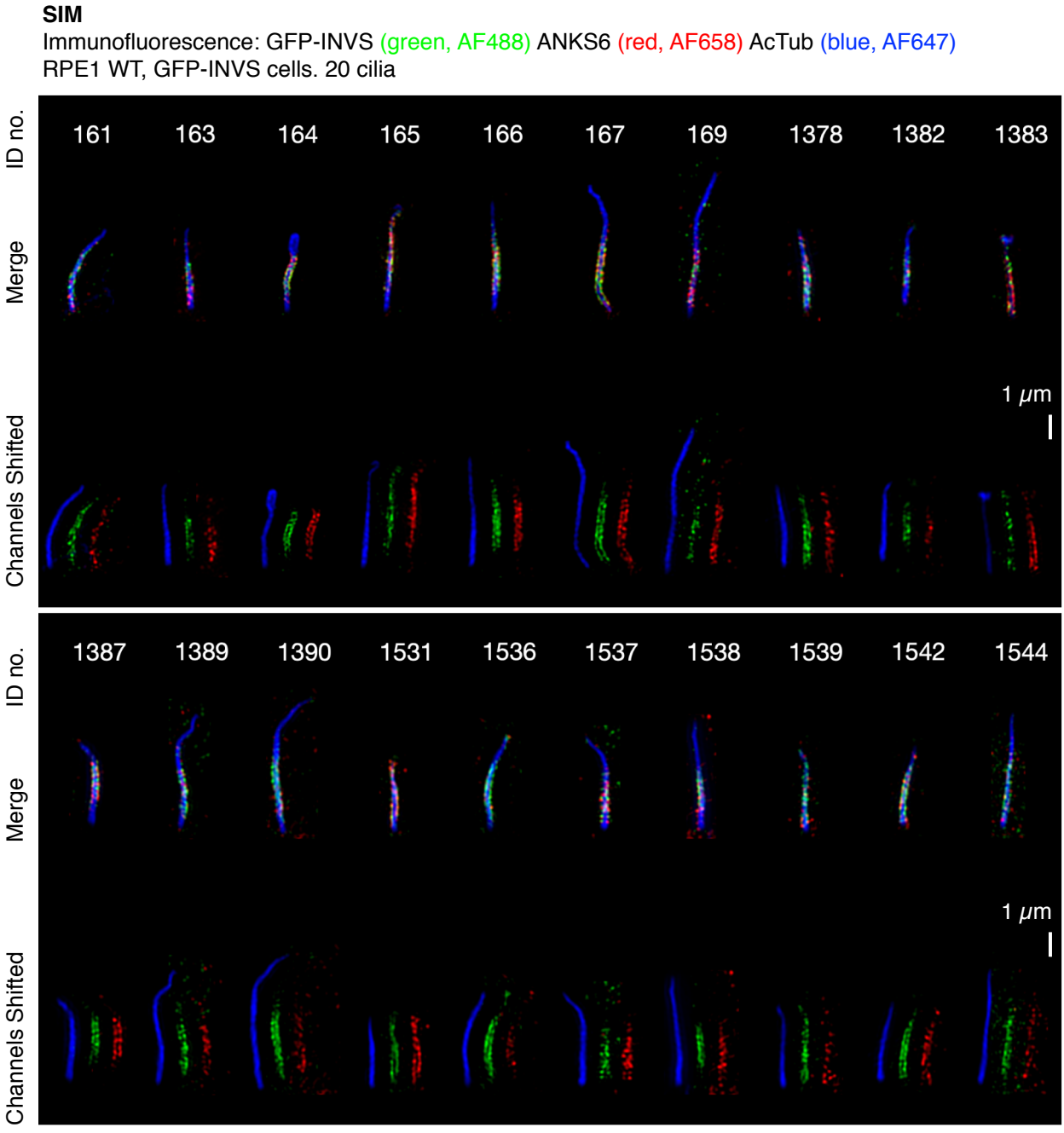

Supplemental Figure S46. Additional SIM reconstructions of ANKS6 in INVS-KO cells rescued with GFP-INVS.

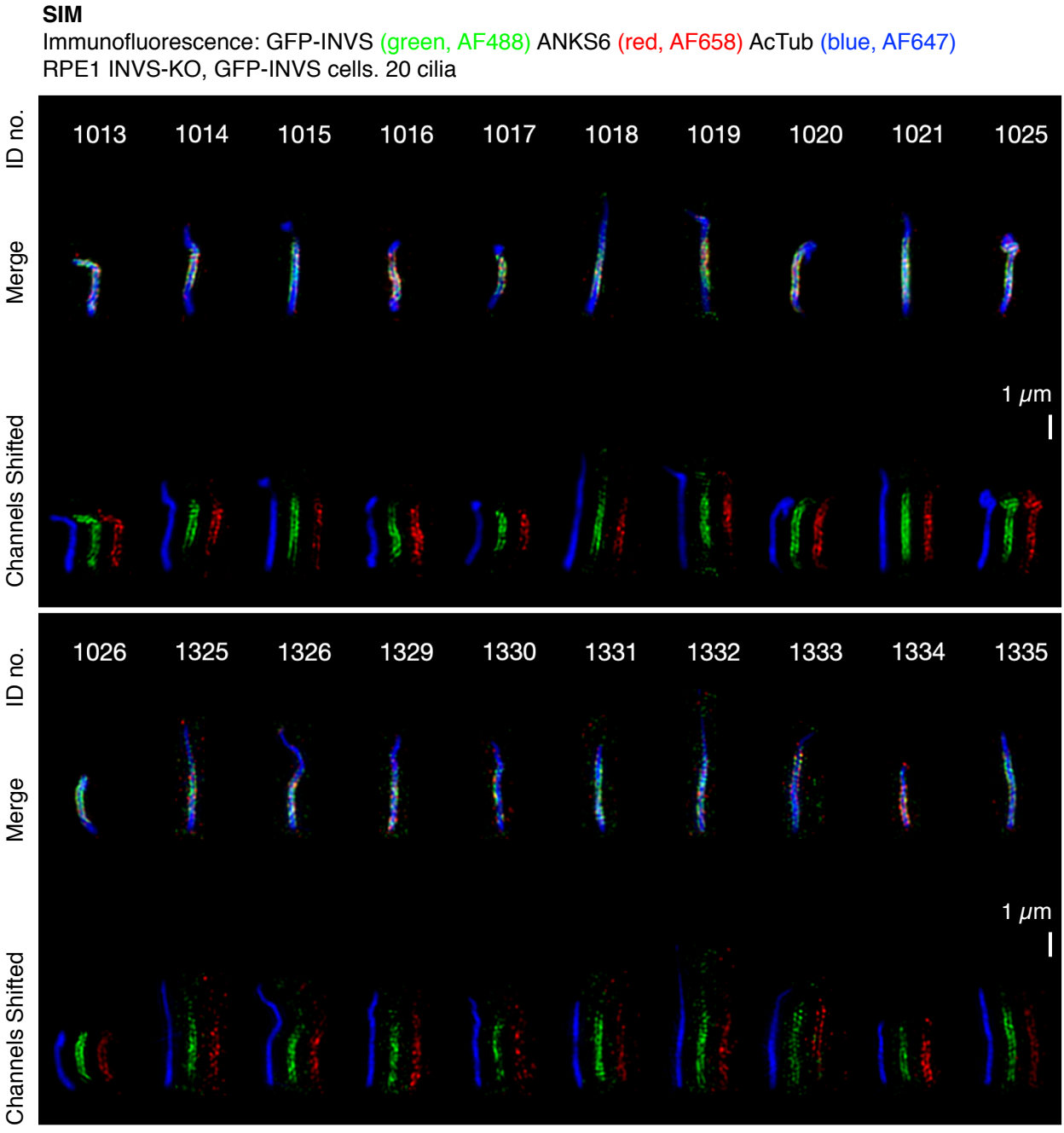

Supplemental Figure S47. SIM reconstructions of ANKS6 in ANKS6-KO cells expressing GFP-INVS.

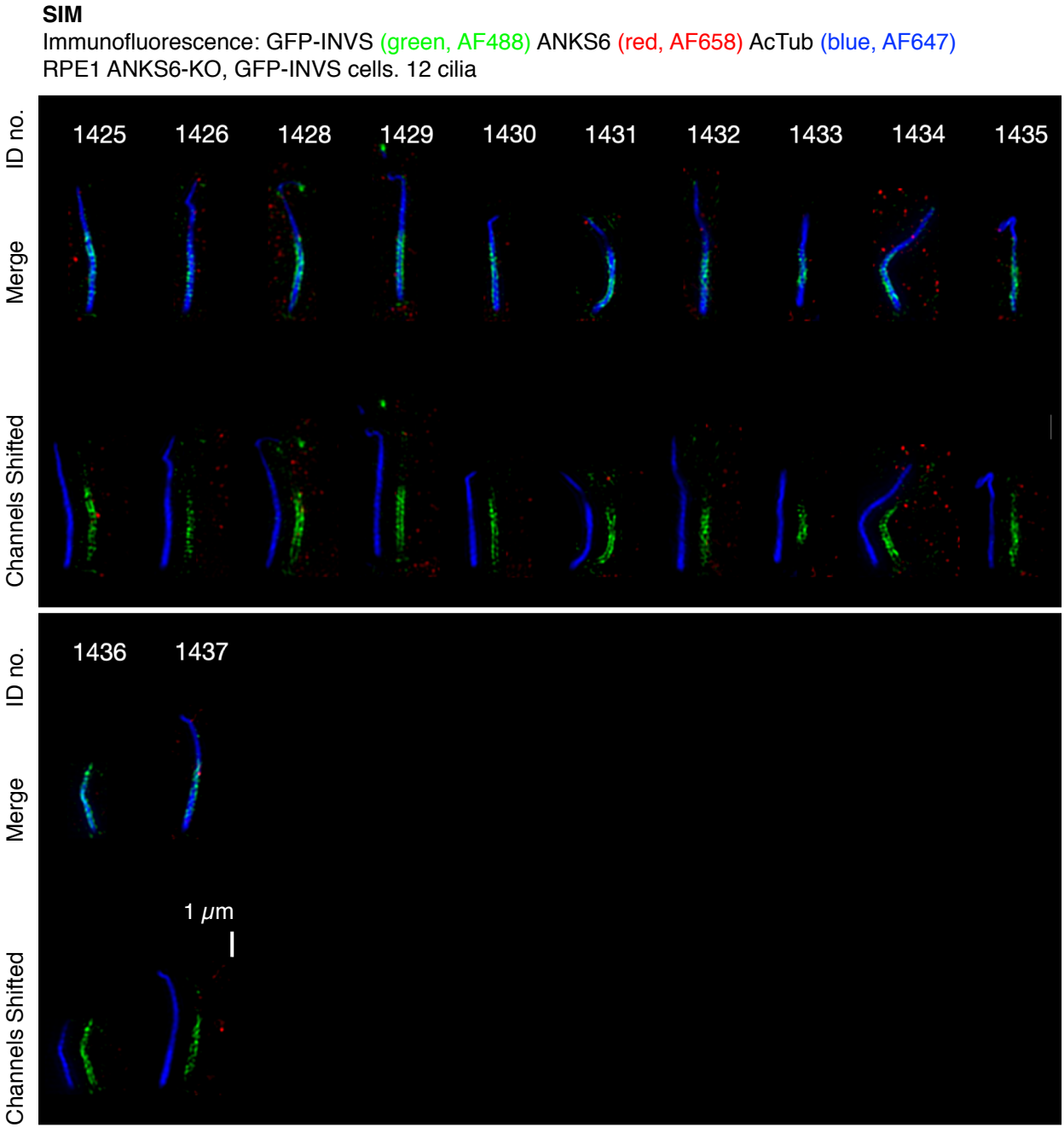

Supplemental Figure S48. Additional SIM reconstructions of ANKS6 in NEK8-KO cells expressing GFP-INVS.

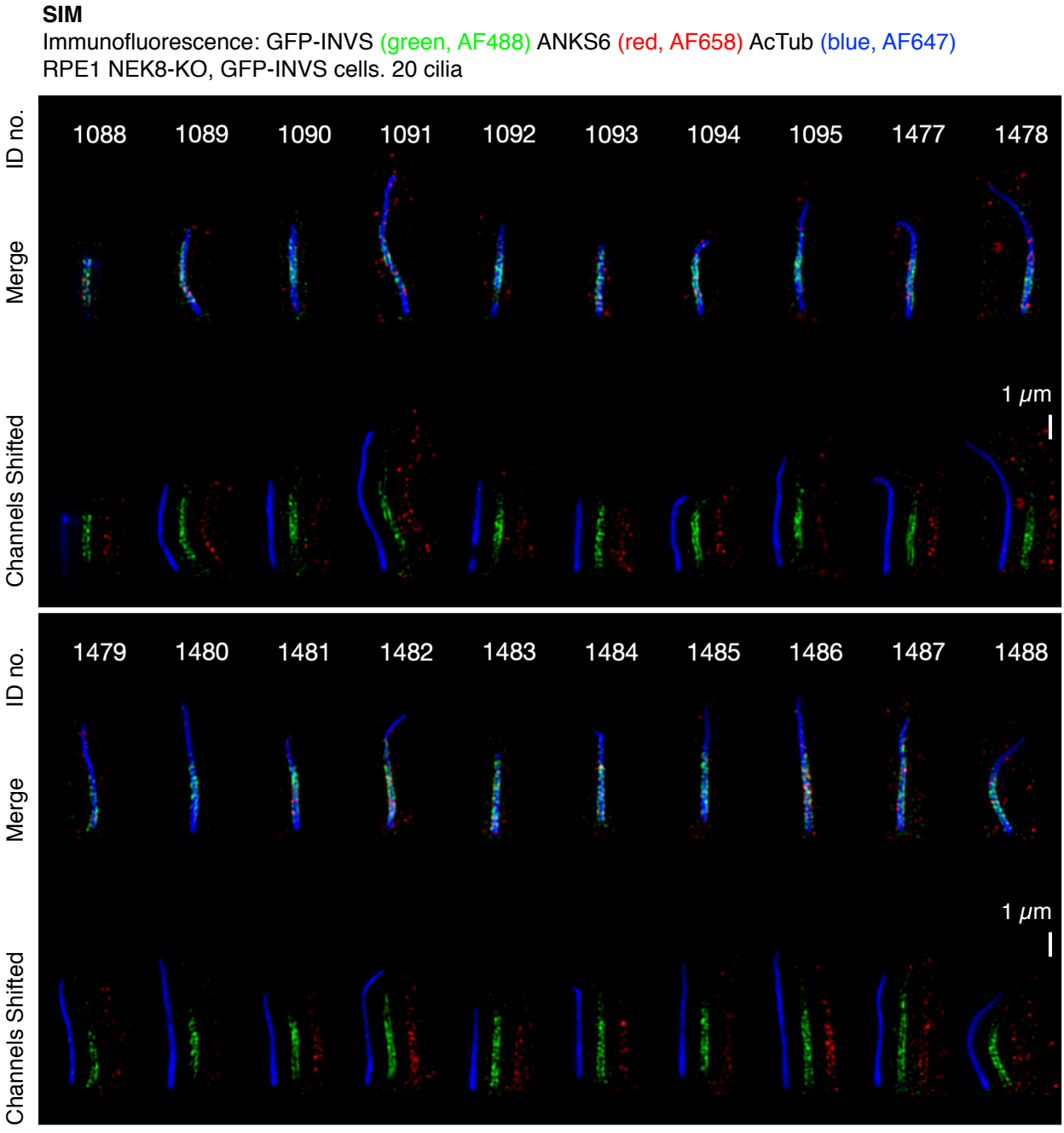

Supplemental Figure S49. Additional SIM reconstructions of ANKS6 in NPHP3-KO cells expressing GFP-INVS.

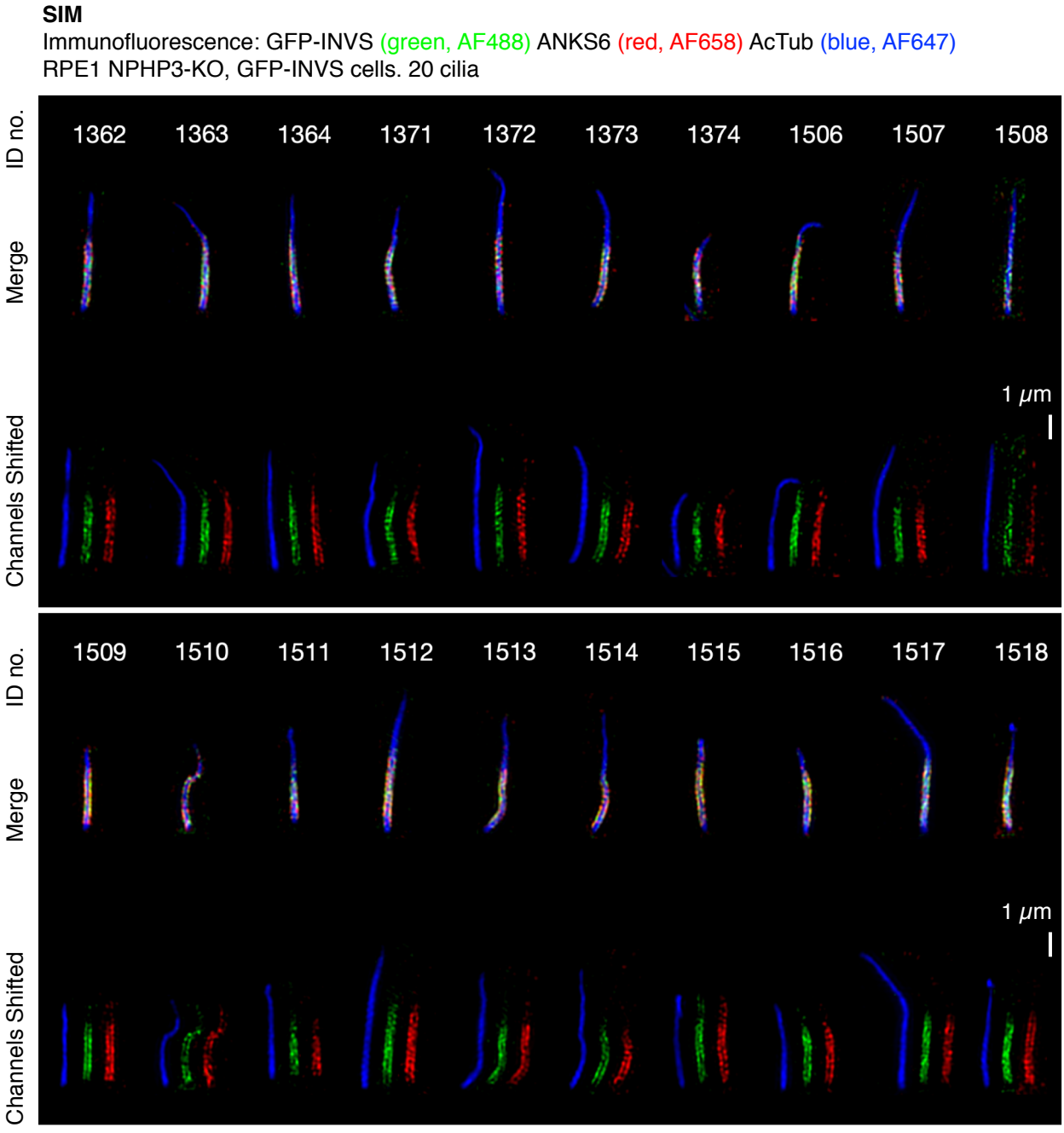

Supplemental Figure S50. DLM of ANKS6 INVc localization in NEK8-KO cells rescued with kinase dead (K33M) or JCK GFP-NEK8 alleles.

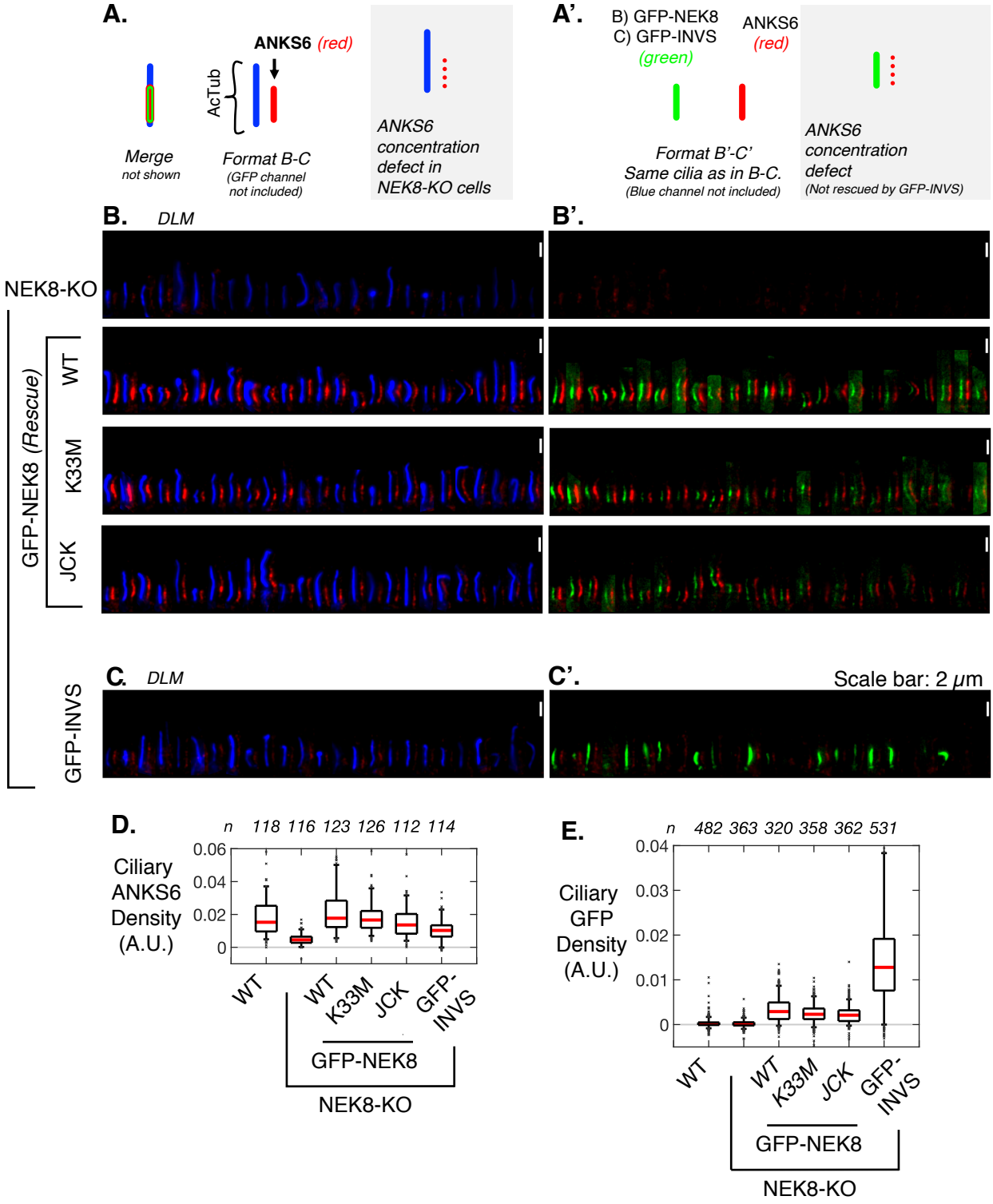

Supplemental Figure S51. NPHP3 INVc localization in NEK8-KO cells rescued with kinase dead (K33M) or JCK GFP-NEK8 alleles.

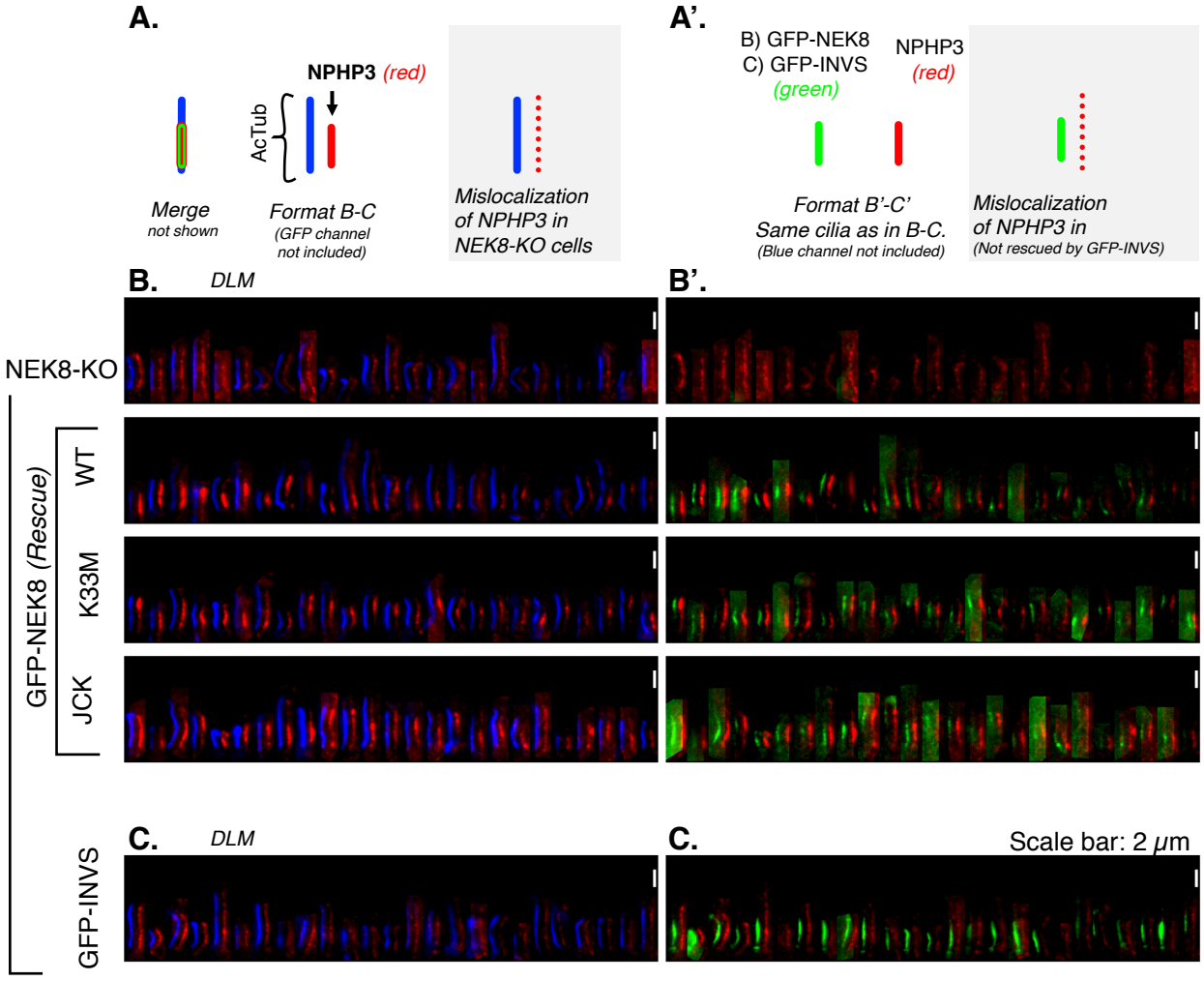

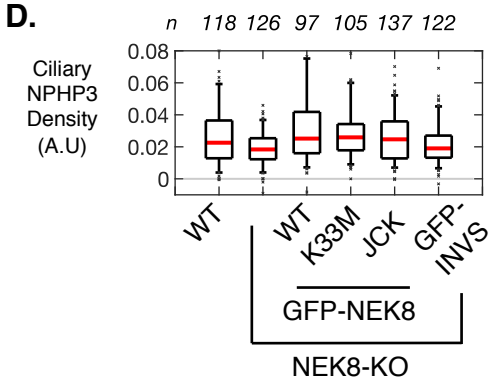

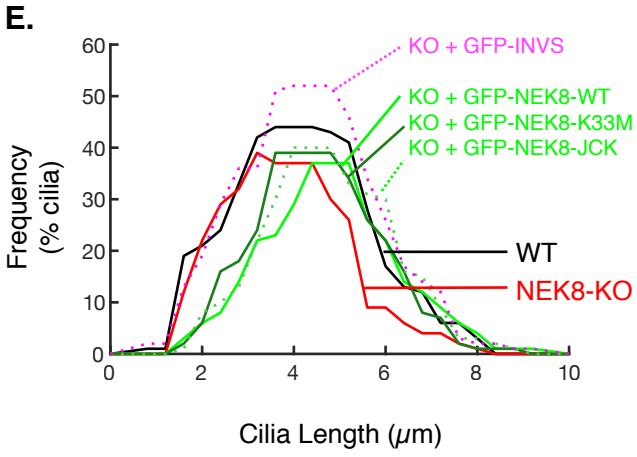

Supplemental Figure S52. SIM reconstructions of the INVc in NEK8-KO cells rescued with kinase dead (K33M) or JCK GFP-NEK8 alleles.

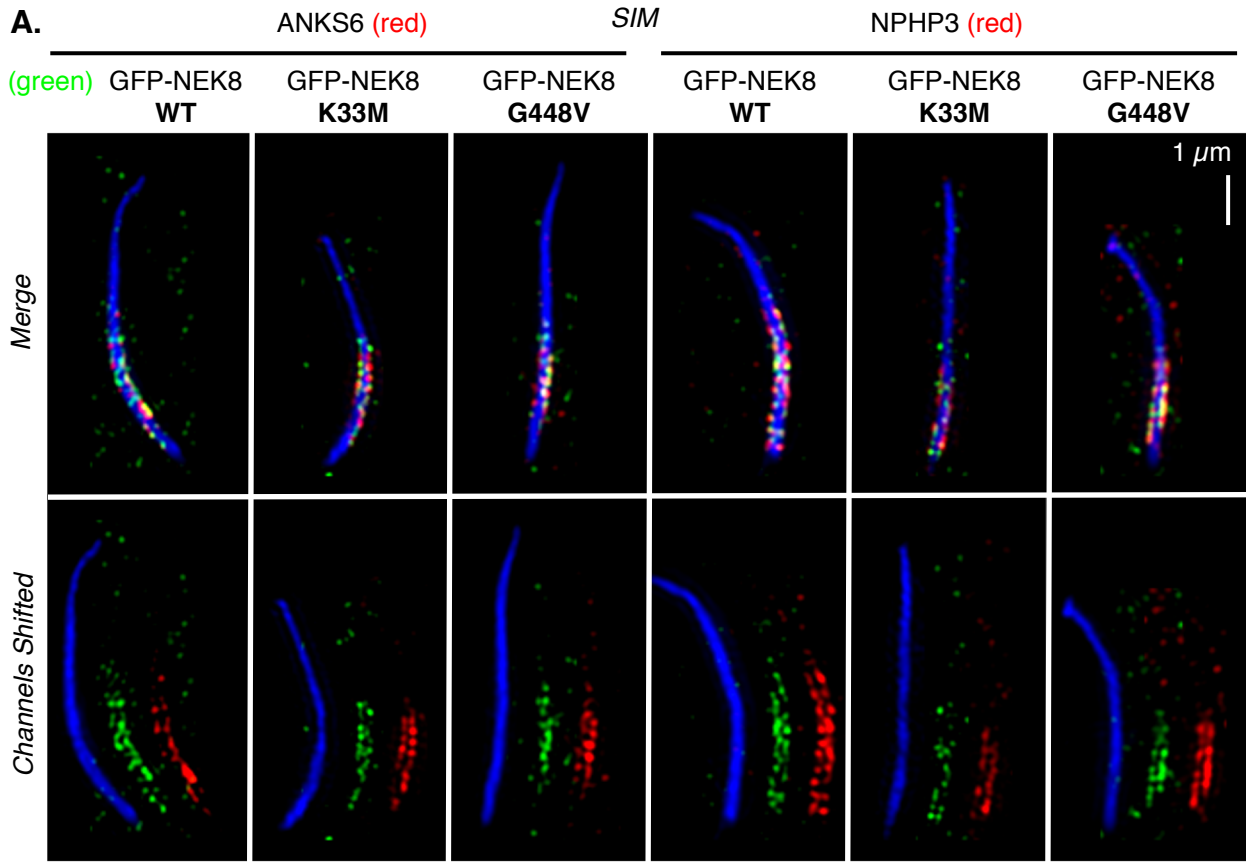

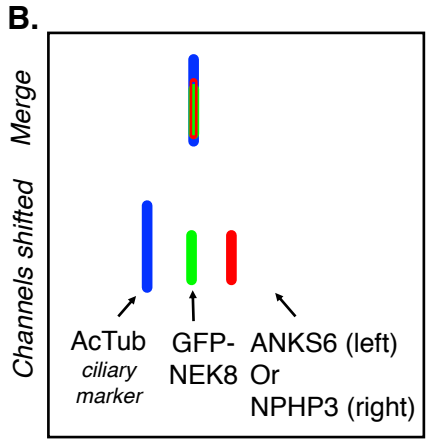

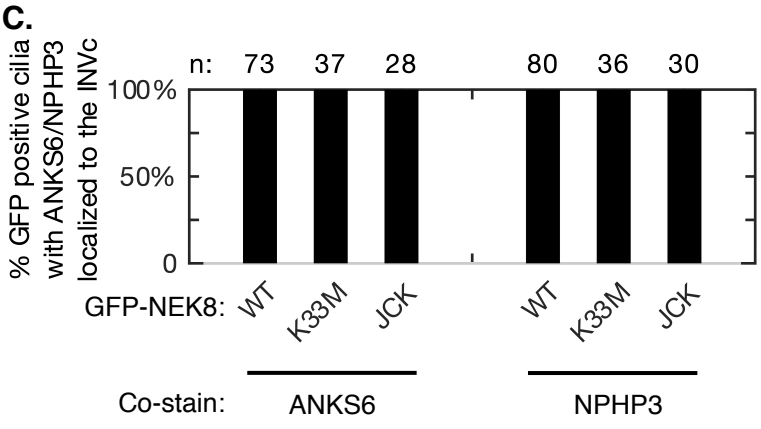

Supplemental Figure S53. Additional SIM reconstructions of ANKS6 in NEK8-KO cells rescued with GFP-NEK8-WT.

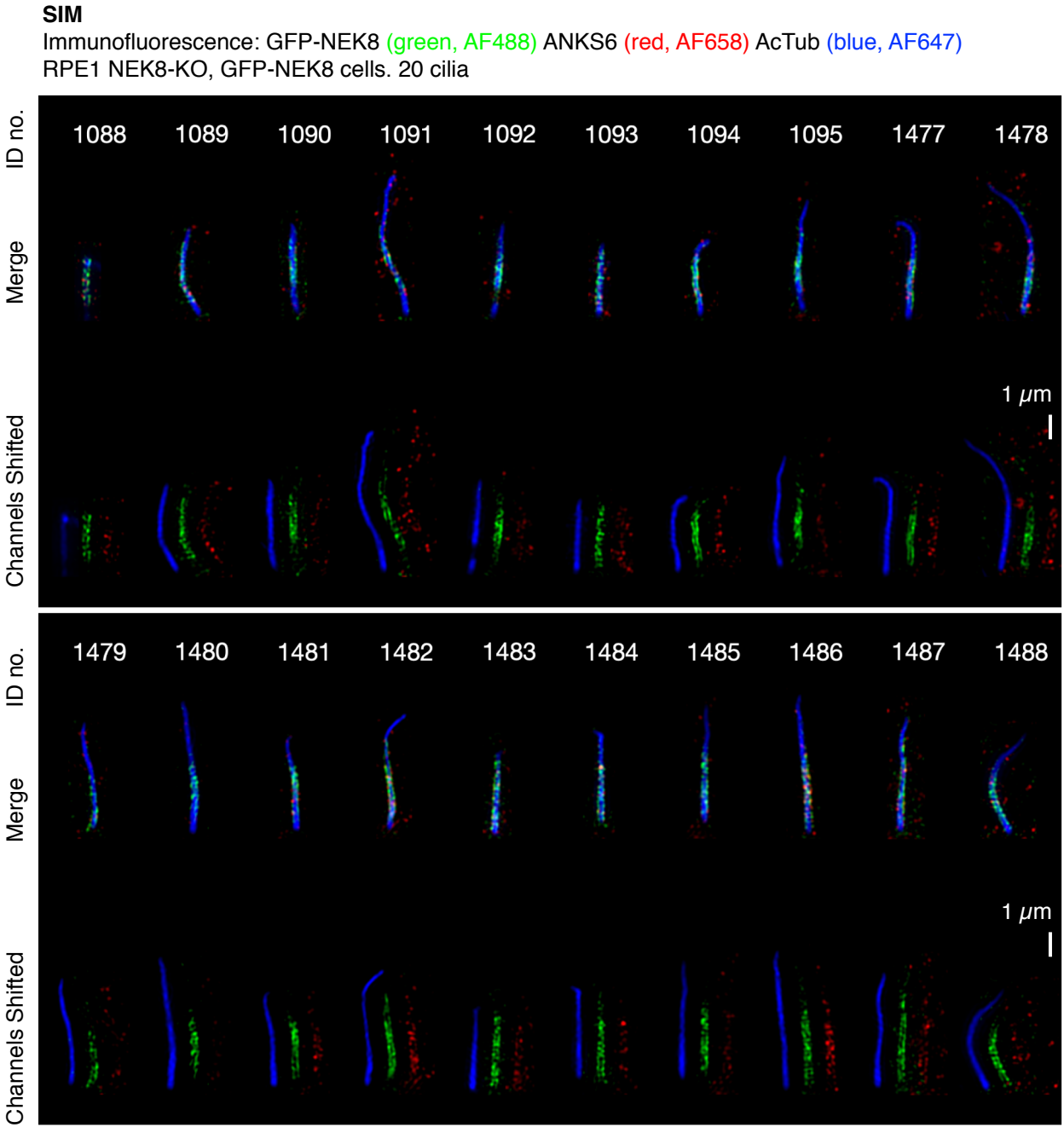

Supplemental Figure S54. Additional SIM reconstructions of ANKS6 in NEK8-KO cells rescued with GFP-NEK8-K33M.

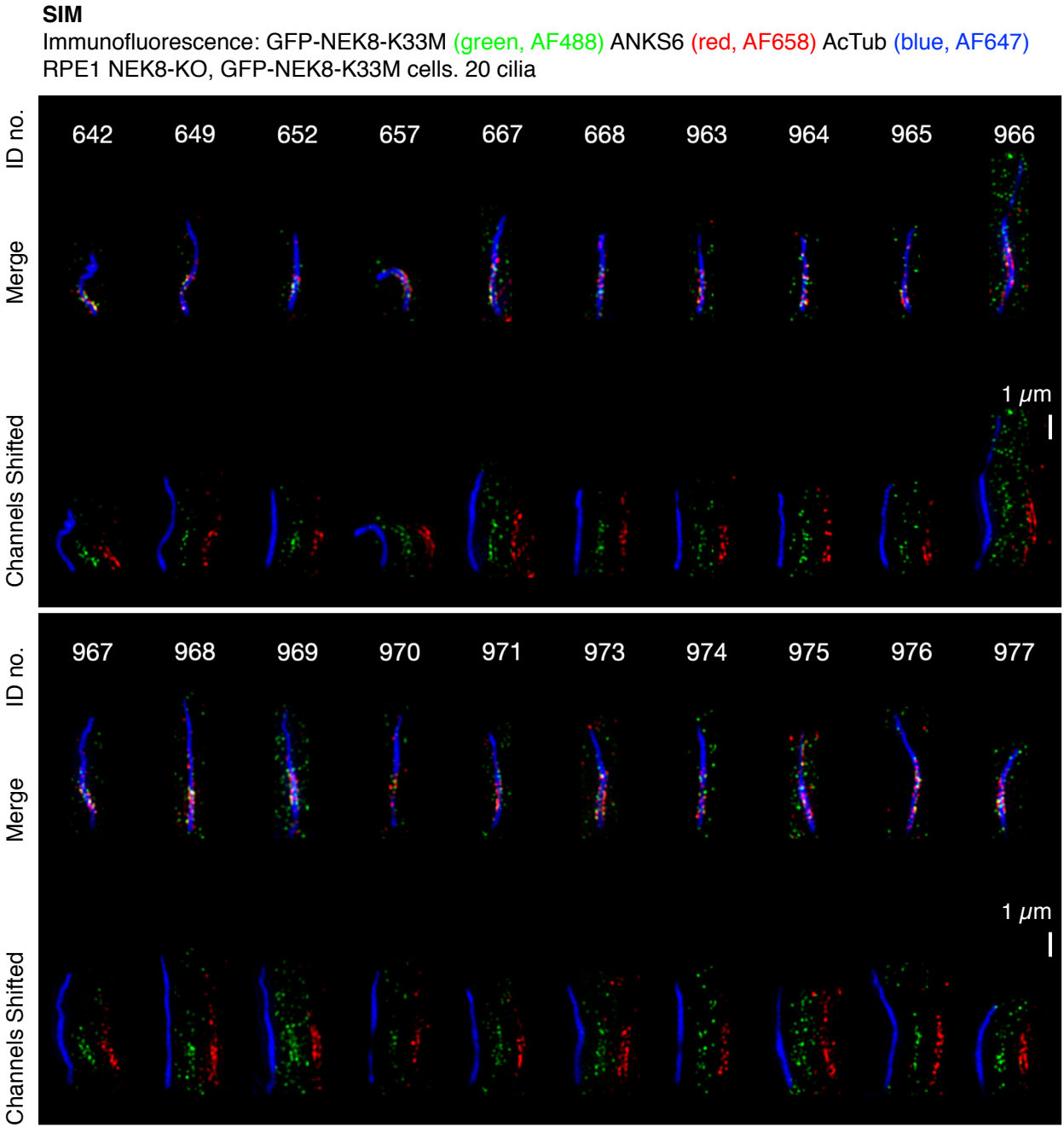

Supplemental Figure S55. Additional SIM reconstructions of ANKS6 in NEK8-KO cells rescued with GFP-NEK8-JCK.

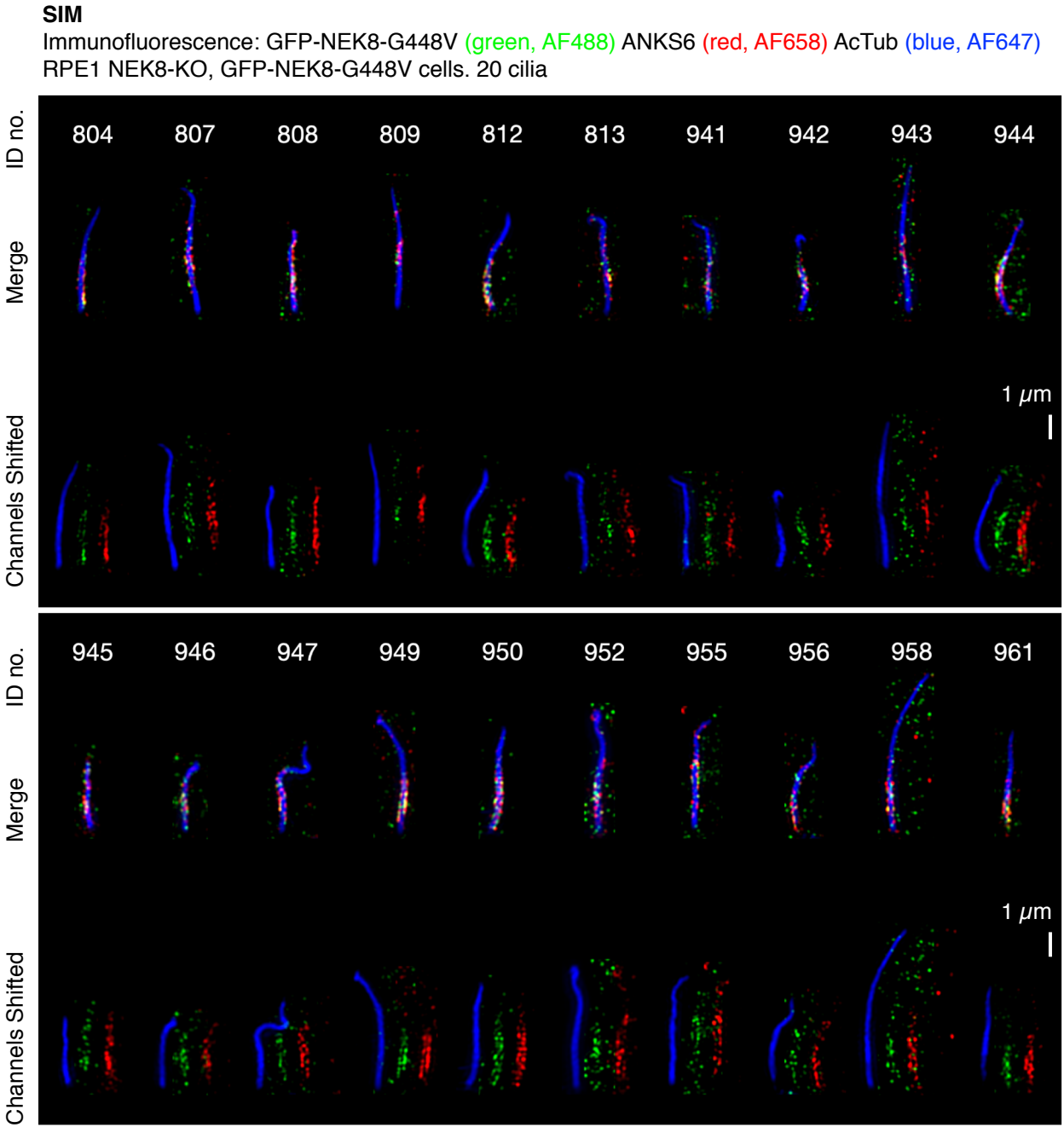

Supplemental Figure S56. Additional SIM reconstructions of NPHP3 in NEK8-KO cells rescued with GFP-NEK8-WT.

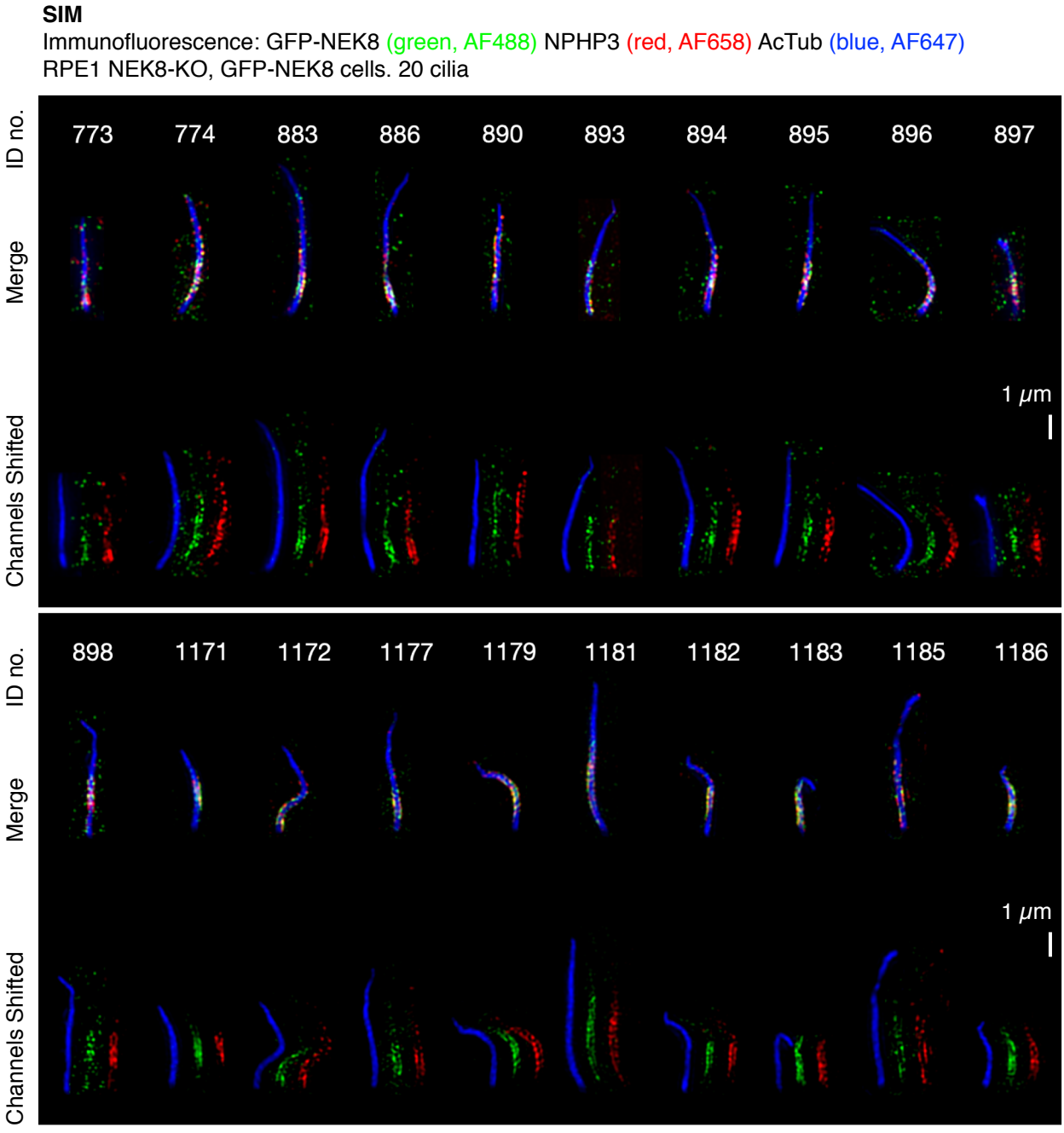

Supplemental Figure S57. Additional SIM reconstructions of NPHP3 in NEK8-KO cells rescued with GFP-NEK8-K33M.

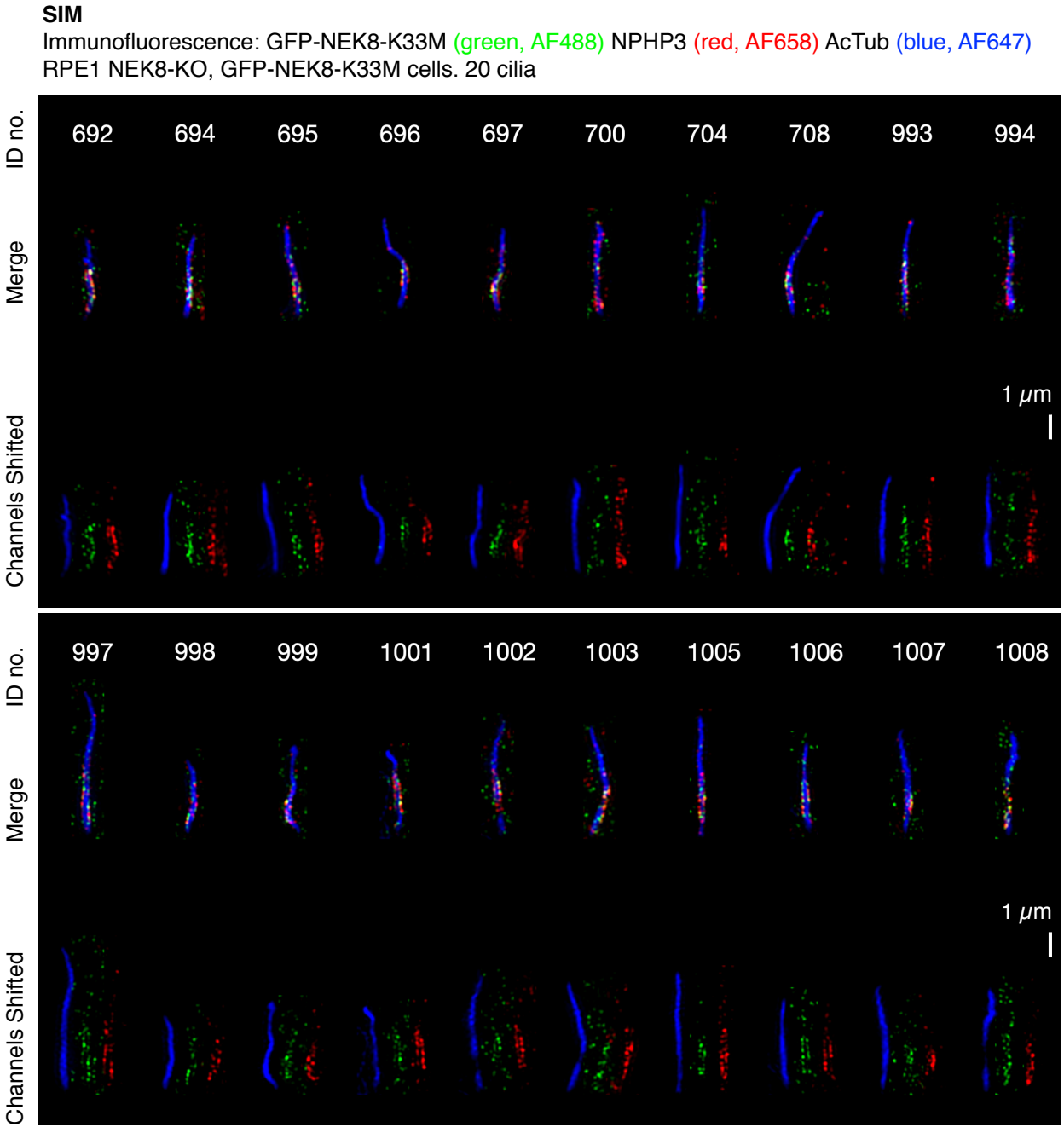

Supplemental Figure S58. Additional SIM reconstructions of NPHP3 in NEK8-KO cells rescued with GFP-NEK8-JCK.

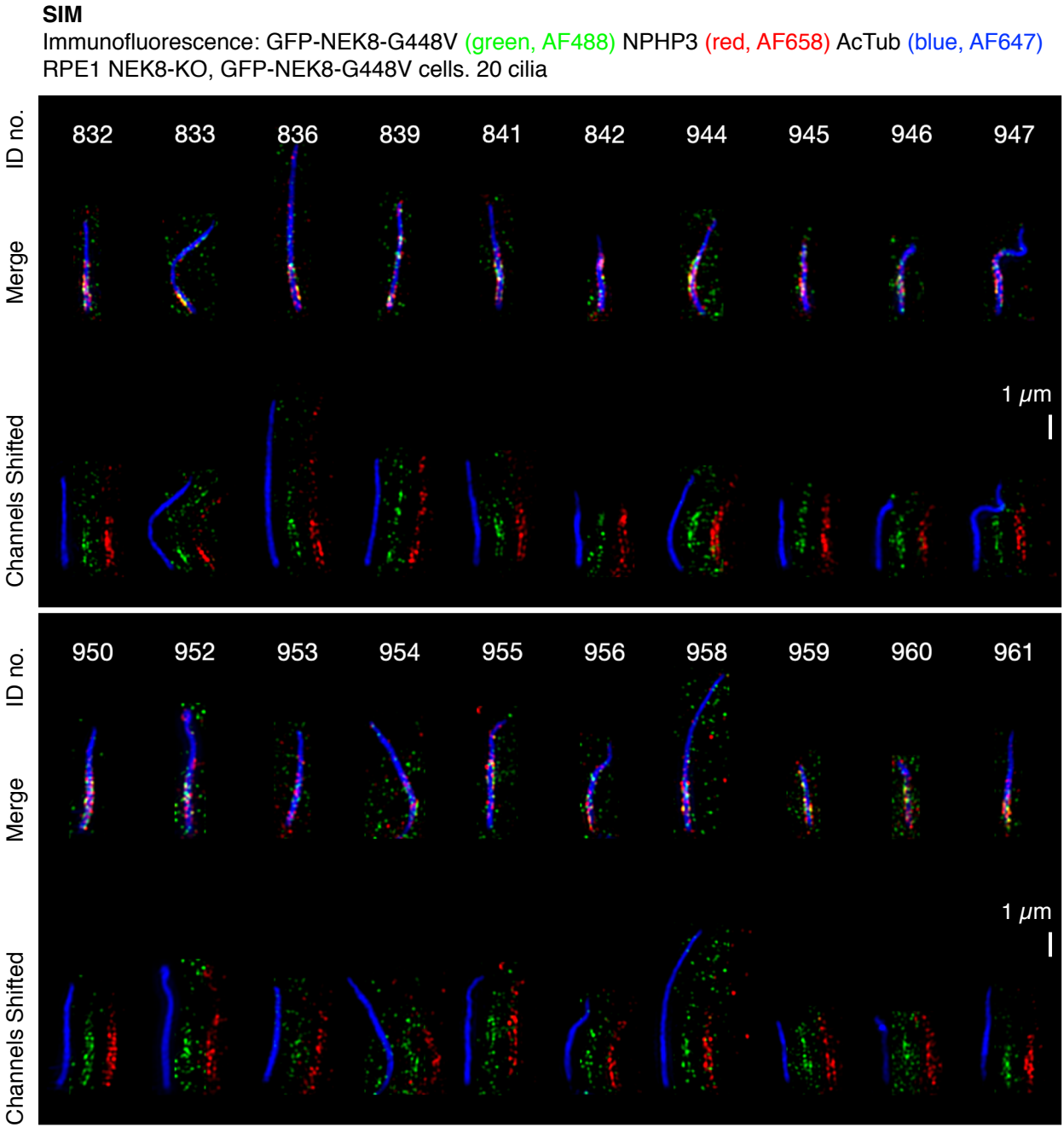

Supplemental Figure S59. A fibrilloid structure provides new insights into observed morphological variation in the INVc.